INVESTIGATION OF ONE- AND TWO-DIMENSIONAL MAGNETIC BEHAVIOUR OF SOME FIRST-ROW TRANSITION METAL COMPOUNDS

H. T. WITTEVEEN

INVESTIGATION OF ONE- AND TWO-DIMENSIONAL MAGNETIC BEHAVIOUR OF SOME FIRST-ROW TRANSITION METAL COMPOUNDS

PROEFSCHRIFT

TER VERKRIJGING VAN DE GRAAD VAN DOCTOR IN DE WISKUNDE EN NATUURWETENSCHAPPEN AAN DE RIJKSUNIVERSITEIT TE LEIDEN, OP GEZAG VAN DE RECTOR MAGNIFICUS DR. A. E. COHEN, HOOGLERAAR IN DE FACULTEIT DER LETTEREN, VOLGENS BESLUIT VAN HET COLLEGE VAN DEKANEN TE VERDEDIGEN OP DINSDAG 26 JUNI 1973 TE KLOKKE, 16.15 UUR

DOOR

HARMEN TJEERD WITTEVEEN

GEBOREN TE DEN HAAG IN 1944

Druk: Judels & Brinkman B.V. - Delft

PROMOTOR: DR. W. J. A. MAASKANT

Het in dit proefschrift beschreven onderzoek werd verricht onder leiding van
Prof. Dr. E. W. Gorter. †

voor Tricky Dick, vanwege zijn
voortreffelijke beerputten

voor Biesheuvel, omdat hij zich zo magnifiek
heeft laten uitrangeren, en aan alle andere
Biesheuveltjes, opdat zij het voorbeeld van
hun grote voorganger zullen navolgen

voor Heit en Mem
en natuurlijk ook voor Ellen

CONTENTS

CHAPTER I - INTRODUCTION

I-1 Introduction

During the last decennium both experimental and theoretical physicists have shown a growing interest in one- and two-dimensional magnetic systems. One of the reasons is that one expects that magnetic systems with a low dimension are generally more amenable to theoretical calculations than are three-dimensional systems. Also, theoretical interest has been stimulated by many experimental investigations of compounds showing magnetic properties that can be interpreted on the basis of one- and two-dimensional theoretical models.

For non-metallic, crystalline solids these properties are usually closely related to the crystal structure. As a rule of thumb one can say that if the compound can be described as having a chain-structure in which the distance between the magnetic ions belonging to different chains is much larger than the distance between the magnetic ions in the chains, the magnetic coupling in the chains (intra-chain coupling) is much stronger than the magnetic coupling between the chains (inter-chain coupling). Under such circumstances the compound can be described approximately as a one-dimensional magnetic system, as is shown by experimental evidence.

Similarly compounds with a layer-structure in which the distance between the magnetic ions in the layers is much smaller than the distance between the layers, often exhibit the characteristics of a two-dimensional magnetic system, i.e. the magnetic coupling in the layers (intra-layer coupling) is much stronger than the coupling between the layers (inter-layer coupling).

In this thesis the magnetic properties of some compounds showing the features of one- and two-dimensional systems are reported. But before passing on to the description of these compounds first a short review will be given of theoretical results obtained for one- and two-dimensional systems.

To interprete experimental results of magnetic systems it is usually necessary to use models that give a simplified description of the magnetic interactions in these systems. The basic properties of the models can be understood from the spin interaction Hamiltonian:

$$H = -2J \sum_{<i,j>} [aS_i^z S_j^z + b(S_i^x S_j^x + S_i^y S_j^y)] ,$$

where J is the exchange parameter between nearest neighbours, $\sum_{<i,j>}$ is the summation over all pairs of ions i and j, and S^x, S^y S^z are the components of spin angular momentum S; the ratio a/b is an anisotropy parameter. In many cases S represents the effective spin operator, utilized in the description of a (2S+1)-fold degenerate ground state of a magnetic ion. Crystal field anisotropy may suppress e.g. the S^x and S^y components and thereby induce anisotropic exchange. In this particular case (a=1 and b=0) the so-called Ising model is obtained, describing the case of extreme anisotropy in the magnetic interactions. If a=b=1 the Hamiltonian denotes the Heisenberg model, in which the magnetic interaction is isotropic. The case a=0, b=1 is called the XY model or planar Heisenberg model if it is required that the spins lie within the xy-plane. Intermediate cases may be described by $0<a<1$ and $0<b<1$.

I-2 Theoretical results for one-dimensional systems

For the one-dimensional (linear-chain) system many exact results and good numerical approximations concerning the thermodynamic properties are available. Calculations of the susceptibility and specific heat as a function of temperature have been reported by several authors for the ferro- and antiferromagnetic Ising chain with spin values S=1/2, 1, 3/2, 2, 5/2 and 3(1-5). For the XY model (transverse coupled chain) theoretical calculations of the energy, specific heat and perpendicular susceptibility are known for spin S=1/2 (1). Within the Heisenberg model Bonner and Fisher (6) have calculated the energy, specific heat and susceptibility for ferro- and antiferromagnetic chains in case S=1/2. For this spin value also the magnetization curves of antiferromagnetic linear chains at zero and non-zero temperature are derived (7, 8). Results for the Heisenberg chain having $S \geq 1$ have been reported by Weng (9). The thermodynamic properties of the classical Heisenberg chain ($S = \infty$) have been described by Fisher (10) and Stanley (11).

An essential property of the truly one-dimensional system having nearest neighbour interaction only, is the absence of long-range ordering at any non-zero temperature. This result holds for both the Ising and the Heisenberg model and all intermediate cases as well (12, 13). Due to this fact the entropy of the magnetic system has to be removed in short-range order processes at decreasing temperature. From this result it is deduced that a broad maximum occurs in the specific heat and susceptibility versus temperature curves of linear-chain systems. An exception has to be made for the susceptibility of the ferromagnetic model, because here the susceptibility diverges for $T \to 0$.

However, compounds of which it is experimentally found that they show one-dimensional properties, are never truly one-dimensional. They always exhibit a weak inter-chain coupling. However weak this coupling may be, it practically always induces a magnetic transition to three-dimensional long-range ordering.

For a two-dimensional array of weakly coupled Ising chains this long-range order transition has been proved by Onsager (14), e.g. on basis of exact calculations for the heat capacity, showing a singularity at finite temperature. It is seen that at high temperature the influence of the inter-chain coupling can be neglected, but that its influence increases at decreasing temperature. For a three-dimensional array of chains no rigorous results are known. Only some approximation methods have been developed by Oguchi (general spin) (15) and Van Tol ($S=1/2$) (16).

I-3 Theoretical results for two-dimensional systems

An essential difference is found between the behaviour of one- and two-dimensional systems (from now on indicated by 1D and 2D systems respectively). As remarked above a 1D system cannot exhibit long-range ordering at a finite temperature in either the Ising or Heisenberg model. For the 2D lattice (e.g. triangular, square and honeycomb lattice), however, it is proved for the Ising model by the exact solution of the partition function, that long-range order sets in at non-zero temperature. Extensive theoretical information about this phenomenon and other properties of 2D Ising lattices is given in a review by Fisher (17).

On the other hand it has been proved rigorously by Mermin and Wagner (12) that in zero magnetic field the 2D Heisenberg model cannot exhibit long-range order at finite temperature. However, for the 2D and 3D ferromagnetic Heisenberg model the so-called high-temperature series expansion method gives results that, at first sight, are in contradiction to the result of Mermin and Wagner. With this

method the partition function in the high-temperature region and thence the susceptibility, are described by a series expansion in powers of a reduced temperature. Analysis of the finite number of terms, known in this expansion, gives an indication for the existence of a finite transition temperature, where the susceptibility diverges (18-20). For high spin values these indications are as nearly as convincing in 2 as in 3 dimensions. But for the 3D model the transition temperature can be identified with the temperature where long-range order sets in, whereas such an identification cannot be made for the 2D isotropic lattice.

For the antifeoormagnetic 2D and 3D Heisenberg model not such a temperature can be found, that corresponds to a singularity in the susceptibility. However, using the so-called staggered susceptibility, which means that in the Hamiltonian a small magnetic field H is included, that changes sign at alternate lattice sites of the antiferromagnetic spin structure, a critical ordering temperature can be located in the limit of zero field (20), as well for the 2D as the 3D case.

Stanley and Kaplan (18) have pointed out that a combination of zero spontaneous magnetization and diverging susceptibility (or staggered susceptibility in the antiferromagnetic case) is possible if the spin correlation function $\langle \vec{S}_o . \vec{S}_r \rangle$ decreases slowly enough with spin separation r.

This intriguing new type of magnetic phase has stimulated many theoretical and experimental investigations. Experimentally, compounds have been found, which approximate the 2D isotropic exchange model very closely. But in many of these compounds a transition from paramagnetism to long-range order is detected at temperatures nearly equal or higher than the 'Stanley-Kaplan transition temperature', that is deduced from the series expansion results. Apparently, any deviation from the ideal isotropic 2D system, like the presence of inter-layer coupling, single-ion anisotropy in the exchange mechanism, dipole-dipole anisotropy, magnetostriction and crystal imperfections, may introduce long-range order at a finite temperature.

The influence of deviations from the ideal isotropic model on the transition temperature has been a subject of several theoretical studies (21-25).

Similar to the linear-chain model also for the 2D Heisenberg model the absence of a singularity in the nearest neighbour correlation implies that the specific heat as a function of temperature shows a broad maximum. In other words, due to the lack of a transition to long-range ordering, the entropy of the spin system has to be removed in short-range order processes. A broad maximum is

also found in the susceptibility curve of the 2D antiferromagnetic Heisenberg model.

Within the Heisenberg model Lines has shown for various spin values that the broad maximum of the antiferromagnetic susceptibility curve of the quadratic lattice just falls within the temperature range where the high-temperature series expansion gives a reliable description of the susceptibility (23). For the temperature region below the maximum no adequate theoretical description of the thermodynamic quantities is known. Only at temperatures well below the transition point there is a reliable description available, viz. spin wave theory (26).

This short review only intends to summarize some theoretical results and problems concerning 1D and 2D systems, that will also return in the discussion of the experimental results described in this thesis. For an extensive review the reader is referred to a forthcoming publication by De Jongh and Miedema (27).

I-4 Experiment

In recent times the system $AX-BX_2$ (A=monovalent ion, e.g. K, Tl, NH_4, Rb, Cs and B=divalent metal ion of the first transition series, e.g. Cr, Mn, Fe, Co, Ni, Cu and X=halogen ion, e.g. F, Cl, Br) has received considerable attention because of the fact that many of the compounds in this system crystallize in structures that could lead to 1D and 2D behaviour. The knowledge of the system $AX-BX_2$ is, however, far from being complete. Therefore, some years ago, a research program has been started at the Department of Solid State Chemistry of the Gorlaeus Laboratories of the University of Leiden with the purpose to make a thorough study of the chemical and physical properties of the compounds in the $AX-BX_2$ system. In this thesis some of the results of this study are reported.

It is known that many of the ABX_3 compounds have the $BaNiO_3$ (h) structure with hexagonal (h) stacking of close packed BaO_3 layers (fig. I-1a) (28-36). In these compounds the B^{2+} ions are octahedrally surrounded by six X^- ions. The octahedra share faces in such a way as to form chains of B^{2+} ions along the c-axis (fig. I-1b). Within these chains the distance between nearest neighbours B ions is about 3Å. The shortest inter-chain B-B distance, i.e. along the a-axis, is about 7Å. As a consequence we have the following types of exchange interaction paths between the B ions. Within the chains the exchange interaction between neighbouring B ions can be a direct exchange B-B and/or about 90° superexchange interaction B-X-B via the three X ions that form the common face of two octahedra. There is also the possibility of superexchange be-

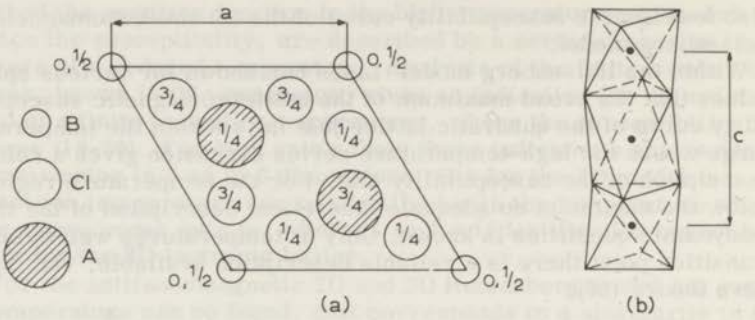

Fig. I-1a $BaNiO_3$ (h) structure, with hexagonal (h) stacking of close packed BaO_3 layers
Fig. I-1b Chains of B^{2+} ions along the c-axis

tween next nearest neighbours in the chains via two X ions, but this type of interaction is usually much smaller than nearest neighbour exchange and will therefore probably play a minor role in the intra-chain coupling.

Between the chains the interaction occurs via at least two non-magnetic ligands. The most probable superexchange is of the type B-X-X-B. Therefore, the inter-chain interaction also will be much smaller than the intra-chain interaction.

The ABX_3 compounds with the $BaNiO_3$ (h) structure are, therefore, expected to show magnetic properties characteristic of a magnetic linear chain. Several of these compounds have been investigated previously (34, 37-44). In this thesis the results of magnetic susceptibility measurements on polycrystalline samples of $ANiCl_3$ (A=Rb, NH_4, Tl, Cs) and $ANiBr_3$ (A=Rb, Cs) are given. As will be discussed in Chapter III the results of these measurements can be interpreted in terms of the linear-chain model.

Of the compounds with composition A_2BX_4 it is known that many among them have the K_2NiF_4 structure (fig. I-2) (45). This structure consists of NiF_2 layers, separated by two KF layers. Within the layers the superexchange interaction path between nearest neighbours involves one non-magnetic ligand (Ni-F-Ni), between nearest layers the superexchange path involves at least two non-magnetic ligands (Ni-F-F-Ni). Roughly speaking, this means that the intra-layer interaction will be much stronger than the inter-layer interaction. Hence, the compounds with the K_2NiF_4 structure could ex-

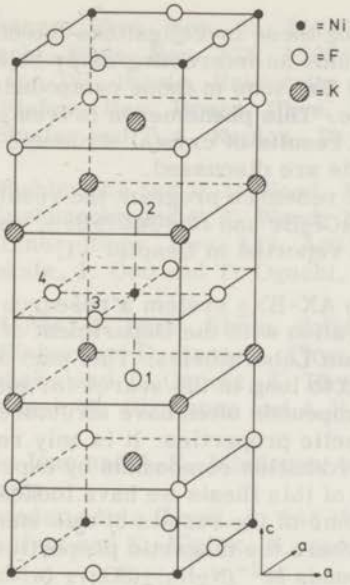

Fig. I-2 Illustration of the K_2NiF_4 structure

hibit the properties of 2D magnetic systems. This is supported by experimental evidence, as discussed in a review that De Jongh has dedicated to the compounds, known in literature, that show 2D properties (46). In particular for X=F many of the A_2BX_4 compounds show the K_2NiF_4 structure. For X=Cl, Br much less is known about A_2BX_4 compounds, although it can be expected that also for this case several compounds crystallize in the K_2NiF_4 structure. This is already known for K_2CrCl_4 (47), Rb_2CrCl_4 (47), $(NH_4)_2$ $CrCl_4$ (48), Cs_2CrCl_4 (49), Rb_2MnCl_4 (50) and Cs_2MnCl_4 (50). The compound $(NH_4)_2$ $CuCl_4$ has a deformed K_2NiF_4 structure (51) (see Chapter II).

Only a few data about the magnetic properties of these compounds are known. Results of neutron diffraction experiments on Rb_2MnCl_4 and Cs_2MnCl_4 have been published by Epstein et al.(50, 52) and recently zero-field susceptibility measurements on $(NH_4)_2$ $CuCl_4$ have been reported by Lécuyer et al.(53).

To enlarge the knowledge of the A_2BX_4 compounds with X=Cl, Br much attention has been paid in our research program to this part

of the $AX-BX_2$ system. During these investigations the compounds $A_2BCl_{4-x}Br_x$ with x=1,2 became an interesting study object because of the special ordering of the Br^- ions in those compounds that possess the K_2NiF_4 structure. This phenomenon is treated in Chapter II. In this chapter also some results of crystal structure investigations on the A_2BX_4 compounds are discussed.

Of the magnetic part of the research program the results for the compounds Rb_2CuCl_4, Rb_2CuCl_3Br and $Rb_2CuCl_2Br_2$, showing the $(NH_4)_2$ $CuCl_4$ structure, are reported in Chapter VI.

In addition to the study of the $AX-BX_2$ system a research program has been developed in cooperation with the Department of Coordination Chemistry of the Gorlaeus Laboratories. This part of inorganic chemistry has been neglected to long in the search for magnetic systems, as coordination compounds often have structures which may lead to interesting magnetic properties. It is only recently that some attention is paid to coordination compounds by experimental physicists. Within the scope of this thesis we have looked mainly for linear-chain systems. Some of the results of this study are reported in Chapter IV and V where the magnetic properties of respectively the linear-chain compounds $M^{2+}(N_2H_5)_2(SO_4)_2$ (with M=Mn, Fe, Co, Ni, Cu) and MnX_2L_2 (with X=Cl, Br and L=pyrazole, pyridine) are discussed.

References

1. S. Katsura, Phys. Rev. 127, 1508 (1962)
2. M. Suzuki, B. Tsujiyama and S. Katsura, J. Math. Phys. 8, 124 (1967)
3. T. Obokata and T. Oguchi, J. Phys. Soc. Jap. 25, 322 (1968)
4. J.A.R. van Veen, H.T. Witteveen and W. Vermin, to be published
5. M.E. Fisher. J. Math. Phys. 4, 124 (1963)
6. J.C. Bonner and M.E. Fisher, Phys. Rev. 135, A640 (1964)
7. R.B. Griffiths, Phys. Rev. 133, A768 (1964)
8. S. Katsura and S. Inawashiro, J. Math. Phys. 5, 1091 (1964)
9. C. Weng, thesis, Carnegie-Mellon University (1968)
10. M.E. Fisher, Am. J. Phys. 32, 343 (1964)
11. H.E. Stanley, Phys. Rev. 179, 570 (1969)
12. N.D. Mermin and H. Wagner, Phys. Rev. Letters 17, 1133 (1966)
13. L.D. Landau and E.M. Lifschitz, 'Statistical Physics' (Pergamon Press, Ltd. London, 1958, p482)

14. L. Onsager, Phys. Rev. 65, 117 (1944)
15. T. Oguchi, Phys. Rev. 133, A1098 (1964)
16. M.W. van Tol, thesis, University of Leiden (1972)
17. M.E. Fisher, Rep. Progr. Phys. 30, Part 2, 615 (1969)
18. H.E. Stanley and T.A. Kaplan, Phys. Rev. Letters 17, 913 (1966)
19. G.S. Rushbrooke and P.J. Wood, Molecular Phys. 1, 257 (1958)
20. G.S. Rushbrooke and P.J. Wood, Molecular Phys. 6, 409 (1963)
21. M.E. Lines, Phys. Rev. 133, A841 (1964)
22. T. Obokata, I. Ono and T. Oguchi, J. Phys. Soc. Jap. 23, 516 (1967)
23. M.E. Lines, J. Phys. Chem. Solids 31, 101 (1970)
24. M.E. Fisher and D. Jasnow, Phys. Rev. B3, 907 (1971)
25. T. Ishikawa and T. Oguchi, J. Phys. Soc. Jap. 31, 1021 (1971)
26. D.J. Breed, K. Gilijamse and A.R. Miedema, Physica 45, 205 (1969)
27. L.J. de Jong and A.R. Miedema, to be published in Advances in Physics
28. J.J. Lander, Acta Cryst. 4, 148 (1951)
29. H.J. Seifert and K. Klatyk, Z. anorg. allgem. Chem. 342, 1 (1966)
30. M. Amit, A. Zodkevitz and J. Makovsky, Isr. J. Chem. 8, 737 (1970)
31. A. Zodkevitz, J. Makovsky and Z.H. Kalman, Isr. J. Chem. 8, 755 (1970)
32. D.J.W. Ydo, thesis, University of Leiden (1960)
33. H.J. Seifert, Z. anorg. allgem. Chem. 307, 137 (1961)
34. N. Achiwa, J. Phys. Soc. Jap. 27, 561 (1969)
35. G.N. Tischenko, Tr. Kristallogr. Akad. Nauk. SSSR 11, 93 (1955), Chem. Abstr. 55, 16251g (1956)
36. A.F. Wells, J. Chem. Soc. 1947, 1662 (1947)
37. F.J. Rioux and B.C. Gerstein, J. Chem. Phys. 50, 758 (1969)
38. F.J. Rioux and B.C. Gerstein, J. Chem. Phys. 53, 1789 (1970)
39. J. Smith, B.C. Gerstein, S.H. Liu and G. Stucky, J. Chem. Phys. 53, 418 (1970)
40. V.J. Minkiewicz, D.E. Cox and G. Shirane, J. Phys. Colloque C1, suppl. au no. 2-3, 892 (1971)
41. D.E. Cox and V.J. Minkiewicz, Phys. Rev. B4, 2209 (1971)
42. R.W. Asmussen and H. Soling, Z. anorg. allgem. Chem. 283, 3 (1956)
43. H.T. Witteveen and J.A.R. van Veen, J. Chem. Phys. 58, 186 (1973)
44. P.A. Montano, E. Cohen, H. Shechter and J. Makovsky, Phys. Rev. B7, 1180 (1973)

45. D. Balz and K. Plieth, Z. Elektrochem. 59, 545 (1955)
46. L.J. de Jongh, P. Bloembergen and J.H.P. Colpa, Physica 58, 305 (1972)
47. H.J. Seifert and K. Klatyk, Z. anorg. allgem. Chem. 334, 113 (1964)
48. H.D. Hardt and G. Streit, Z. anorg. allgem. Chem. 373, 97 (1970)
49. H.J. Seifert and K. Klatyk, Naturw. 49, 539 (1962)
50. A. Epstein, E. Gurewitz, J. Makovsky and H. Shaked, Phys. Rev. B2, 3703 (1970)
51. R.D. Willett, J. Chem. Phys. 41, 2243 (1964)
52. E. Gurewitz, A. Epstein, J. Makovsky and H. Shaked, Phys. Rev. Letters 25, 1713 (1970)
53. B. Lécuyer, J.P. Renard and A. Herpe, C.R. Acad. Sc. Paris, t. 275 Serie B, 73 (1972)

CHAPTER II - EXPERIMENTAL EQUIPMENT, SAMPLE PREPARATION AND CHARACTERIZATION

II-1 Experimental Equipment

Magnetic susceptibility measurements were carried out by means of a commercial P(rinceton) A(pplied) R(esearch) Parallel Field Vibrating Sample Magnetometer Model 150. This type of magnetometer was first described by Foner (1). The mechanical system of the instrument is mounted on a liquid-nitrogen-shielded liquid-helium dewar (Janis Research Company), containing a superconducting magnet. A small sample of the compound to be investigated is placed in a sample holder located at the end of a rod that is vibrated parallel to the field direction of the superconducting solenoid (frequency about 82 Hz). This induces an AC voltage in a set of stationary pick-up coils located at the centre of the solenoid. The associated electronic system measures this induced voltage from which the magnetic properties of the sample are deduced.

By means of a throttle valve a continuous flow of liquid helium is transferred from the liquid helium bath of the cryostat to the sample chamber. At the bottom of the sample chamber a small heat exchanger is located that controls the temperature of the helium vapour stream emerging from this heat exchanger. The current supplied to the heating coil is governed by a PAR Cryogenic Temperature Controller Model 152, that utilizes an uncalibrated GaAs diode as temperature sensor. The helium vapour stream evades at the top of the sample chamber. With this system the temperature in the sample zone may be maintained at any temperature between 4.2 K and 300 K. By evacuating the sample chamber the temperature can be lowered to 2 K.

The temperature in the sample zone is measured with a calibrated GaAs diode. This diode was calibrated in the temperature region 2-90 K by means of a Cryocel Ge resistance thermometer calibrated at the Department of Thermometry of the Kamerlingh Onnes Labora-

tory of the University of Leiden, and kindly lent to us by this department.

Between 70 K and 300 K the diode voltage appeared to be linearly dependent on the temperature within the uncertainty of the temperature measurement (the uncertainty is rising from 0.1 K at the lowest temperatures to 0.5 K in the higher temperature region), so that only at room temperature another calibration point was necessary.

The current for the calibrated diode is delivered by a constant current supply of 10μA.

The voltage of the diode is measured with a Hewlett-Packard 3420A DC Differential Voltmeter.

The superconducting magnet of Westinghouse is made of Nb-T_i wire and has a 1 inch bore. The homogeneity is about 2.5% in a spherical volume with 1 inch diameter, and the maximum field is 56 kOe.

By combining the coil constant (the magnetic field strength is proportional to the magnet current: 10 A corresponds to 11.7 kOe) and the current (supplied) to the superconducting coil by a Westinghouse magnet power supply) measured with a 0.01Ω precision resistor, the magnetic field strength is calculated. The calibration of the magnetometer is obtained by measuring at room temperature the saturation magnetization of a pure Ni sample of which weight and magnetic moment per gram atom at room temperature are known.

Some additional zero-field susceptibility and spin-flop measurements in the liquid-helium and liquid hydrogen temperature region (Chapter IV, VI) have been carried out by S. Hillaert at the Kamerlingh Onnes Laboratory by means of a radio frequency twin-T-bridge at frequencies in the range 250-300 kHz. This apparatus will be described in detail elsewhere (2).

F.W. Klaaijsen at the Kamerlingh Onnes Laboratory carried out heat capacity measurements by means of the heat pulse method on some of the compounds described in this thesis. Preliminary results are reported here. A detailed description of his apparatus and his measurements will be published elsewhere (3).

The ESR measurements both at room temperature and liquid-nitrogen temperature, described in Chapter III and VI were carried out by H. Vos at X-band frequency (about 9.2 GHz) with a commercial Varian E3 instrument.

In Chapter IV the results of ESR measurements at liquid-hydrogen temperature are described. These measurements were carried out by J. van Dijk at the Department of Chemistry of the Technological University of Delft by means of a Varian E3 instrument.

The ESR measurements at X-band and Q-band (35.5 GHz), described in Chapter IV and V were carried out by B. Nieuwenhuyse and P.G. van den Akker of the Technological University of Twente with

a Varian V-4502/3-10A spectrometer of which details have been published elsewhere (4).
X-ray powder diffraction patterns of all compounds were obtained by means of a Philips PW1050 diffractometer that is also suited for the investigation of hygroscopic samples.

For a structure analysis of some compounds described in this chapter (II-2.5) neutron powder diffraction experiments were carried out at the 'Reactor Centrum Nederland' in Petten by B. van Laar.

Chemical analysis of the samples used for the magnetic measurements have been carried out by J.A. Smit of the Department of Coordination Chemistry of the Gorlaeus Laboratories and at the Organic Institute TNO in Utrecht.

For several compounds differential thermal analysis experiments have been carried out by E. Kruissink by means of a Mettler Vacuum Thermal Analyzer TA1.

Many calculations in this thesis were carried out with the IBM 360/65 computer at the University Computer Centre of Leiden.

II-2 Sample Preparation and Characterization

II-2.1 The compounds $ANiCl_3$ (A=Tl, NH_4, Rb, Cs) and $ANiBr_3$ (A=Rb, Cs)

Polycrystalline samples of the yellow compounds $RbNiCl_3$, $TlNiCl_3$ and $CsNiCl_3$ were prepared by melting stoichiometric amounts of ACl (A=Tl, Rb, Cs) and $NiCl_2$ in an evacuated and sealed silica tube for one day at 800°C and heating afterwards for several days at 350-500°C. $NiCl_2$ was prepared by dehydration of $NiCl_2.6H_2O$ in a stream of dry HCl gas at 450-550°C during 3-4 hours.

The yellow compound NH_4NiCl_3 was prepared by mixing stoichiometric amounts of NH_4Cl and $NiCl_2$ in an agate mortar and heating afterwards the mixture in a sealed gold tube for several days at 400°C under a pressure of about 1 kbar.

The redbrown compounds $RbNiBr_3$ and $CsNiBr_3$ and also the compounds $RbNiCl_3$ and $CsNiCl_3$ were prepared as described by Asmussen and Soling (5). $NiCO_3$ and AX (A=Rb, Cs, X=Cl, Br) in the ratio 1.5:1 were dissolved in concentrated HX-solution. These solutions were partly evaporated over concentrated H_2SO_4. The needle-like crystals were filtered off, washed with acetone and dried over P_2O_5. It was found that the $RbNiCl_3$ and $CsNiCl_3$ samples obtained in this way, were magnetically purer than the samples obtained from the melt (see Chapter III). Also the longer it took for the samples to crystallize (maximum about one month), the better they were.

Because of the hygroscopic nature of $NiCl_2$ and the compounds prepared all treatments were carried out in a glove box filled with dry nitrogen. The same has been done for all other hygroscopic compounds discussed in this chapter.

The results of the chemical analysis of the compounds are listed in Table II-1. As already discussed in Chapter I, the compounds in Table II-1 crystallize in the hexagonal $BaNiO_3$ (h) structure (fig. I-1). The a- and c-axes of the chemical unit cell of the compounds, obtained from X-ray powder diffraction patterns, are given in Table II-2. These values are in good agreement with those found by other authors (5-11).

Table II-1 Chemical analyses of the $ANiX_3$ compounds

Compound	Ni(exp)%	Ni(theor)%	X(exp)%	X(theor)%
$TlNiCl_3$	15.86	15.89	28.62	28.79
NH_4NiCl_3	31.51	32.06	57.51	58.09
$RbNiCl_3$	23.31	23.43	42.35	42.45
$CsNiCl_3$	19.49	19.70	35.33	35.69
$RbNiBr_3$	15.29	15.29	62.60	62.45
$CsNiBr_3$	13.60	13.61	55.43	55.57

Table II-2 Cell constants of the $ANiX_3$ compounds

Compound	a-axis (Å)	c-axis (Å)	Ref.
$TlNiCl_3$	6.864(2)	5.882(2)	
	6.84	5.88	6
NH_4NiCl_3	6.927(3)	5.919(5)	
	6.9216	5.915	7
$RbNiCl_3$	6.958(2)	5.904(2)	
	6.95	5.90	8
	6.955(1)	5.906(1)	9
$CsNiCl_3$	7.173(2)	5.942(3)	
	7.18	5.93	10
$RbNiBr_3$	7.308(2)	6.201(2)	
	7.268(8)	6.208(8)	9
$CsNiBr_3$	7.485(2)	6.230(3)	
	7.50	6.24	11
	7.49	6.24	9,5

As in all tables in this thesis the values between parentheses indicate the uncertainty in the last digit.

II-2.2 Ordering of X and X' halogen ions in $A_2BX_{4-x}X'_x$ compounds (X=0, 1, 2) with K_2NiF_4 structure

A description of the K_2NiF_4 structure has already been given in Chapter I. One aspect of this structure, however, deserves more attention.

The anions in the K_2NiF_4 structure are distributed over two crystallographic positions. If the anions in A_2BX_4 halides with the K_2NiF_4 structure are partly replaced by larger, and thus more polarizable halogen ions it is expected that these larger anions prefer the sites denoted by 1 and 2 in fig. I-2. The anions in these positions are coordinated by five A ions and one B ion. The linear configuration A^+-X-B^{2+} of this anion coordination is more favourable for more polarizable anions than the linear configuration B^{2+}-X-B^{2+} of the other anion coordination (sites denoted by 3 and 4 in fig. I-2).

In $A_2BX_2X'_2$ halides with the K_2NiF_4 structure where X' is a larger, more polarizable halogen ion than the X ion, one expects, therefore, that due to the equal number of X and X' ions a new kind of octahedra $[BX_4X'_2]$ is formed, where the X ions lie within the equatorial plane of the octahedron (sites 3 and 4) and the X' ions occupy the sites above and beneath this plane (1 and 2).

For the same reason one expects two possibilities for A_2BX_3X' halides: a structure in which $[BX_6]$ octahedra along with an equal number of $[BX_4X'_2]$ octahedra occur and a structure in which only $[BX_5X']$ octahedra occur. From our experiments no indications are found for the latter possibility (see below).

To investigate the conjecture about the ordering of the X and X' halogen ions we have tried to prepare $A_2BX_{4-x}X'_x$ compounds (x = 1, 2) with the K_2NiF_4 structure for the combinations (F, Cl), (Cl, Br) and (Cl, I). The attempts for the case (F, Cl) were not very successful, but for the combination (Cl, Br) the expected behaviour is found indeed, as described in detail below.

That for the combination (F, Cl) the expectations are not fulfilled is not so surprising because the ratio between the radii of the Cl^- ion and the F^- ion ($r(Cl^-)/r(F^-)$) is much larger than $r(Br^-)/r(Cl^-)$. Using the Ahrens radii these ratio are 1.36 and 1.05 respectively (12, 13).

For some compounds with the combination (Cl, I) for which $r(I^-)/r(Cl^-)=1.21$, also indications for an ordering between Cl and I are found.

Most of the compounds described below were prepared by melting stoichiometric amounts of the commercial products ACl, ABr and AI (A=K, Tl, NH_4, Rb, Cs) and the compounds BCl_2 (B=Mg, Cr, Mn, Fe, Co, Ni, Cu) for 1 or 2 days at 600°C in an evacuated and sealed silica tube and annealing afterwards at temperatures 300-400°C for about 2 weeks. If for a particular compound another preparation method is used, this will be mentioned there.

II-2.3 The compounds $A_2MgCl_{4-x}Br_x$ (x=0, 1, 2)

The Mg compounds are of course not of interest for the magnetic part of our research program. But the phenomenon of the ordering between Cl and Br ions in those compounds with the K_2NiF_4 structure can be studied well.

From phase-diagram investigations of the systems ACl-$MgCl_2$ (A=K, Rb, Cs) the existence of the compounds A_2MgCl_4 (A=K, Rb, Cs) was already known (14, 15). However, the crystal structure had not yet been determined.

We have prepared these compounds as described above. $MgCl_2$ was prepared by heating Mg powder at 900°C for 4 hours in a stream of dry HCl gas.

Analysis of the X-ray diffraction patterns of the white polycrystalline samples of these compounds revealed that K_2MgCl_4 and Rb_2MgCl_4 have the K_2NiF_4 structure and that Cs_2MgCl_4 probably possesses the so-called β-K_2SO_4 structure. In this structure Mg is tetrahedrally surrounded by Cl ions, whereas the tetrahedra are isolated from each other.

Besides these compounds the white compound $(NH_4)_2MgCl_4$ was prepared by mixing in an agate mortar stoichiometric amounts of NH_4Cl and $MgCl_2$ and heating the mixture in a sealed gold tube for several days at about 350°C under a pressure of about 1 kbar. In the X-ray diffraction pattern a K_2NiF_4 phase was detected along with peaks that could not be indexed. It is possible that these peaks are due to an unknown impurity. Also for the other Mg compounds small or very small, unknown peaks were present in the diffraction patterns.

The compound Tl_2MgCl_4 could not be prepared and probably does not exist. The reaction product was always found to consist of TlCl and $TlMgCl_3$.

Other Mg compounds prepared are K_2MgCl_3Br, $K_2MgCl_2Br_2$, Rb_2MgCl_3Br and $Rb_2MgCl_2Br_2$ that all have the K_2NiF_4 structure. All compounds prepared are hygroscopic.

The unit cell parameters of all Mg compounds with the K_2NiF_4

structure are listed in Table II-3. The values of the a- and c-axes indicate well the expected occupation of sites 1 and 2 (fig. I-2) by the Br^- ions. The value of the c-axis increases strongly when the amount of Br in the compound increases, caused by the larger radius of the Br^- ion compared to the radius of the Cl^- ion (using the Ahrens radii: $r(Cl^-)=1.81$ Å, $r(Br^-)=1.96$ Å (12, 13)). The differences in the values of the a-axes are much smaller.

Table II-3 Cell dimension of compounds with K_2NiF_4 structure

Compound	a-axis (Å)	c-axis (Å)
K_2MgCl_4	4.939(2)	15.581(6)
K_2MgCl_3Br	4.944(2)	16.081(5)
$K_2MgCl_2Br_2$	4.918(3)	16.639(7)
Rb_2MgCl_4	4.987(1)	16.174(4)
Rb_2MgCl_3Br	5.004(5)	16.61 (1)
$Rb_2MgCl_2Br_2$	5.028(4)	16.97 (1)
$(NH_4)_2MgCl_4$	4.984(3)	16.152(8)
$K_2CrCl_2Br_2$	5.091(5)	16.02 (1)
Rb_2CrCl_4	5.131(4)	15.74 (1)
$Rb_2CrCl_2Br_2$	5.158(4)	16.41 (1)
$Rb_2CrCl_2I_2$	5.225(7)	17.40 (1)
Cs_2CrCl_4	5.208(7)	16.42 (2)
Rb_2MnCl_4	5.049(2)	16.172(4)
Rb_2MnCl_3Br	5.060(3)	16.588(8)
$Rb_2MnCl_2Br_2$	5.073(2)	16.924(3)
$Rb_2MnCl_2I_2$	5.162(3)	17.84 (1)
Cs_2MnCl_4	5.135(3)	16.88 (1)
Cs_2MnCl_3Br	5.169(3)	17.25 (1)
$(NH_4)_2MnCl_4$	5.049(2)	16.148(7)
$(NH_4)_2MnCl_2Br_2$	5.055(5)	16.83 (1)
$(NH_4)_2MnCl_2I_2$	5.102(4)	17.71 (1)

II-2.4 Structural information from ESR powder spectra of Mn^{2+}-doped Rb_2MgCl_4, Rb_2MgCl_3Br and $Rb_2MgCl_2Br_2$

To obtain evidence for the idea concerning the occupation of sites 1 and 2 in the K_2NiF_4 structure (fig. I-2) by the Br ions ESR powder spectra of the compounds Rb_2MgCl_4, Rb_2MgCl_3Br and $Rb_2MgCl_2Br_2$ doped with Mn^{2+} were obtained, since it is known that this method is very useful in elucidating the symmetry and geometry of coordi-

nation polyhedra around Mn^{2+} (16, 17).

For the synthesis of the Mn^{2+}-doped compounds about 0.5% of $MnCl_2$ was added to the reagents necessary for the preparation of the pure Mg compounds. $MnCl_2$ was obtained by dehydrating commercial $MnCl_2.4H_2O$ at 350°C for 4 hours in a stream of dry HCl gas.

The ESR powder spectra were run at room temperature as the first derivative of the absorption line on Varian instruments operating at X- and Q-band frequency and described in detail elsewhere (4). The spectral calculations were carried out using a Fortran IV program written by R.D. Dowsing (16) and modified by J. Reedijk of the Department of Coordination Chemistry of the Gorlaeus Laboratories.

In Table II-4 the ESR spectral data of the Mn^{2+}-doped compounds are listed, together with assignments and calculated bands. An illustrative Q-band spectrum is drawn in Fig. II-1.

The spectra of the compounds were analyzed according to the spin Hamiltonian:

$$H = g\beta\vec{H}.\vec{S} + D\,[S_z^2 - S(S+1)/3] + E(S_x^2 + S_y^2) + \vec{S}.\vec{A}.\vec{I}.$$

Higher-order zero-field terms, that are usually very small (4, 16, 17), are neglected in the Hamiltonian.

As the influence of the term $\vec{S}.\vec{A}.\vec{I}.$ is small and only results into a splitting of the absorption lines into six hyperfine components, the centre of these six lines was taken as the maximum of the resonance lines. According to theory (16, 17), powder lines are found for transitions, where the magnetic field points along the principal axes of the zero-field tensor. Extra powder lines occur for some transitions, where the field lies in one of the principal planes and not along the axes (4, 17).

For a first analysis of the spectra, the diagrams of Dowsing and Gibson (16) were used, after which the parameters were slightly varied to seek a best fit with the observed resonance lines.

The spectra of $Rb_2MgCl_2Br_2$ doped with Mn could be interpreted with $D=0.350(3)cm^{-1}$ and $E=0.00(3)cm^{-1}$, indicating a strictly axial Mn species. Since it seems reasonable to assume that Mn takes the positions of Mg in the lattice, these zero-field parameters can be ascribed to a species $[MnCl_4Br_2]$ having the Br^- ions trans to each other, i.e. with Br^- at sites 1 and 2 (see fig. I-2).

Both at X- and Q-band frequency the spectrum of the Mn-doped Rb_2MgCl_4 compound consists of a single line split into six hyperfine components; the parameters are g=2.00 and D=0.00, i.e. there is no detectable axial splitting. These parameters can be explained

Table II-4 Calculated and observed ESR bands (Gauss) for Mn^{2+} in $Rb_2MgCl_{4-x}Br_x$ (x=0, 1, 2)

Compounds and parameters[a]	X-band Observed	Calcd.	ν=9.521 GHz Int.[b]	Dir.[c]	Q-band Observed	Calcd.	ν=35.550 GHz Int.	Dir.
Rb_2MgCl_4								
g = 2.00(1)	3400	3401			12700	12690		
A = 88(1) G								
$Rb_2MgCl_2Br_2$	1175 vs[d]	1190	2.06	x, y	1970 m	1985	0.31	xz, yz
					2075 m	2117	0.38	x, y
g = 2.00 (1)	1640 vw				2300 m	2309	1.92	z
						3617	0.95	x, y
D = 0.350(3) cm^{-1}	3375 w[e]				4400 s	4600	1.10	xz, yz
					4700 m			
E = 0.000(3) cm^{-1}	4130 m	4150	1.88	x, y		5186	3.08	z
					6970 s	7024	2.13	x, y
A = 87(1) G	5600 m	5665	1.70	xz, yz	8250 m	8225	0.95	xz, yz
					8685 s	8712	2.98	x, y
	9300 m	9350	1.22	xz, yz	11250 vs	11256	3.07	x, y
	10950 m	11050	2.75	x, y	12700 vs[e]	12685	3.46	z
					13875 m	13893	2.75	x, y
					15900 s	15950	2.60	xz, yz
					16000 s	15975	2.70	xz, yz

[a] Uncertainties in the least significant digit are between parantheses

[b] Calculated intensity according to ref. 16

[c] Orientation of axes and planes

[d] s = strong, m = medium, w = weak, v = very

[e] Observed without hyperfine splitting

by assuming a regular octahedral species $[MnCl_6]$, just as expected for Mn ions substituting at Mg positions. The value for the hyperfine coupling constant, $A(^{55}Mn)$, is - within experimental error - equal to that found in K_4CdCl_6 doped with Mn^{2+} (18).

The spectra of Mn doped Rb_2MgCl_3Br appeared to be a complete summation of the spectra of Rb_2MgCl_4 and $Rb_2MgCl_2Br_2$, indicating the presence of both $[MnCl_6]$ and $[MnCl_4Br_2]$. No other species, such as $[MnCl_5Br]$, could be detected.

Finally a few remarks concerning the observed spectra should be made. In the first place it is seen from Table II-4 that the calculated band at 5186 Gauss (Q-band) does not completely agree with the observed spectrum; it appeared,however, that the position of this band is strongly dependent upon very small cubic splittings (of the order of 10^{-4} cm^{-1}). Secondly, the lines at g=2.00 for the bromide compounds appeared to have no hyperfine splitting. We do not have a clear explanation for this phenomenon, but one could think of exchange coupling between Mn ions, or the presence of an impurity.

Conclusions

The results discussed above, allow the following conclusions:

1. In Rb_2MgCl_4 the Mn^{2+} dope has octahedral symmetry, as reflected by the regular $[MnCl_6]$ species found from the ESR spectra.
2. In $Rb_2MgCl_2Br_2$ the coordination of the Mn^{2+} dope has D_{4h} symmetry, in agreement with a tetragonal species $[MnCl_4Br_2]$. This can be explained by assuming an ordering of the Br^- ions at sites 1 and 2 (Fig. I-2).
3. ESR powder spectra of Mn^{2+}-doped Rb_2MgCl_3Br show the presence of both $[MnCl_6]$ and $[MnCl_4Br_2]$ species. The presence of other species, like $[MnCl_5Br]$ could not be detected. Although nothing can be said about a possible ordering of the two species, it is clear that only these two occur (in a 1 : 1 ratio).

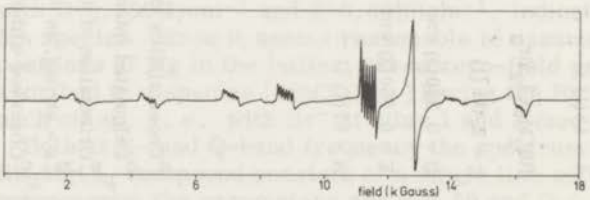

Fig. II-1 Experimental first derivative Q-band spectrum of Mn^{2+}-doped $Rb_2MgCl_2Br_2$

II-2.5 The compounds $A_2CuCl_{4-x}Br_x$ (x=0, 1, 2)

As we are interested in compounds $A_2CuCl_{4-x}Br_x$ with the K_2NiF_4 structure, we scanned various possiblities for the A ions. Cs_2CuCl_4 has been reported to have the β-K_2SO_4 structure (19, 20), which structure is not interesting for our investigations. K_2CuCl_4 has also been reported to have the β-K_2SO_4 structure (21, 22). However, we believe that the compound does not exist as we were not able to prepare it by melting and annealing of stoichiometric amounts of KCl and $CuCl_2$; the reaction product resulted in a mixture of KCl and $KCuCl_3$. Moreover, we could index the reported X-ray powder diffraction diagram (22) of a sample that was prepared by dehydration of $K_2CuCl_4.2H_2O$, as a mixture of KCl and $KCuCl_3$.

For A=Tl no compound of the composition A_2CuCl_4 could be prepared. The reaction product was found to exist of $TlCuCl_3$ and probably Tl_3CuCl_5.

As has been remarked in Chapter I (Section I-4) the compound $(NH_4)_2CuCl_4$ has a deformed K_2NiF_4 structure (23). As shown in fig. II-2, the long axis of a distorted octahedron in the Cu-layers (bc-plane; according to convention the a-axes of the K_2NiF_4 structure are now replaced by the b- and c-axis) is always perpendicular to the long axis of the neighbouring octahedra in this plane. Due to this distortion the structure is no longer tetragonal, but orthorhombic (space-group Cmca), as the four-fold axis is lost. The b- and c-axes, however, are equal within the experimental uncertainty.

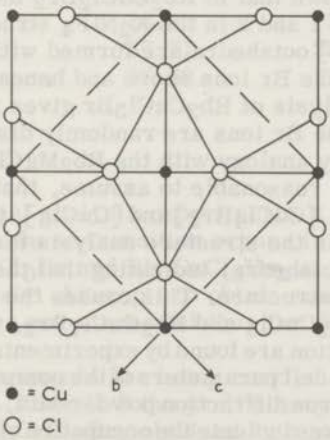

Fig. II-2 bc-plane of the $(NH_4)_2CuCl_4$ structure, in which indicated the deformed $[CuCl_6]$ octahedra. The crystallographic unit cell is shown by the dashed line

As an extension of the knowledge of these Cu compounds we have prepared the compounds Rb_2CuCl_4, Rb_2CuCl_3Br, and $Rb_2CuCl_2Br_2$ by the method described above. $CuCl_2$ was prepared by dehydrating the commercial product $CuCl_2.2H_2O$ at 200°C for 5 hours in a stream of dry HCl gas.

It was also possible to obtain the compounds by slow evaporation of solutions of RbCl and/or RbBr and $CuCl_2$ in absolute methyl alcohol at a temperature of about 75°C.

Rb_2CuCl_4 could also be prepared by dehydration of $Rb_2CuCl_4.2H_2O$ at 250-300°C for 5 hours in a stream of dry HCl gas. $Rb_2CuCl_4.2H_2O$ was obtained by evaporating an aqueous solution of $CuCl_2.2H_2O$ and RbCl. The compounds are hygroscopic. They tend to be less hygroscopic with growing Br content.

The X-ray powder patterns of the compounds could be indexed, assuming the $(NH_4)_2CuCl_4$ structure. However, these diffraction data could not be used for a detailed calculation of the structure parameters because the intensity of many reflections was influenced by preferential orientation of the polycrystalline samples in the sample holder. Attempts to remove this preferential orientation were not successful. Therefore, neutron diffraction measurements were carried out at room temperature because preferential orientation can be largely avoided in this way.

A detailed structure analysis by means of the neutron diffraction data will be published elsewhere (24). Here only those results, relevant to this thesis, are given.

In ref. 24 it is shown that in $Rb_2CuCl_2Br_2$ the Br ions, as expected, occupy the sites 1 and 2 in the K_2NiF_4 structure (fig. I-2) and that only $[CuCl_4Br_2]$ octahedra are formed with the Cu and Cl ions in the bc-plane and the Br ions above and beneath it.

The structure analysis of Rb_2CuCl_3Br gives reasonable results if it is assumed that the Br ions are randomly distributed over the positions 1 and 2. By analogy with the Rb_2MgCl_3Br compound (Section II-2.4) it is reasonable to assume, that only two kinds of octahedra, occur viz. $[CuCl_4Br_2]$ and $[CuCl_6]$, in the ratio 1 : 1. No evidence was found in the structure analysis for an ordering between these two kinds of octahedra, indicating that they are distributed at random through the structure. This causes the compound to be less well defined than Rb_2CuCl_4 and $Rb_2CuCl_2Br_2$. Other indications for the random distribution are found by experiments described in Chapter VI. The values of the unit cell parameters of the compounds described, calculated from the neutron diffraction powder data, are given in Table II-5. The values of these axes indicate the occupation of sites 1 and 2 by Br ions.

In Table II-6 the results of the chemical analysis of the samples used for the magnetic measurements, are listed.

Table II-5 Cell dimensions of compounds $A_2CuCl_{4-x}Br_x$ (x=0, 1, 2) with A=NH_4, Rb

Compound	a-axis (Å)	b-axis (Å)	c-axis (Å)
Rb_2CuCl_4 [a]	15.540(4)	7.198(2)	7.190(4)
Rb_2CuCl_3Br [a]	15.937(7)	7.217(3)	7.222(7)
$Rb_2CuCl_2Br_2$ [a]	16.256(7)	7.254(3)	7.261(7)
$(NH_4)_2CuCl_4$ [b]	15.46 (2)	7.20 (1)	7.20
$(NH_4)_2CuCl_2Br_2$ [c]	16.15 (1)	7.244(5)	7.244(5)

a) Cell dimensions obtained from neutron powder diffraction experiments
b) Cell dimensions obtained from ref. 23
c) Cell dimensions obtained from X-ray powder diffraction patterns

Table II-6 Chemical analysis of the $Rb_2CuCl_{4-x}Br_x$ compounds (x=0, 1, 2)

Element (%)	Rb_2CuCl_4	Rb_2CuCl_3Br	$Rb_2CuCl_2Br_2$
Cu (exp)	16.73	14.96	13.56
Cu (cal)	16.89	15.10	13.66
Cl (exp)	37.71	25.35	15.17
Cl (cal)	37.69	25.28	15.24
Br (exp)	-	19.05	34.20
Br (cal)	-	18.99	34.35

By means of thermal analysis experiments it is detected that probably a crystallographic phase transition occurs in the compounds Rb_2CuCl_4, Rb_2CuCl_3Br and $Rb_2CuCl_2Br_2$ at 222±3°C, 220±3°C and 215±3°C respectively. Attempts to obtain more information about this transition were not successful thus far (24).

For A=NH_4 experiments are being carried out for the compounds $A_2CuCl_{4-x}Br_x$. In Table II-5 the preliminary results for the cell constants of $(NH_4)_2CuCl_2Br_2$ obtained by means of X-ray powder diffraction patterns, are listed. For comparison the known axes of $(NH_4)_2CuCl_4$ are given too in this table (23).

II-2.6 The compounds $A_2CrCl_{4-x}Br_x$ (x=0, 1, 2)

It is known that the compounds A_2CrCl_4 with A=NH_4, Rb, Cs have the K_2NiF_4 structure (25-28), whereas indications are found that this is also the case for K_2CrCl_4 (26).

We have tried to prepare the unknown compound Tl_2CrCl_4, but we did not succeed. Probably this compound does not exist, just as is found for the other Tl compounds: Tl_2MgCl_4 and Tl_2CuCl_4 (see Section II-2.3 and II-2.5).

Of compounds $A_2CrCl_{4-x}Br_x$ (x=1, 2) with the K_2NiF_4 structure it is expected again that an ordering exists between the Cl and Br ions. To investigate this ordering we have tried to prepare these compounds with A=K, NH_4, Rb, Cs. Also for the combination (Cl, I) several attempts were made. But due to the difficulties that arised with the preparation of pure $CrCl_2$, which compound is very hygroscopic and sensitive to oxygen, no pure samples of the compounds could be obtained.

In several X-ray powder diffraction patterns of the reaction products a K_2NiF_4 phase was detected, but often the reflections due to other phases, were too strong to obtain reliable results for the cell constants of these K_2NiF_4 phases. Up to now only for some compounds reasonable data are obtained (Table II-3). For the Rb compounds it is noticed that the c-axis is increasing much faster than the a-axis when Cl is replaced partly by Br or I, indicating that the Br and I ions prefer to occupy sites 1 and 2 in the K_2NiF_4 structure indeed. For Rb_2CrCl_4 and Cs_2CrCl_4 the values of the axes are in good agreement with the values published by Seifert et al.(26).

In spite of the problems that are met in the preparation of the Cr compounds the results mentioned above are encouraging enough to continue the investigations of this part of our research program.

II-2.7 The compounds $A_2MnCl_{4-x}Br_x$ (x=0, 1, 2)

It is known that the compound Rb_2MnCl_4 crystallizes in the K_2NiF_4 structure (29). This is also the case for Cs_2MnCl_4, but this compound shows a high-temperature phase (β-K_2SO_4 structure) above 310°C (27, 30).

Phase diagram experiments on the system KCl-$MnCl_2$ did not indicate the existence of K_2MnCl_4 (29). This is in accordance with our experience that K_2MnCl_4 cannot be prepared. The same result is found for Tl_2MnCl_4. The reaction product from the melt of stoichiometric amounts of TlCl and $MnCl_2$ was always composed of TlCl and $TlMnCl_3$.

For the magnetic part of our investigations Rb_2MnCl_4 and

Cs_2MnCl_4 were prepared by the melting method (described above). Due to the incongruent melting point of Rb_2MnCl_4 (at 460°C) the reaction product contained small amounts of $Rb_3Mn_2Cl_7$ and RbCl. Therefore, the reaction product was powdered again and annealed for a few weeks at about 350°C. After this treatment no impurities could be detected in the sample by means of X-ray diffraction.

However, susceptibility measurements of several samples of Rb_2MnCl_4 and Cs_2MnCl_4 revealed that still paramagnetic impurities were present, probably due to impurities in the starting compound $MnCl_2$. Especially in the low-temperature region (4-100 K) the susceptibility curve was influenced too much by these impurities.

Therefore, it was tried to obtain purer samples by means of another preparation method, using the hydrated compounds.

A precipitate of $Rb_2MnCl_4.2H_2O$ was obtained by dissolving $MnCO_3$ and RbCl in the ratio 1:2 in an HCl solution. $Cs_2MnCl_4.2H_2O$ could be prepared best by slow evaporation of an aqueous solution of $MnCl_2.4H_2O$ and CsCl in the ratio 3:1.

With differential thermal analysis of these compounds it was determined, that dehydration started at about 80°C. By heating the hydrated compounds for several days at about 150°C in an Ar atmosphere samples of Rb_2MnCl_4 and Cs_2MnCl_4 were obtained that were purer from a magnetic point of view than the samples prepared from the melt.

We tried to prepare the compound $(NH_4)_2MnCl_4$ in two ways. Firstly stoichiometric amounts of $MnCl_2$ and NH_4Cl were mixed and heated in a sealed gold tube for several days in the temperature region 300-400°C under a pressure of about 1 kbar. The X-ray diffraction patterns revealed the presence of a K_2NiF_4 phase in combination with relatively large amounts of other phases of the system NH_4Cl-$MnCl_2$.

Therefore $(NH_4)_2MnCl_4.2H_2O$ was prepared in the same way as described above for $Rb_2MnCl_4.2H_2O$. Thermal analysis showed that the dehydration process in $(NH_4)_2MnCl_4.2H_2O$ starts at about 115°C and that at about 160°C the compound starts to decompose due to the sublimation of NH_4Cl.

The X-ray diffraction patterns of samples obtained by heating $(NH_4)_2MnCl_4.2H_2O$ for several days at 120°C in an Ar atmosphere revealed a pure K_2NiF_4 phase for the compound $(NH_4)_2MnCl_4$. But susceptibility measurements in the low-temperature region indicated again the presence of impurities, probably due to the sublimation of a small amount of NH_4Cl, already at the preparation temperature. Several attempts to improve the purity by varying time, temperature and Ar pressure were not successful.

Besides the A_2BX_4 compounds mentioned above, several compounds

of the type $A_2MnCl_{4-x}Br_x$ (x=1, 2) with the K_2NiF_4 structure were prepared by means of the melting method for A=Rb, Cs and by means of the method described above, in which gold tubes are used, for $A=NH_4$. Also some compounds with the combination (Cl, I) could be obtained. In several of the samples prepared, small amounts of AX, other phases of the diagram AX-$MnCl_2$ (X=Cl, Br, I) and unknown impurities were present.

The unit cell parameters of the compounds are listed in Table II-3. It is noticed again from the values of these parameters that the Br or I ions preferably occur at the positions 1 and 2 in the K_2NiF_4 structure (fig. I-2). The cell parameters of Rb_2MnCl_4 and Cs_2MnCl_4 agree with those reported in literature (29, 30).

The compound $Cs_2MnCl_2Br_2$ could not be prepared. For most samples of the compounds Cs_2MnCl_3Br the X-ray reflections were rather broad, indicating that these samples were not well crystallized. Probably $Cs_2MnCl_2Br_2$ is not stable enough, whereas Cs_2MnCl_3Br is a borderline case. Thermal analysis of Cs_2MnCl_3Br revealed a phase transition (possibly to the β-K_2SO_4 structure) at 295°C, just as is the case for Cs_2MnCl_4 (see above).

For the case x=1 and $A=NH_4$ ($(NH_4)_2MnCl_3Br$) more phases were detected in the reaction product.

As a last remark about the chemical properties of the compounds described, it is mentioned that they are all hygroscopic.

The results of the susceptibility measurements of the Mn compounds are not reported in this thesis but will be published elsewhere (31).

II-2.8 The compounds A_2BCl_4 with B=Fe, Co, Ni

Of the compounds A_2BCl_4 (B=Fe, Co, Ni) no K_2NiF_4 phases are known in literature (27). Our investigations did not reveal any new compounds having this structure. Therefore, these compounds are not treated here.

II-2.9 The compounds $M^{2+}(N_2H_5)_2(SO_4)_2$ with M=Mn, Fe, Co, Ni, Cu

The compounds $M^{2+}(N_2H_5)_2(SO_4)_2$ (M=Mn, Fe, Co, Ni, Cu) are prepared by adding a solution of the metal sulfates MSO_4 in hot water to a hot solution of $N_2H_6SO_4$ in water (in the ratio MSO_4:$N_2H_6SO_4$ = 1:2) (32-34). In most cases the compounds $M(N_2H_5)_2(SO_4)_2$ immediately separate as powders, except for M=Mn, where cooling down to about 10°C is necessary to obtain the solid compound. The powders were collected on a glass filter, washed with water, ethanol and diethyl-ether, and finally dried in vacuo at 40-50°C.

The compounds were checked for purity by metal analysis, of which

the results are listed in Table II-7. The structural and magnetic properties of the compounds are discussed in Chapter IV.

Table II-7 Metal analysis of the compounds $M^{2+}(N_2H_5)_2\ (SO_4)_2$

Compound	metal (cal)%	metal (exp)%
$Mn(N_2H_5)_2\ (SO_4)_2$	17.54	17.94
$Fe(N_2H_5)_2\ (SO_4)_2$	17.78	18.21
$Co(N_2H_5)_2\ (SO_4)_2$	16.58	17.90
$Ni(N_2H_5)_2\ (SO_4)_2$	18.52	19.05
$Cu(N_2H_5)_2\ (SO_4)_2$	19.75	19.68

II-2.10 The compounds MnX_2L_2 with X=Cl, Br and L=pyrazole, pyridine

The slightly pink coloured compounds MnX_2L_2 (X=Cl, Br; L=pyrazole, pyridine) were prepared by blending alcoholic solutions of $MnCl_2 4H_2O$ and pyrazole ($N_2C_3H_5$) or pyridine (NC_5H_5) in a ratio 1:2. The precipitates are filtered off, washed with alcohol and diethylether and finally dried in vacuo at room temperature.

The results of the chemical analysis of the samples are given in Table II-8.

Table II-8 Chemical analysis of the compounds MnX_2L_2 with X=Cl, Br and L=pyrazole, pyridine

Compound	X (exp)%	X (cal)%	Mn (exp)%	Mn (cal)%
$MnCl_2$ (pyrazole)$_2$	26.8	26.8	20.97	20.98
$MnBr_2$ (pyrazole)$_2$	45.0	45.6	15.58	15.66
$MnCl_2$ (pyridine)$_2$	24.9	25.0	19.30	19.34
$MnBr_2$ (pyridine)$_2$	42.9	42.9	14.68	14.73

In Chapter V some preliminary results of single crystal structure investigations on $MnCl_2$(pyrazole)$_2$, carried out by Gorter et al.(35), are reported in combination with the results of susceptibility measurements.

References

1. S. Foner, Rev. Sci. Instrum. 30, 548 (1959)
2. S. Hillaert, to be published
3. F.W. Klaaijsen, to be published
4. R.D. Dowsing, B. Nieuwenhuyse and J. Reedijk, Inorg. Chim. Acta 5, 301 (1971)
5. R.W. Asmussen and H. Soling, Z. anorg. allgem. Chem. 283, 3 (1956)
6. A. Zodkevitz, J. Makovsky and Z.H. Kalman, Isr. J. Chem. 8, 755 (1970)
7. H.F. McMurdie, J. de Groot, M. Morris and H.E. Swanson, J. Research of NBS 73a, 621 (1969)
8. N. Achiwa, J. Phys. Soc. Jap. 27, 561 (1969)
9. R.W. Asmussen, T. Kindt-Larsen and H. Soling, Acta Chem. Scand. 23, 2055 (1969)
10. G.N. Tischenko, Tr. Kristallogr. Akad. Nauk. SSSR 11, 93 (1955); Chem. Abstr. 55, 16251g (1956)
11. G. Stucky, S. d'Agostinho and G. McPherson, J. Am. Chem.Soc. 88, 4828 (1966)
12. R.D. Shannon and C.T. Prewitt, Acta Cryst. B25, 925 (1969)
13. R.D. Shannon and C.T. Prewitt, Acta Cryst. B26, 1046 (1970)
14. W. Klemm, K. Beyersdorfer and J. Oryschkewitz, Z. anorg. allgem. Chem. 256, 25 (1948)
15. B.F. Markov and I.D. Panchenko, Ukrain. Khim. Zhur. 20, 620 (1954)
16. R.D. Dowsing and J.F. Gibson, J. Chem. Phys. 50, 294 (1969)
17. R. Aasa, J. Chem. Phys. 52, 3919 (1970)
18. F.D. Tsay and L. Helmholz, J. Chem. Phys. 50, 2642 (1969)
19. L. Helmholz and R.F. Kruk, J. Am. Chem. Soc. 74, 1176 (1952)
20. B. Morosin and E.C. Lingafelter, J. Phys. Chem. 65, 50 (1961)
21. V. Vasil'kova and G.M. Barnivah, Issled. v. Obl. Khim. i Tekhnel. Mineral'n. Solei i Okislov, Akad. Nauk. SSSR Sb. Statei 1965, 208 (1965); Chem. Abstr. 65, 9831e (1966)
22. E. Joly, C.R. Acad. Sc. Paris, t 272, Serie C, 1302 (1971)
23. R.D. Willett, J. Chem. Phys. 41, 2243 (1964)
24. V. Brandwijk, H.T. Witteveen and D. Jongejan, to be published
25. H.J. Seifert and K. Klatyk, Naturw. 49, 539 (1962)
26. H.J. Seifert and K. Klatyk, Z. anorg. allgem. Chem. 334, 113 (1964)
27. D.J.W. Ydo, thesis, University of Leiden (1960)
28. H.D. Hardt and G. Streit, Z. anorg. allgem. Chem. 373, 97 (1970)
29. H.J. Seifert and F.W. Koknat, Z. anorg. allgem. Chem. 341, 269 (1965)

30. J.J. Foster and N.S. Gill, J. Chem. Soc. 1968, A2625 (1968)
31. H. T. Witteveen, to be published
32. C.K. Prout and H.M. Powell, J. Chem. Soc. 1961, 4177 (1961)
33. D.W. Hand and C.K. Prout, J. Chem. Soc. A 1966, 168 (1966)
34. A. Nieuwpoort and J. Reedijk, J. Inorg. Chim. Acta (in press)
35. S. Gorter and G. Verschoor, to be published

CHAPTER III - MAGNETIC SUSCEPTIBILITIES OF POLYCRYSTALLINE SAMPLES OF THE COMPOUNDS $ANiCl_3$ (A=Tl, NH_4, Rb, Cs) AND $ANiBr_3$ (A=Rb, Cs)

III-1 Introduction

As discussed in Chapter I-4 many of the ABX_3 compounds (A = monovalent ion, e.g. K, Tl, NH_4, Rb, Cs; B = divalent metal ion of the first transition series, e.g. Cr, Mn, Fe, Co, Ni, Cu; X = halogen ion e.g. F, Cl, Br) have the $BaNiO_3$ (h) structure (fig. I-1). On the basis of this structure these compounds are expected to show magnetic properties of a linear-chain system.

In this chapter, the results of magnetic susceptibility measurements in the temperature region 2-200 K for polycrystalline samples of $ANiCl_3$ (A=Tl, NH_4, Rb, Cs) and $ANiBr_3$ (A=Rb, Cs) are given.

For two of these compounds, $RbNiCl_3$ and $CsNiCl_3$, the susceptibility has already been investigated by Achiwa (1) and Smith et al. (2). Asmussen and Soling (3) have measured the susceptibility of $RbNiX_3$ and $CsNiX_3$ (X=Cl, Br), but only down to 85 K.

Achiwa interpreted his experimental results in terms of the antiferromagnetic Heisenberg linear-chain system with spin S=1 by assuming that

$$\chi(\text{Heisenberg, } S=1) = \chi(\text{Heisenberg, } S=\tfrac{1}{2}) \times \frac{\chi(\text{Ising, } S=1)}{\chi(\text{Ising, } S=\tfrac{1}{2})} ,$$

where theoretical results were already known for linear-chain systems in the right-hand side of the equation (2, 4, 5). Smith et al.(2), however, used the model for antiferromagnetic Heisenberg linear chains with $S=\infty$ (scaled to finite S) (6), after having found out that their results could not be described by the Ising antiferromagnetic linear-chain system with S=1.

In the meantime numerical results for antiferromagnetic Heisenberg linear chains with 3 to 7 spins S=1 were reported by Weng in his thesis (7). By extrapolation from these results he obtained the susceptibility as a function of temperature for infinite, antiferromagnetic Heisenberg chains with S=1. It is to be expected that this method gives better results than the previous ones. Smith and

Friedberg (8) have used these calculations in combination with an interpolation scheme - also developed by Weng, for the calculation of the susceptibility curve of antiferromagnetic Heisenberg linear-chain systems with spin $S > 1$ - for the description of the linear-chain antiferromagnetism in $CsMnCl_3.2H_2O$, where $S=5/2$.

We have remeasured the susceptibility of $RbNiCl_3$ and $CsNiCl_3$ to interpret the results in terms of the theory of Weng (section III-2). We have also measured the susceptibility of the compounds $TlNiCl_3$, NH_4NiCl_3, $RbNiBr_3$, and $CsNiBr_3$, of which it is known that they have the $BaNiO_3$ (h) structure.

In section III-3 it is tried to estimate the order of magnitude of the inter-chain interaction by comparing the experimentally determined values of the 3D ordering temperature to the theoretical transition temperature, calculated by means of Green function techniques.

III-2 Results and discussion

III-2.1 ESR Spectra

Of all Ni compounds described in this paper ESR spectra were obtained at X-band frequency (~9.2 GHz), both at room temperature and liquid nitrogen temperature (77 K). In fig. III-1 the ESR spectrum of $CsNiCl_3$, run as the first derivative of the absorption line, at liquid nitrogen temperature is shown. The shape of the spectra of the other compounds is identical.

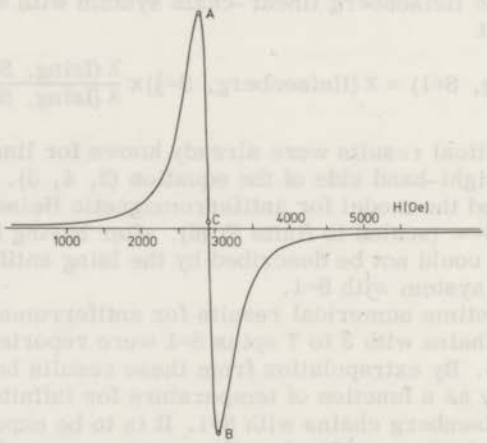

Fig. III-1 ESR spectrum of $CsNiCl_3$ at 9.2 GHz and 77 K

At room temperature the peak to peak distance in the spectra (point A and B in fig. III-1) is about 1300-1700 Oe for the $ANiCl_3$ compounds and about 2300-2500 Oe for the $ANiBr_3$ compounds. At 77 K the peak to peak distances are reduced to about 300-650 Oe and about 1200 Oe for the $ANiCl_3$ and $ANiBr_3$ compounds respectively.

From the point with minimum slope in the absorption line (C in fig. III-1 halfway between A and B) the g-values, listed in Table III-1, are calculated.

III-2.2 Susceptibility

In fig. III-2, 3, 4 the results of the susceptibility measurements, corrected for diamagnetism according to the tables of Selwood (9), are shown. At 2.0 K the magnetization of all compounds was nearly

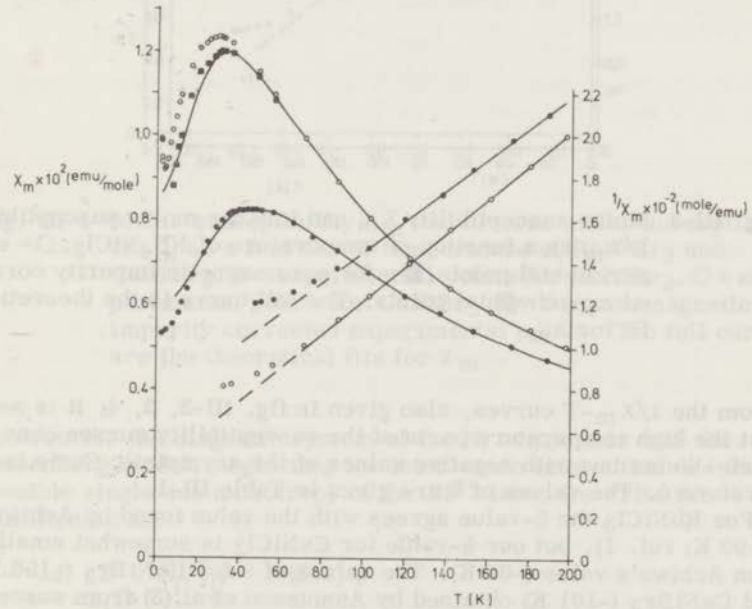

Fig. III-2 Molar susceptibility χ_m and inverse molar susceptibility $1/\chi_m$ as a function of temperature of $RbNiCl_3$ and $CsNiCl_3$. ● = experimental points for $RbNiCl_3$. ○ = experimental points for $CsNiCl_3$. ■ = for paramagnetic impurity corrected experimental points. The full curves are the theoretical fits for χ_m

linearly dependent upon the magnetic field up to about 15 kOe. The susceptibility measurements were carried out at about 10 kOe.

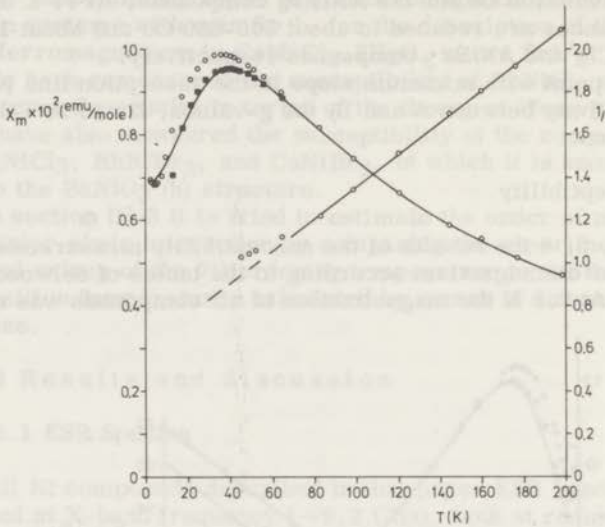

Fig. III-3 Molar susceptibility χ_m and inverse molar susceptibility $1/\chi_m$ as a function of temperature of NH_4NiCl_3. ○ = experimental points. ■ = for paramagnetic impurity corrected experimental points. The full curve is the theoretical fit for χ_m

From the $1/\chi_m$-T curves, also given in fig. III-2, 3, 4, it is seen that the high temperature parts of the susceptibility curves obey the Curie-Weiss law with negative values of the asymptotic Curie temperature θ. The values of θ are given in Table III-1.

For $RbNiCl_3$ the θ-value agrees with the value found by Achiwa (-100 K; ref. 1), but our θ-value for $CsNiCl_3$ is somewhat smaller than Achiwa's value (-69 K). The values of θ for $RbNiBr_3$ (-156 K) and $CsNiBr_3$ (-101 K) obtained by Asmussen et al. (3) from susceptibility measurements down to 85 K, agree well with our values.

All susceptibility curves show the broad maximum, expected for antiferromagnetic linear-chain systems.

It is known that usually the magnetic systems with hexacoordinated Ni^{2+} ions can be described by the Heisenberg model. Achiwa's single crystal measurements on $RbNiCl_3$ and $CsNiCl_3$ have already shown that anisotropy in these compounds above the transition point of 3D

magnetic ordering is hardly detectable. Therefore it seems reasonable to assume that also the compounds $TlNiCl_3$, NH_4NiCl_3, $RbNiBr_3$, and $CsNiBr_3$ can be described with the Heisenberg model.

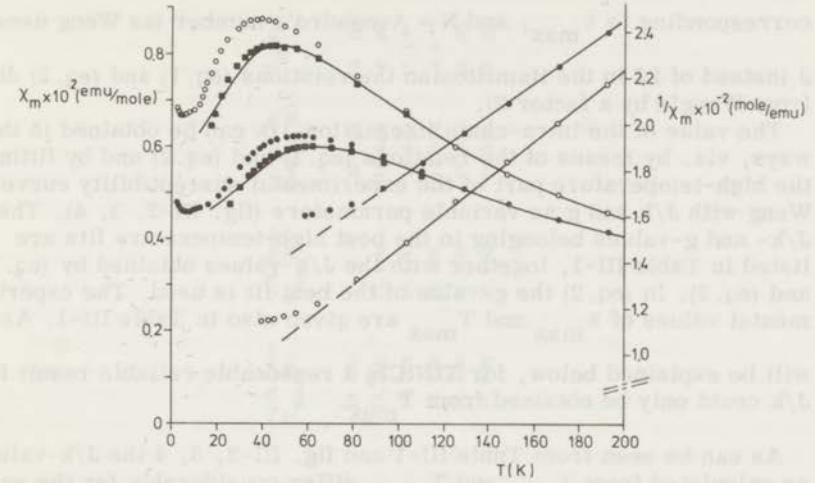

Fig. III-4 Molar susceptibility χ_m and inverse molar susceptibility $1/\chi_m$ as a function of temperature of $RbNiBr_3$ and $CsNiBr_3$. ● = experimental points for $RbNiBr_3$. ○ = experimental points for $CsNiBr_3$. ■ = for paramagnetic impurity corrected experimental points. The full curves are the theoretical fits for χ_m

To describe the magnetic system of the Ni compounds with the Heisenberg model, neglecting the inter-chain interaction and the possible single-ion anisotropy of the Ni^{2+} ions, we write the Hamiltonian as:

$$H = -2J \sum_{<i,j>} \vec{S}_i . \vec{S}_j, \qquad (S=1) ,$$

where the parameter J for magnetic interaction between nearest neighbours in the chains has negative sign for antiferromagnetic coupling. The summation is over all pairs of ions in the chains.

On the basis of this Hamiltonian Weng obtained the theoretical susceptibility as a function of temperature for antiferromagnetic Heisenberg chains. For this susceptibility curve the following rela-

tions hold: $kT_{max}/|J| = 2.7$ (eq. 1) and $|J|\chi_{max}/Ng^2\beta^2 = 0.0872$ (eq. 2), where χ_{max} = maximum of the susceptibility, T_{max} = temperature corresponding to χ_{max}, and N = Avogadro's number (as Weng uses J instead of 2J in the Hamiltonian the relations (eq. 1) and (eq. 2) differ from Weng's by a factor 2).

The value of the intra-chain interaction J/k can be obtained in three ways, viz. by means of the relations (eq. 1) and (eq. 2) and by fitting the high-temperature part of the experimental susceptibility curve of Weng with J/k and g as variable parameters (fig. III-2, 3, 4). The J/k- and g-values belonging to the best high-temperature fits are listed in Table III-1, together with the J/k-values obtained by (eq. 1) and (eq. 2). In (eq. 2) the g-value of the best fit is used. The experimental values of χ_{max} and T_{max} are given also in Table III-1. As will be explained below, for $TlNiCl_3$ a reasonable reliable result for J/k could only be obtained from T_{max}.

As can be seen from Table III-1 and fig. III-2, 3, 4 the J/k-values, as calculated from χ_{max} and T_{max}, differ considerably for the same compound. If the theoretical high-temperature fit is extended to lower temperatures, it is noticed that the theoretical curves do not fit very well with the experimental susceptibility curves in the region around the broad maxima. An exception can be made for $RbNiCl_3$ (fig. III-2). For this compound a very reasonable fit is found; the J/k-values, calculated from (eq. 1) and (eq. 2), differ by about 10%.

Comparing Achiwa's susceptibility data for $RbNiCl_3$ and $CsNiCl_3$ (1) with our results for these compounds it is seen that for $RbNiCl_3$ the data agree much better than for $CsNiCl_3$. In an extensive review of compounds with 1D, 2D and 3D properties, De Jongh (10) has fitted Achiwa's single crystal susceptibility data for $CsNiCl_3$ around the susceptibility maximum to Weng's theory. A very reasonable fit was obtained for $J/k = -13K$ and $g = 2.20$. These values agree well with those belonging to our best fit in the high-temperature region (Table III-1).

We can explain the differences between our susceptibility data for $CsNiCl_3$ and Achiwa's (our $\chi_{max} > \chi_{max}$ (Achiwa), our $T_{max} < T_{max}$ (Achiwa)) and a minimum in our susceptibility curve at very low temperatures), if we assume the presence of a paramagnetic impurity with a small asymptotic Curie temperature in our $CsNiCl_3$

Table III-1. Physical properties of the $ANiX_3$ compounds

Compound	θ(K)	$\chi_{max} \times 10^3$ (emu/mole)	T_{max}(K)	g from ESR	g from best fit	-J/k from T_{max}(K)	-J/k from χ_{max}(K)	-J/k from best fit (K)	T_N(K)	$\lvert J'/J \rvert$
$TlNiCl_3$	-	-	50(2)	2.24(1)	-	19 (1)	-	22 (1)	13 (2)	2×10^{-2}
NH_4NiCl_3	- 78(2)	9.85(5)	36(1)	2.23(1)	2.17(2)	13.3(3)	15.4(4)	16.0(5)	9 (2)	2×10^{-2}
$RbNiCl_3$	-101(2)	8.30(5)	45(1)	2.23(1)	2.18(2)	16.7(3)	18.7(4)	18.5(5)	11.1 *	2×10^{-2}
$CsNiCl_3$	- 56(2)	12.35(5)	30(1)	2.25(1)	2.18(2)	10.9(3)	12.6(4)	13.0(5)	4.5 **	6×10^{-3}
$RbNiBr_3$	-155(2)	6.25(5)	56(1)	2.22(1)	2.16(2)	20.8(3)	24.4(4)	25.5(5)	23 (2)	4×10^{-2}
$CsNiBr_3$	- 95(2)	8.75(5)	40(1)	2.27(1)	2.16(2)	14.8(3)	17.4(4)	18.5(5)	14 (2)	3×10^{-2}

The values between parentheses indicate the uncertainty in the last digit.

* refs. 1, 22

** refs. 1, 22, 23

sample. By analogy, we assume that the deviation from the theoretical results found for NH_4NiCl_3, $RbNiBr_3$, and $CsNiBr_3$ (fig. III-3, 4) are also due to paramagnetic impurities in these samples. For $RbNiCl_3$ no minimum in the susceptibility curve is found, whereas the theoretical fit is much better too than for the other compounds, indicating that in this sample of $RbNiCl_3$ impurities do not play an important role.

In order to check the validity of our assumption regarding the influence of paramagnetic impurities, we have measured the susceptibility of some other samples of $RbNiCl_3$ and $CsNiBr_3$, for which X-ray powder diffraction patterns had shown some small reflections due to the presence of an unknown impurity. As expected χ_{max} shifted to higher and T_{max} to lower values, relative to the purer samples. Also, we found for $RbNiCl_3$ a minimum in the susceptibility curve at 10K. For $CsNiBr_3$ the minimum shifted to a higher temperature ($\sim$10K).

In the high-temperature region the influence of the impurities can be neglected, so that the J/k-values obtained from the best fits in this region are the most trustworthy ones, as confirmed by De Jongh's fit of Achiwa's susceptibility data (see above). It seems reasonable to assume that the impurities are of the kind $NiX_2.xH_2O$ (X = Cl, Br). It is known that the compounds $NiX_2.6H_2O$ have low, antiferromagnetic transition points and small θ-values. (11, 12). Of the other hydrates no magnetic data are available.

Assuming now that the difference between χ_{max} (theoretical) and χ (experimental) at the temperature T_{max} (theoretical) is caused by an impurity with a small asymptotic Curie temperature ($\theta \approx 0$); the contribution to the experimental susceptibility curve can be calculated roughly with the Curie-law:

$$\chi(\text{impurity}) = C/T$$

Correcting the experimental susceptibility in this way, the points indicated in fig. III-2, 3, 4 are obtained. It is seen that the agreement between theoretical and corrected experimental results is satisfactory, although small differences still exist between T_{max} (exp.) and T_{max} (theor.) and in the temperature region just below T_{max}, where just as found for the pure $RbNiCl_3$ sample (fig. III-2)

the experimental susceptibility is somewhat higher than the theoretical susceptibility.

We conclude that Weng's theory gives a reasonably accurate description of the antiferromagnetic Heisenberg linear-chain system with S=1.

Very recently Montano et al. (13) applied the spin-wave approximation to linear-chain antiferromagnets, especially to $RbNiCl_3$ and $CsNiCl_3$, using Achiwa's results in the temperature region up to about 60K. Good agreement is obtained between experimental results and theoretical calculations on the basis of the spin-wave approximation in the temperature region around T_{max} using $J/k=-(18.9\pm0.7)K$, $D/k=(1.6\pm0.4)K$ and $J/k=-(15.9\pm0.4)K$, $D/k=(0.35\pm0.15)K$ for $RbNiCl_3$ and $CsNiCl_3$ respectively. Here D is the axial splitting parameter due to the single-ion anisotropy of the Ni^{2+} ions.

However, it is well-known that spin-wave theory gives only reliable results in temperature regions up to about $0.5T_N$ and, therefore, cannot be applied with success to the paramagnetic region. So the reasonable agreement between the values for the intra-chain interaction, obtained by Montano et al., and our values has to be a coincidence. Confirmation of this idea could be obtained from Montano indeed (14).

As already has been remarked, there were some problems in obtaining a reliable result for the J/k-values of $TlNiCl_3$. We have measured several samples of this compound, but for none of them it was possible to obtain a reasonable fit for the high-temperature part of the susceptibility curve, because this part of the curve did not fall off fast enough with increasing temperature. Also, the high-temperature part varied from one sample to another.

Zodkevitz et al. (15) have remarked that the linewidth of the reflections in the X-ray diffraction pattern of $TlNiCl_3$ was larger than for the other Ni compounds, probably due to a large number of stacking faults in the crystal structure. The same effect was noticed by us. It is, therefore, possible that the deviations of the experimental susceptibility from the theoretical curve, are caused by poor crystallization of the samples. Of all samples measured, however, T_{max} was found in the temperature region 48-52K, so that we can reasonably calculate by means of (eq. 1) the following J/k-value: $J/k=-(18.5\pm1.0)K$. In the susceptibility curves of $TlNiCl_3$ minima were found at low temperatures due to paramagnetic impurities. Therefore, the J/k-value, obtained from T_{max}, may be too small,

just as for the other Ni compounds. Knowing, for these compounds, the magnitude of the difference between the J/k-values, obtained from T_{max} and from the high-temperature fit respectively, we expect the following J/k-value for $TlNiCl_3$: $J/k = -(22\pm1)K$.

From Table III-1 it is seen that the g-values obtained from ESR measurements are all somewhat larger than the g-values obtained from the best fits. At the moment we cannot give an explanation for this.

From Table III-1 it can also be seen that the intra-chain interaction for $CsNiBr_3$ is of the same magnitude as J/k for $RbNiCl_3$, although the distance between nearest neighbours in $CsNiBr_3$ is much larger (3.115Å) than in $RbNiCl_3$ (2.952Å) (see Table II-2). In $RbNiBr_3$ (distance = 3.101Å) the J/k-value is even much larger than in $RbNiCl_3$. The exchange mechanism in the various compounds is essentially the same, except for the replacement of Cl^- by Br^-. It seems reasonable to assume, therefore, that the superexchange via the Br^- ions is stronger than via the Cl^- ions. This effect has also been found in the linear-chain compounds $CuCl_2$ (pyridine)$_2$ and $CuBr_2$ (pyridine)$_2$ (16) and the layer-type compounds Rb_2CuCl_4, Rb_2CuCl_3Br and $Rb_2CuCl_2Br_2$ (see Chapter VI).

In fig. III-5 the dependence of J/k of the $ANiCl_3$ compounds (obtained from the high-temperature fits) upon the distance between nearest neighbours in the chains is illustrated. As could be expected, because the interaction mechanism in the chains is the same for all compounds, the intra-chain interaction decreases with increasing distance. It can be noticed too, that the result for $TlNiCl_3$ fits very well in this picture.

Because of the uncertainties in the J/k-values and the small range of r-values, it could not be determined, whether the dependence is linear or can be described by a powerlaw $J/k=ar^{-n}$ or an exponential function $J/k=e^{-ar}$ (r is the distance between nearest neighbours), as could be demonstrated for some other sets of compounds. (17-19)

III-2.3 Transition points and inter-chain interaction

It has been proved theoretically that in an Ising or Heisenberg chain with nearest neighbour interaction only, no spontaneous magnetization, that is, long-range order can occur for $T>0$ (20, 21). But, due to the usually relatively weak inter-chain coupling in compounds with '1D magnetic properties', for all of these compounds a transition point, showing features of 3D long-range order, can be found.

For the compounds described in this paper, antiferromagnetic

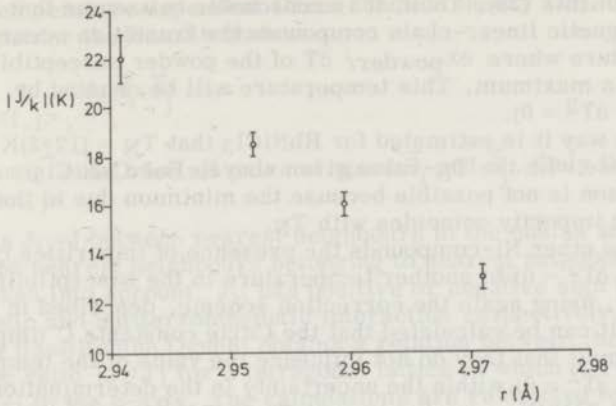

Fig. III-5 The intra-chain interaction $|J/k|$ as a function of the distance r between nearest neighbour Ni^{2+} ions in the chains for $ANiCl_3$ (A=Tl, NH_4, Rb, Cs)

transition points are known for $RbNiCl_3$ (T_N = 11.1K (1, 22)) and $CsNiCl_3$ (T_N=4.5K (1, 23, 24)). Although it is much easier to find T_N by means of susceptibility measurements on single crystals, it is also possible to determine reliable values of T_N in polycrystalline samples of linear-chain compounds. There are strong indications for several antiferromagnetic linear-chain compounds that T_N occurs at the maximum of $\partial\chi/\partial T$ of the powder susceptibility curve (25).

As can be noticed from Achiwa's measurements on single crystals of $RbNiCl_3$ and $CsNiCl_3$ (11) the parallel susceptibility $\chi_{//}$ (magnetic field //c-axis) falls off very sharply below the transition point, whereas the perpendicular susceptibility $\chi_{\perp}$ (magnetic field $\perp$ c-axis) varies only very little below this point. Comparison of the single crystal measurements with the powder susceptibility curves, also measured by Achiwa, shows that $\partial\chi_{powder}/\partial T$ reaches a maximum at the transition point indeed. Another example is given by the linear-chain compound $CuCl_2.2NC_5H_5$ for which De Jongh (10) has alleged, by combining several experimental data (26, 27) that a transition point occurs at about 1.7K, at which temperature the powder susceptibility starts to fall off considerably. For the antiferromagnetic linear-chain compound $Fe(N_2H_5)_2(SO_4)_2$ the temperature at which $\partial\chi_{powder}/\partial T$ reaches its maximum (see Chapter IV), agrees well with the transition temperature as found by means of specific heat

measurements (28). Thus, it is reasonable to assume that in antiferromagnetic linear-chain compounds the transition occurs at the temperature where $\partial \chi_{powder} / \partial T$ of the powder susceptibility curve reaches a maximum. This temperature will be denoted by $T(\partial^2 \chi / \partial T^2 = 0)$.

In this way it is estimated for $RbNiCl_3$ that $T_N = (12 \pm 2)K$, in accordance with the T_N-value given above. For $CsNiCl_3$ such a comparison is not possible because the minimum due to the paramagnetic impurity coincides with T_N.

For the other Ni-compounds the presence of impurities could shift $T(\partial^2 \chi / \partial T^2 = 0)$ to another temperature in the susceptibility curve. However, using again the correction scheme, described in Section III-2.2, it can be calculated that the Curie constants C (impurity) are so small that they do not influence the value of the temperature $T(\partial^2 \chi / \partial T^2 = 0)$ within the uncertainty in the determination T_N.

For all $TlNiCl_3$ samples investigated, $T(\partial^2 \chi / \partial T^2 = 0)$ was located in the temperature region 11-15K. It seems, therefore, reasonable to assume that the transition point is $T_N = (13 \pm 2)K$.

The T_N-values found for the various compounds are given in Table III-1, including the already known T_N-values. It is seen for the $ANiCl_3$ compounds that with increasing distance between nearest neighbour-chains (a-axis) the value of T_N decreases (in Table III-1 the compounds have been arranged according to increasing a-axis). Because the superexchange mechanism is the same for all compounds, this result indicates that the inter-chain interaction decreases with the lenghtening of the most probable inter-chain superexchange path Ni-Cl-Cl-Ni (see Chapter I). An exception is found for NH_4NiCl_3, for which T_N is lower than the T_N-value of $RbNiCl_3$, although the distance between nearest neighbour-chains is smaller in NH_4NiCl_3 (6.927Å) than in $RbNiCl_3$ (6.958Å) (see Table II-2). An explanation for this deviation can possibly be ascribed to the relatively rough method used for the determination of T_N.

By comparing the $ANiCl_3$ compounds (A=Rb, Cs) and the corresponding $ANiBr_3$ compounds the stronger influence of the Br^-ions in the inter-chain superexchange is found again. Although the distance between the chains in $ANiBr_3$ is larger than in $ANiCl_3$ the transition temperatures in $ANiBr_3$ are about 2-3 times higher than in $ANiCl_3$, corresponding to a larger inter-chain interaction in the bromides.

Using the experimentally determined temperatures T_N and intrachain interactions J, an estimate for the ratio of J and the interchain interaction J' can be given by means of a theory developed by Oguchi for antiferromagnetic linear chains on the basis of double-

time temperature dependent Green function theory (29).
We consider the Hamiltonian:

$$H = - \sum_{<i,j>} 2J_{ij} \vec{S}_i . \vec{S}_j ,$$

where $\sum_{<i,j>}$ runs over all pairs of spins $\vec{S}_i$ and $\vec{S}_j$. Only the interactions $J_{ij}=J$ between nearest neighbours in the chains and $J_{ij}=J'$ between nearest neighbours belonging to nearest neighbour-chains are taken into account. J_{ij} has positive or negative sign for ferromagnetic and antiferromagnetic interaction respectively. By means of this Hamiltonian Oguchi obtains a relation between the Néel point and the ratio $|J'/J|$ for a tetragonal lattice in which the chains are parallel to the c-axis. The calculations are restricted to the case that there is a single preferred direction of antiferromagnetic alignment in the ordered state of the spin system and that there are only two ferromagnetic sublattices. As Oguchi gives only four pairs of values (T_N, $|J'/J|$), we have calculated with Oguchi's formula, the whole curve of T_N vs $|J'/J|$ (fig. III-6).

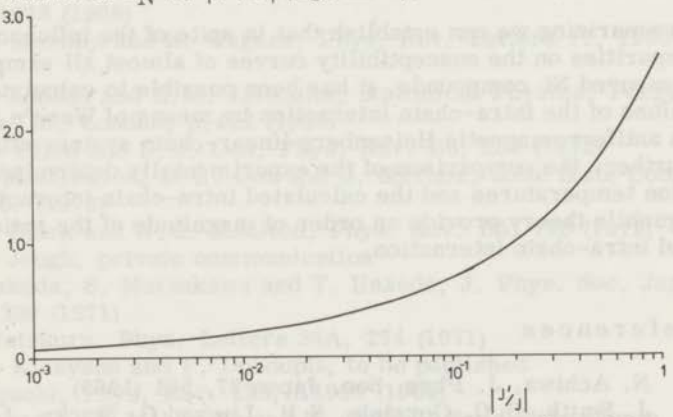

Fig. III-6 The ratio of the inter-chain interaction J'/k and the intra-chain interaction J/k, $|J'/J|$, as a function of T_N

In the literature on the compounds $RbNiCl_3$ and $CsNiCl_3$ two different possibilities for the spin structure are mentioned (22-24, 30). The most probable magnetic structure consists of an antiferromagnetic sequence of spins along the c-axis (direction of the chains), along

with a screw spiral propagating in the basal plane (23). The wavelength of the screw spiral is commensurate with the lattice and has a value 3a (a=a-axis of the chemical unit cell).

No data are known about the magnetic structure of the other Ni compounds, but it seems reasonable to assume that these compounds have a similar structure.

So the restriction about the single preferred direction of spin alignment is not in accordance with the spin structure. Further the unit cell is hexagonal, whereas Oguchi's calculations hold for a tetragonal structure. So the ratio $|J'/J|$ of the Ni compounds, listed in Table III-1, can only be a rough estimate.

Comparison of the $|J'/J|$-values among each other shows that $CsNiCl_3$ has the smallest value, that is, is the best approximation of a linear-chain system. For the other $ANiCl_3$ compounds $|J'/J|$ has nearly the same value.

Although in $ANiBr_3$ (A=Rb, Cs) the distance between the chains is enlarged and the J/k-values are larger compared to $ANiCl_3$, the ratio $|J'/J|$ is larger. This means that the superexchange interaction via the Br^-ions between the chains is stronger than via the Cl^-ions, as was already remarked above.

Summarizing we can establish that in spite of the influence of small impurities on the susceptibility curves of almost all samples of the measured Ni compounds, it has been possible to calculate reliable values of the intra-chain interaction by means of Weng's results for an antiferromagnetic Heisenberg linear-chain system with S=1. Further, the comparison of the experimentally determined transition temperatures and the calculated intra-chain interactions within Oguchi's theory provide an order of magnitude of the ratio of inter- and intra-chain interaction.

References

1. N. Achiwa, J. Phys. Soc. Japan 27, 561 (1969)
2. J. Smith, B.C. Gerstein, S.H. Liu and G. Stucky, J. Chem. Phys. 53, 418 (1970)
3. R.W. Asmussen and H. Soling, Z. Anorg. Allgem. Chem. 283, 3 (1956)
4. M. Suzuki, B. Tsujiyama and S. Katsura, J. Math. Phys. 8, 124 (1967)
5. J.C. Bonner and M.E. Fisher, Phys. Rev. 135, A640 (1964)
6. M.E. Fisher, Am. J. Phys. 32, 343 (1964)
7. C. Weng, Thesis, Carnegie-Mellon University (1968)

8. T. Smith and S.A. Friedberg, Phys. Rev. 176, 660 (1968)
9. P.W. Selwood, Magnetochemistry, Interscience Publishers Inc., New York (1956)
10. J. de Jongh and A.R. Miedema, Advances in Physics (to be published)
11. T. Hoseda, H. Kobayashi and H. Date, J. Phys. Soc. Japan 14, 1724 (1959)
12. R.D. Spence, H. Forstat, G.A. Khan and G. Taylor, J. Chem. Phys. 31, 555 (1959)
13. P.A. Montano, E. Cohen and H. Shechter, Phys. Rev. B6, 1053 (1972)
14. P.A. Montano, private communication
15. A. Zodkevitz, J. Makovsky and Z.H. Kalman, Isr. J. Chem. 8, 755 (1970)
16. D.G. Jeter and W.E. Hatfield, J. Inorg. Nucl. Chem. 34, 3055 (1972)
17. K.W. Rogers, L. Finegold and B. Morosin, Phys. Rev. B6, 1058 (1972)
18. D. Bloch, J. Phys. Chem. Solids 27, 881 (1966)
19. M.T. Hutchins, K.J. Birgenau and W.P. Wolf, Phys. Rev. 168, 1026 (1968)
20. W.D. Mermin and H. Wagner, Phys. Rev. Letters 17, 1133 (1966)
21. L.D. Landau and E.M. Lifschitz, Statistical Physics, Pergamon Press Ltd, London, p.482 (1958)
22. W.B. Yelon and D.E. Cox, Phys. Rev. B6, 204 (1972)
23. V.J. Minkiewicz, D.E. Cox and G. Shirane, Solid State Comm. 8, 1001 (1970)
24. R.H. Clark and W.G. Moulton, Phys. Rev. B5, 788 (1972)
25. J. de Jongh, private communication
26. K. Takeda, S. Matsukawa and T. Haseda, J. Phys. Soc. Japan 30, 1330 (1971)
27. M. Matsuura, Phys. Letters 34A, 274 (1971)
28. F.W. Klaaysen and F. Dokoupil, to be published
29. T. Oguchi, Phys. Rev. 133, A1098 (1964)
30. A. Epstein, J. Makovsky and H. Shaked, Solid State Comm. 9, 249 (1971)

CHAPTER IV - LINEAR-CHAIN ANTIFERROMAGNETISM IN THE COMPOUNDS $M^{2+}(N_2H_5)_2(SO_4)_2$ WITH M=Mn, Fe, Co, Ni AND Cu

IV-1 Introduction

As part of a research program on the magnetic properties of coordination-compounds having chain structures, which may be expected to behave as one-dimensional magnetic systems, susceptibility and specific heat measurements on polycrystalline samples of the compounds $M^{2+}(N_2H_5)_2(SO_4)_2$ with M = Mn, Fe, Co, Ni and Cu (catena-bis(hydrazinium)-bisμ(sulfato) metal (2+) compounds) have been carried out at low temperatures (2-80K). In this chapter the results of the susceptibility measurements and some preliminary results of the specific heat measurements (carried out by F.W. Klaaijsen at the Kamerlingh Onnes Laboratory at Leiden and to be published in detail elsewhere (1)) on these compounds are discussed.

A single-crystal structure determination presented by Prout and Powell (2) has shown that the Zn ions in the triclinic compound $Zn(N_2H_5)_2(SO_4)_2$ are coordinated by four oxygens belonging to four different, bridging SO_4 groups and by two monodentate N_2H_5 groups, together forming a distorted octahedral coordination around the metal ion. The SO_4 groups are bridging between two adjacent Zn ions, forming chains of metal ions along the b-axis (fig. IV-1).

Additional structure, magnetic and spectroscopic studies by Hand and Prout (3) and Nieuwpoort and Reedijk (4) on similar compounds with M = Cr, Mn, Fe, Co, Ni, Cu and Cd have shown that all these compounds possess the same geometrical arrangement and that most of the measurements (4) can be interpreted on the basis of a tetragonal, compressed octahedral geometry with an additional rhombic distortion. The susceptibility and ESR measurements (4) on some of these compounds showed the presence of a small magnetic interaction between the metal ions.

The metal-metal distances in the chains are about 5.3Å. This large distance is prohibitive for the occurrence of direct magnetic interaction between the metal atoms. If intra-chain interaction is present, it would be mainly due to a superexchange mechanism via the path M-O-S-O-M. The chains are linked to each other via

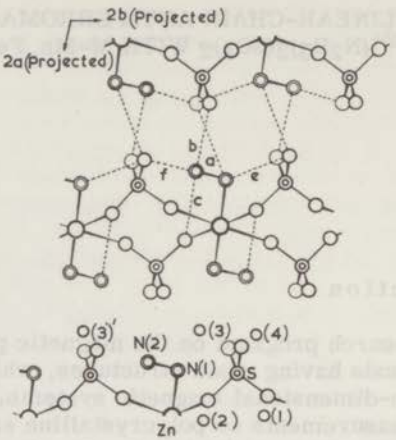

Fig. IV-1 Structure of $Zn(N_2H_5)_2(SO_4)_2$. The linear complex is shown in the centre. Hydrogen bonds within the complex and between a pair of neighbouring complexes are shown by broken lines (the figure and lettering are after Prout and Powell (2)). In addition there is a hydrogen bond d from N(2) to an oxygen atom similar to O(3)' but belonging to another complex nearer to the observer

terminal nitrogen atoms of the N_2H_5 groups, which form hydrogen bonds with SO_4 groups of neighbouring chains. It can, therefore, be expected that the magnetic interaction between the chains (inter-chain interaction) is weaker than the intra-chain interaction, although the distance between the metal atoms along the c-axis (5.8Å) is roughly equal to the distance within the chains (along b-axis, 5.3Å).

In Section IV-2 it is shown that the susceptibility measurements can be interpreted in terms of the one-dimensional linear-chain model, indicating that, as expected, the intra-chain interaction is relatively much stronger than the inter-chain interaction.

The preparation method of the compounds was already discussed in Chapter II-2.8. The results of a metal analysis are listed in Table II-7.

IV-2 Results and discussion

In Chapter I-1 a short discussion was given of various models that are usually necessary to give a simplified description of the magnetic

interactions in magnetic systems, viz. the Heisenberg, Ising and XY model. The magnetic properties of many compounds can be described adequately by the Heisenberg or Ising model, whereas only a few experimental examples are known of the XY model. The former model gives a good description of magnetic systems with S-state ions (e.g. Mn^{2+}), because for these ions single-ion anisotropy and anisotropy in the exchange mechanism are usually very small. The Heisenberg model is also successful for many Cu^{2+} and Ni^{2+} compounds. Many Co^{2+} compounds show strongly anisotropic properties, that can be approximately described by the Ising model. The properties of Fe^{2+} compounds are very often intermediate between those expected for a Heisenberg and Ising system. More details about the models applied to the description of the compounds discussed in this chapter, are given below for each compound individually.

The so-called Dzialoshinsky-Moriya term $D.\vec{S}_i x \vec{S}_j$, that describes the antisymmetrical part of the superexchange interaction (6, 7), is not included in the discussion above. Obviously this is allowed if the exchange is isotropic, but in case of anisotropic exchange this term can influence the magnetic behaviour. Due to the low crystal symmetry of the compounds $M(N_2H_5)_2(SO_4)_2$ it is quite well possible that, in particular in the cases M = Fe and Co, the Dzialoshinsky-Moriya term influences the magnetic behaviour. However, from our powder susceptibility measurements no reliable impression about this influence can be obtained. Therefore, this term is not taken into account in the discussion of the results.

IV-2.1 $Ni(N_2H_5)_2(SO_4)_2$

In fig. IV-2a the molar powder susceptibility χ_m and inverse molar susceptibility $1/\chi_m$ of $Ni(N_2H_5)_2(SO_4)_2$ as a function of temperature are shown. As can be seen in fig. IV-2b the magnetization at 2.2K is linearly dependent upon the magnetic field strength up to about 25kOe. Above 25kOe the curve shows an anomalous behaviour, which was found to be a common feature of the other $M(N_2H_5)_2(SO_4)_2$ compounds described below. The susceptibility was measured at a magnetic field of about 5.5kOe.

The $1/\chi_m$-curve obeys the Curie-Weiss law down to about 35K with an asymptotic Curie temperature $\theta = -9.5$K (Table IV-1). The broad maximum that is found in the χ-curve at low temperature (fig. IV-2a) is characteristic for antiferromagnetic dimers, linear-chain and two-dimensional systems. On basis of the crystal structure it seems therefore reasonable to interpret the magnetic properties of the compound in terms of an antiferromagnetic linear-chain system,

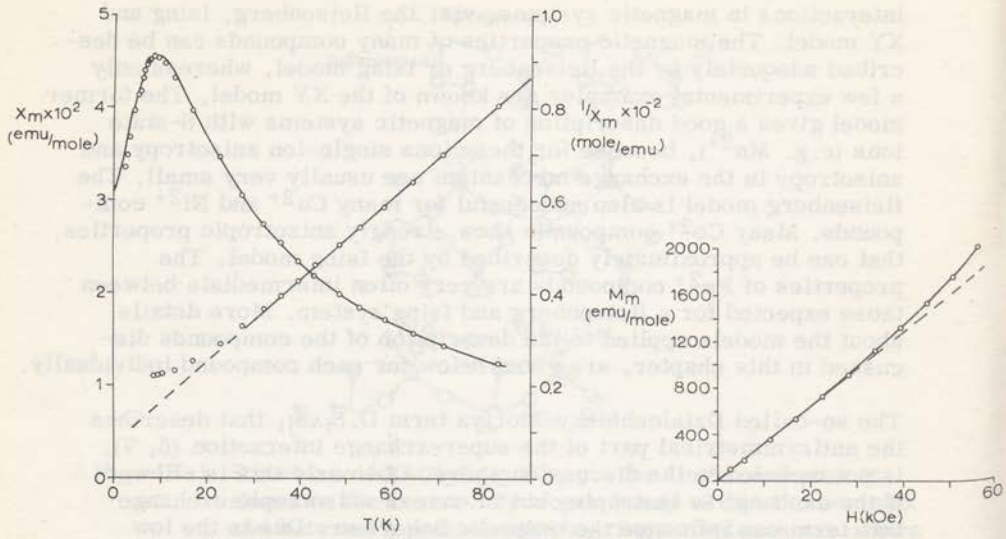

Fig. IV-2a Molar susceptibility χ_m and inverse molar susceptibility $1/\chi_m$ of $Ni(N_2H_5)_2(SO_4)_2$ as a function of temperature t; o = experimental points; ——: theoretical fit for $J/k = -3.35K$ according to Weng's results. The straight line through the $1/\chi_m$ data represents the Curie-Weiss law

Fig. IV-2b Magnetization curve of $Ni(N_2H_5)_2(SO_4)_2$ at 2.2K

that, as has been remarked above, can probably be described by the Heisenberg model. In this case a = b = 1 in the Hamiltonian

$$H = -2J \sum_{<i,j>} [aS_i^Z S_j^Z + b(S_i^X S_j^X + S_i^Y S_j^Y)] \quad (1)$$ (see Chapter I-1),

where J indicates now the exchange between nearest neighbours in the chains and has negative sign for antiferromagnetic coupling. The inter-chain interaction and the single-ion anisotropy of the Ni^{2+} ions are neglected at this stage of the analysis. It can be inferred from the specific heat measurements (1) and from a corresponding entropy determination that, as usual for Ni^{2+} compounds, the magnitude of the spin is S=1. In 1968 Weng has published in his thesis (7) numerical results for antiferromagnetic Heisenberg linear chains of 3 to 7 spins S=1. By extrapolation of his results to an infinite number of

spins he obtained the susceptibility and specific heat as a function of temperature for antiferromagnetic Heisenberg chains with S=1 (7).

By fitting our susceptibility results to Weng's theoretical susceptibility curve one obtains a value for the intra-chain interaction. With the variable parameters J/k and g the high-temperature part of the experimental curve (fig. IV-2a) is fitted well to the theoretical curve for J/k = -3.35K (Table IV-2) and g = 2.17. The g-value is in good agreement with the value of about 2.2, that is usually found for the spectroscopic splitting factor of Ni^{2+} compounds.

From the experimentally determined values of the maximum in the susceptibility χ_{max} and of the temperature $T_{max}(\chi)$ at which χ_{max} occurs (Table IV-1) values for J/k are also obtained by means of the following relations, derived by Weng:

$$kT_{max}(\chi)/|J| = 2.7 \quad (2) \text{ and}$$

$$|J|\chi_{max}/Ng^2\beta^2 = 0.0872 \quad (3),$$

where N = Avogadro's number and β = Bohr magneton. Using the g-value from the high-temperature fit, the J/k-values are calculated (Table IV-2).

The differences between the three obtained J/k-values fall within experimental error. It is seen in fig. IV-2a that, if the high-temperature fit is extended to the lower temperature region, agreement between experiment and theory remains good. Thus, we can describe our susceptibility data well by Weng's theory, assuming $J/k = -(3.3 \pm 0.1)K$.

Applying Weng's theoretical results to fit the high-temperature part of the experimental specific heat curve (corrected for the lattice contribution) the value J/k = -2.7K is obtained. From the temperature $T_{max}(C) = 3.7K$ (C=specific heat) and Weng's theoretical relation for $T_{max}(C)$: $kT_{max}(C)/|J| = 1.8$ it is found that J/k = -2.0K. Not only is a large difference observed between the two J/k-values as obtained from the specific heat data, but also between these two values and the J/k-value, calculated from the susceptibility.

This discrepancy cannot be explained at present, but the disagreement may be due to the occurrence of single-ion zero-field splitting. Because of the strongly distorted octahedral coordination of the Ni ion it is possible that the zero-field splitting parameter D cannot be neglected and may even be of the same order of magnitude as J.

As far as known no theory is available which describes antiferromagnetic Heisenberg chains including zero-field splitting of the S=1 state, so that even a qualitative study of the influence of D on the susceptibility and specific heat is not feasible. However, from a

recently published theory for S=1 dimers including zero-field splitting, it is seen that neglection of D does not influence the susceptibility of the dimers very much (8). For the magnetic specific heat curve it is expected that the broad maximum in this curve originates from the contribution of the broad maximum of a Schottky anomaly, caused by the zero-field splitting (9) and the broad maximum due to the antiferromagnetic dimer interaction. By extension to linear chains it is understandable that the magnetic specific heat curve cannot be fitted with Weng's results, whereas a good fit is found for the susceptibility curve.

Other antiferromagnetic linear-chain Ni^{2+} compounds, $RbNiCl_3$ and $CsNiCl_3$, have much larger J/k values (10, 11) and are less distorted from cubic symmetry so that $D \ll J$ (see also Chapter III). The experimental susceptibility of these compounds can be fitted well using Weng's theory (Chapter III). A comparison with specific heat results is not possible, because only a few specific heat data are known for $CsNiCl_3$ (12).

Compounds having linear-chain properties practically always show a magnetic transition, where 3D long-range order sets in, due to the inter-chain interaction. The specific heat measurements did not indicate such a transition point down to 1.5K, indicating that the inter-chain interaction is much weaker than the intra-chain interaction.

A last remark about $Ni(N_2H_5)_2(SO_4)_2$ concerns the 'anomalous' behaviour of the magnetization curve (fig. IV-2b). Such behaviour is predicted by several theoretical investigations on antiferromagnetic Heisenberg and Ising linear-chain models with spin $S=\frac{1}{2}$ and 1 (7, 13-16) and has been measured experimentally for e.g. the linear-chain compounds $Cu(NH_3)_4SO_4.H_2O$ (17) and $CuCl_2.2NC_5H_5$ (18). For the other compounds described below, similar magnetization curves are found.

IV-2.2 $Mn(N_2H_5)_2(SO_4)_2$

The observed susceptibility of $Mn(N_2H_5)_2(SO_4)_2$ is shown in fig. IV-3. The susceptibility was field independent up to about 10kOe. The measurements were carried out at a field strength of about 2.7kOe. The curve shows the broad maximum, that on basis of the crystal structure, is typical for an antiferromagnetic linear-chain system. The asymptotic Curie temperature $\theta=-5.5$K (Table IV-1).

The magnetic system of Mn^{2+} compounds can be described by the Heisenberg model. ESR measurements revealed (4) that the single-ion anisotropy of $Mn(N_2H_5)_2(SO_4)_2$ is very small

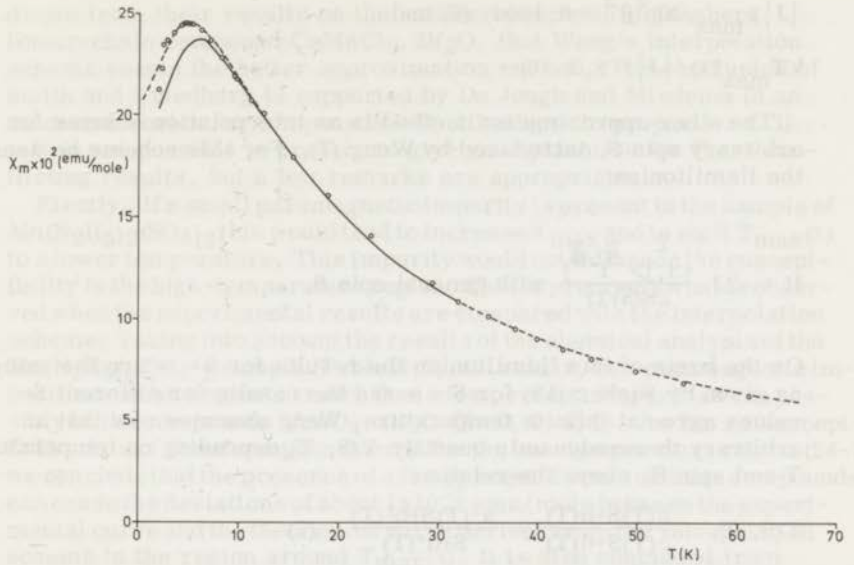

Fig. IV-3 Molar susceptibility χ_m of $Mn(N_2H_5)_2(SO_4)_2$ as a function of temperature. o = experimental points; ___: best fit obtained, using Wengs interpolation scheme for J/k =-0.59K and g=2.01; ---: best fit obtained, using the scaling method for J/k= -0.615K and g=2.01

($D = 0.025 \pm 0.005\ cm^{-1}$), so that it can be neglected.

Within the Heisenberg model one knows two theoretical approximations for the description of antiferromagnetic linear chains with S=5/2. By scaling at high temperature the exact results of Fisher (19) for an antiferromagnetic linear chain with $S = \infty$ to the series expansion results of Rushbrooke and Wood (20), Wagner and Friedberg (21) obtained eq. (4) for the molar susceptibility:

$$\chi_m = \frac{Ng^2\beta^2 S(S+1)}{3kT} \cdot \frac{1+U(K)}{1-U(K)} \quad (4)$$

where U(K) = coth K-1/K and K=2JS(S+1)/kT. The sign of J is again negative. In this approximation χ_{max} and $T_{max}(\chi)$ for S=5/2 are related to J by:

$|J|\chi_{max}/Ng^2\beta^2 = 0.1004$ (5) and

$kT_{max}(\chi)/|J| = 8.2$ (6).

The other approximation method is an interpolation scheme for arbitrary spin S, introduced by Weng (7). For this scheme he uses the Hamiltonian

$$H = -2J \frac{\sum_{<i,j>} \vec{S}_i \cdot \vec{S}_j}{2S(S+1)} \text{ with general spin S.}$$

On the basis of this Hamiltonian the results for $S = \infty$ are the same as given by Fisher (19) for $S = \infty$ and the results for different S-values agree at infinite temperature. Weng assumes now that an arbitrary thermodynamic quantity Y(S, T) depending on temperature T and spin S, obeys the relation

$$Y(S, T) = \frac{a(T)S+b(T)}{c(T)S+d(T)} = \frac{a'(T)S+b'(T)}{S+d'(T)} \quad (7)$$

where a'(T), b'(T) and d'(T) depend on temperature but are independen of S. Tabulating the known numerical results (13) for antiferromagnetic Heisenberg linear chains with $S=\frac{1}{2}$, the numerical results (7) for S=1 and the exact results (19) for $S = \infty$ on a reduced temperature scale $kT/2|J|S(S+1)$, the unknown constants a'(T), b'(T) and d'(T) can be calculated for each value of $kT/2|J|S(S+1)$. In this way the suceptibility and specific heat curves for arbitrary spin value are obtained. By means of this interpolation scheme it is found that for S=5/2:

$|J|\chi_{max}/Ng^2\beta^2 = 0.0949$ (8) and

$kT_{max}(\chi)/|J| = 9.8$ (9).

Using eq. (5), (6), (8), (9), the experimental values for χ_{max} and $T_{max}(\chi)$ (Table IV-1) and the value g = 2.01, as found by Nieuwpoort and Reedijk (4), the J/k-values in Table IV-2 are derived. Also in this table are given the J/k-values obtained from the fits to the high-temperature part of the susceptibility curve (fig. IV-3) with g = 2.01 and J/k as variable parameter. It is noticed in fig. IV-3 that the best result is found by means of the scaling method of Wagner and Friedberg (21).

This is in contradiction with Smith and Friedberg's conclusion (22)

drawn from their results on the antiferromagnetic Heisenberg linear-chain compound $CsMnCl_3.2H_2O$, that Weng's interpolation scheme seems the better approximation method. The conclusion of Smith and Friedberg is supported by De Jongh and Miedema in an extensive review on compounds with 1D magnetic properties (23).

It is not possible at present to give an explanation for these conflicting results, but a few remarks are appropriate.

Firstly, if a small paramagnetic impurity is present in the sample of $Mn(N_2H_5)_2(SO_4)_2$ this would tend to increase χ_{max} and to shift $T_{max}(\chi)$ to a lower temperature. This impurity would not influence the susceptibility in the high-temperature region. This is precisely what is observed when the experimental results are compared with the interpolation scheme. Taking into account the results of the chemical analysis of the $Mn(N_2H_5)_2(SO_4)_2$ sample (Table II-7), it is clear, that paramagnetic impurities cannot amount to more than a few percent. Impurities can possibly be the compounds $MnSO_4.xH_2O$ (X = 0, 1, 4, 5). As far as susceptibility data of these compounds exist for the low-temperature region (24-27), we conclude that the presence of a few percent of some of these compounds can cause the deviations of about $1x10^{-2}$ emu/mole between the experimental curve and the theoretical curve derived from the interpolation scheme in the region around $T_{max}(\chi)$. It is also concluded from these data that at higher temperatures the experimental susceptibility curve can hardly have been influenced by the impurities.

In the second place the presence of anisotropy in the magnetic system would also cause a shift of χ_{max} to lower temperatures and to higher values (7, 13). But, as has already been remarked, the anisotropy is very small and can at most have a minor influence on the susceptibility curve.

Further it is noticed that $Mn(N_2H_5)_2(SO_4)_2$ is not equally good an example of a 1D system as $CsMnCl_3.2H_2O$. Whereas in the latter compound (22, 28) $T_{max}(\chi)/T_N = 6.3$, for $Mn(N_2H_5)_2(SO_4)_2$ it is found, by means of specific heat measurements (1), that $T_N = 2.09K$, hence $T_{max}(\chi)/T_N = 2.3$. This indicates that in this compound the inter-chain interaction is much stronger than in $CsMnCl_3.2H_2O$. Neutron scattering experiments on some antiferromagnetic linear-chain compounds demonstrate that up to temperatures of about $2T_N$ to $4T_N$ the effect of inter-chain interaction is noticeable (28, 29), in other words, 3D correlations are found between the chains. Because of this phenomenon and the fact that the theoretical approximation holds for pure 1D systems only, it can be expected that in linear-chain compounds, where $T_{max}(\chi)$ is about 2 to 3 times T_N (hence, with a relatively large inter-chain interaction) the susceptibility shows deviations from the theoretical picture in the region below and at $T_{max}(\chi)$. It is possible that the 3D correlations in linear-

chain systems above T_N cause an increase of the susceptibility above T_N, compared to the susceptibility of an ideal 1D system.

Probably one, or a combination of more of the phenomena described above explains the difference between the conclusion of Smith and Friedberg (22) and our results for $Mn(N_2H_5)_2(SO_4)_2$.

From the specific heat data $T_{max}(C) = (2.5\pm0.3)K$ is determined. The uncertainty in this value is rather large due to overlap of the strong peak, caused by the 3D ordering at $T_N = 2.09K$, with the broad maximum in the specific heat curve. By means of the relation $kT_{max}(C)/|J| = 5.6$, obtained with the interpolation scheme (eq. 7), the value $J/k = -(0.45\pm0.05)K$ is calculated (Table IV-2). This value is in agreement with the one obtained from $T_{max}(\chi)$.

It has also been possible to determine J/k by means of a paramagnetic line-width study, in particular the so-called '10/3 effect'. The great advantage of this method is that, if some special conditions are fulfilled, the magnetic exchange can be calculated from the ratio between the line widths of two ESR signals recorded at two different frequencies (e.g. in X- and Q-band) at room temperature. The special conditions are that only dipolar interaction and isotropic magnetic exchange are present and that the latter is stronger than the former. Kubo and Tomita (30) have derived the following expression for the linewidth ΔH of the ESR signal as a function of the measuring frequency:

$$\Delta H = \frac{H_d^2}{H_e}\left[1+(5/3)\exp\{-\tfrac{1}{2}(f_o/f_e)^2\}+(2/3\exp\{-2(f_o/f_e^2\}\right] \quad (10)$$

where H_d = dipolar field and the range of f_o should be comparable to the frequency f_e that is correlated to the exchange field $H_e(f_e = g\beta H_e/h)$. In the limit $H_e \gg H_o(f_o = g\beta H_o/h)$ ΔH is 10/3 as large as in the limit $H_o \gg H_e$.

Pleau and Kokoszka (31) employed (eq. 10) to calculate the ratio of linewidths at two frequencies in terms of the magnetic field H_e. To relate H_e to J they used the expression

$$(g\beta H_e/h)^2 = (8/3)zS(S+1)J^2 \quad (11),$$

given by Moriya (32). Here z = number of magnetic nearest neighbours.

Because the compound $Mn(N_2H_5)_2(SO_4)_2$ fulfills the conditions required for the application of the '10/3 effect', the ESR signals of this compound were recorded at room temperature at the frequencies 9.5 GHz (X-band) and 35.5 GHz (Q-band). The spectra were recorded

as the derivative of the absorption curve with a Varian V-4502/3-10A spectrometer of which details have been published elsewhere (33). The measured linewidths were (241±4) and (212±4) Oe at X- and Q-band frequency respectively, resulting in a linewidth ratio 0.88±0.03 and an intra-chain interaction $J/k = -(0.52 \pm 0.08)$K, calculated by means of eq. (10) and (11) (Table IV-2; see also Chapter V-2.2 and fig. V-6). Within experimental uncertainty this value is in agreement with the J/k-values obtained via susceptibility and specific heat measurements.

IV-2.3 $Cu(N_2H_5)_2(SO_4)_2$

In fig. IV-4 the χ_m-curve of $Cu(N_2H_5)_2(SO_4)_2$ is depicted. The susceptibility at 2.1K was field independent up to about 35 kOe. The plotted data refer to measurements at about 10 kOe.

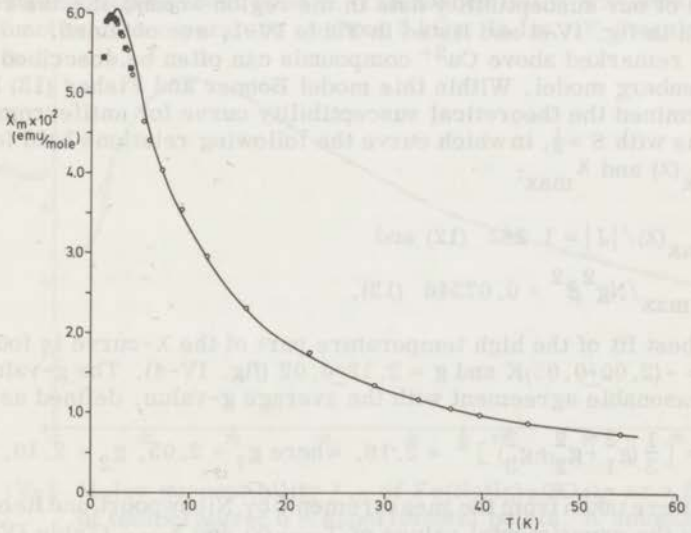

Fig. IV-4 Molar susceptibility χ_m of $Cu(N_2H_5)_2(SO_4)_2$ as a function of temperature. o = experimental points; ■ = experimental points obtained from zero-field susceptibility measurements. ——: best theoretical fit for $J/k = -2.00$K and $g = 2.12$

The susceptibility curve (as measured with our apparatus down to 2.1K) did not exhibit the broad maximum as found for the Ni and Mn compound (fig. IV-2a, 3). From the reciprocal susceptibility versus

temperature curve it was determined that $\theta = -(3\pm1)$K (Table IV-1). By analogy with the Ni and Mn compound one would expect an antiferromagnetic intra-chain interaction. Probably the intra-chain interaction is so small that the expected broad maximum only occurs below or in the neighbourhood of 2.1K. To obtain experimental data in the temperature region below 2.1K, zero-field susceptibility measurements were performed with a twin-T-bridge at a frequency of about 300 kHz. A detailed description of this apparatus will be published elsewhere (34). With this bridge the real part χ' and the imaginary part χ'' of the complex susceptibility $\chi = \chi' - i\chi''$ are measured simultaneously. The measurements on $Cu(N_2H_5)_2(SO_4)_2$ showed that (at the measuring frequency) χ'' was practically zero. The measurements were carried out in the liquid helium temperature region (1.2-4.2K).

Scaling the relative zero-field susceptibility measurements to some of our susceptibility data in the region around 4K, the results, shown in fig. IV-4 and listed in Table IV-1, are obtained.

As remarked above Cu^{2+} compounds can often be described by the Heisenberg model. Within this model Bonner and Fisher (13) have determined the theoretical susceptibility curve for antiferromagnetic chains with $S = \frac{1}{2}$, in which curve the following relations hold for $T_{max}(\chi)$ and χ_{max}:

$$kT_{max}(\chi)/|J| = 1.282 \quad (12) \text{ and}$$

$$|J|\chi_{max}/Ng^2\beta^2 = 0.07346 \quad (13).$$

The best fit of the high temperature part of the χ-curve is found for $J/k = -(2.00\pm0.05)$K and $g = 2.12\pm0.02$ (fig. IV-4). The g-value is in reasonable agreement with the average g-value, defined as

$$g_{av} = [\tfrac{1}{3}(g_1^2+g_2^2+g_3^2)]^{\frac{1}{2}} = 2.16, \text{ where } g_1 = 2.05,\ g_2 = 2.10,\ g_3 = 2.34$$

were taken from the measurements by Nieuwpoort and Reedijk (4). Using the experimental values of $T_{max}(\chi)$ and χ_{max} (Table IV-1), the g-value from the high-temperature fit and eq. (12) and (13) the intra-chain coupling is calculated to be $J/k = -1.65$K and $J/k = -2.10$K respectively (Table IV-2).

It is noticed that the theoretical fit and the experimental curve agree well except in the region around $T_{max}(\chi)$, where a small discrepancy might well be related to the small anisotropy in the magnetic system, which is suggested by the presence of small differences between the g-values (4). Another explanation could be found

in the presence of interactions other than those arising from nearest neighbours.

The value $C_{max}(exp)/R=0.34$, (R= gas constant = 8.31J/mole K), obtained from the specific heat measurements agrees very well with the theoretically expected value (13) for an antiferromagnetic Heisenberg linear-chain system with $S=\frac{1}{2}$: $C_{max}(theor)/R=0.35$.

With the experimental value $T_{max}(C)=1.8K$ and the theoretical relation (13) $kT_{max}(C)/J=0.962$ the intra-chain interaction is calculated to be $J/k=-1.87K$ (Table IV-2). This value is in good agreement with the value obtained from the best fit of the susceptibility curve.

IV-2.4 $Fe(N_2H_5)_2(SO_4)_2$

The experimental susceptibility of $Fe(N_2H_5)_2(SO_4)_2$ is shown in fig. IV-5. At 2.0K the susceptibility was independent of the magnetic field strength up to about 20 kOe. The susceptibility was measured as a function of temperature at about 5 kOe. In fig. IV-5 again a

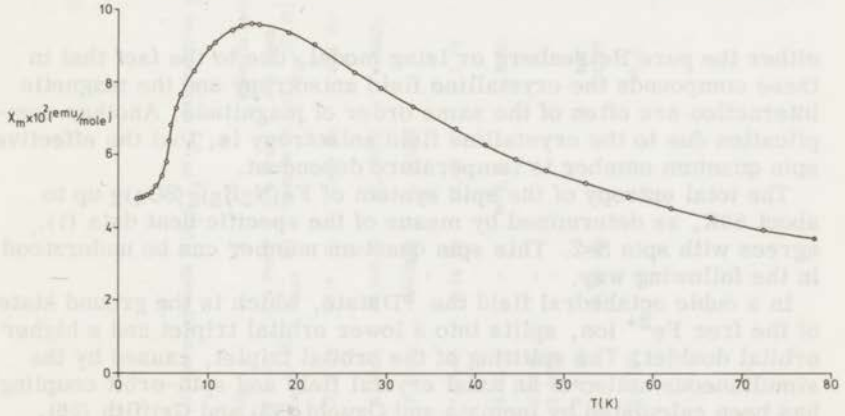

Fig. IV-5 Molar susceptibility χ_m of $Fe(N_2H_5)_2(SO_4)_2$ as a function of temperature; o = experimental points. A smooth curve is drawn through the experimental points

broad maximum is noticed. The high-temperature part of the reciprocal susceptibility curve obeys the Curie-Weiss law with an asymptotic Curie temperature $\theta=-(13\pm1)K$ (Table IV-1).

The theoretical interpretation of the susceptibility gives rise to serious problems. As already remarked, it is usually not possible to describe the magnetic properties of Fe^{2+} compounds by means of

Table IV-1. Experimental values of susceptibility measurements

Compound	θ(K)*	$\chi_{max} \times 10^2$ (emu/mole)	T_{max}(K)
$Ni(N_2H_5)_2(SO_4)_2$	- 9.5(5)	4.51(5)	8.7(2)
$Mn(N_2H_5)_2(SO_4)_2$	- 5.5(5)	24.50(25)	4.8(2)
$Cu(N_2H_5)_2(SO_4)_2$	- 3 (1)	5.95(5)	2.1(2)
$Fe(N_2H_5)_2(SO_4)_2$	-13 (1)	9.65(10)	15.3(3)
$Co(N_2H_5)_2(SO_4)_2$	-22 (1)	9.10(10)	5.7(2)

* Uncertainties in the last digit are indicated in parentheses in this Table and in Table IV-2

either the pure Heisenberg or Ising model, due to the fact that in these compounds the crystalline field anisotropy and the magnetic interaction are often of the same order of magnitude. Another complication due to the crystalline field anisotropy is, that the effective spin quantum number is temperature dependent.

The total entropy of the spin system of $Fe(N_2H_5)_2(SO_4)_2$ up to about 80K, as determined by means of the specific heat data (1), agrees with spin S=2. This spin quantum number can be understood in the following way.

In a cubic octahedral field the ^5D state, which is the ground state of the free Fe^{2+} ion, splits into a lower orbital triplet and a higher orbital doublet. The splitting of the orbital triplet, caused by the simultaneous action of an axial crystal field and spin-orbit coupling, has been calculated by Inomata and Oguchi (35) and Griffith (36). From their energy level diagram it can be concluded that, if the effective spin value at low temperature is S=2, the ratio δ/λ (δ = ground state splitting and λ = spin-orbit coupling parameter) is fairly large and positive: $\delta/\lambda \approx 10$. This conclusion is in accordance with the results, obtained from magnetic and Mössbauer measurements by Nieuwpoort and Reedijk (4), that the octahedral coordination of the Fe ion is deformed into a compressed, tetragonal structure with four spectrochemically weak oxygen ligands in the equatorial plane and two spectrochemically strong nitrogen ligands in the axial direction. This deformation leads to a zero-field splitting parameter D.

Table IV-2. Listing of J/k values and $|J'/J|$ for compounds $M(N_2H_5)_2(SO_4)_2$ obtained from several methods

Compound	Susceptibility results: Theoretical model	J/k from $T_{max}^{(\chi)}$ (K)	J/k from χ_{max} (K)	J/k from best fit (K)	Specific heat results: J/k from $T_{max}^{(C)}$ (K)	J/k from best fit (K)	J/k from ESR line width	Estimated value of J/k (K)	$\|J'/J\|$
$Ni(N_2H_5)_2(SO_4)_2$	Heisenberg model	- 3.2 (1)	-3.4 (1)	-3.35 (5)	- 2.0 (1)	-2.7 (1)	-	≈-3.3	$<1\times10^{-2}$
$Mn(N_2H_5)_2(SO_4)_2$	interpolation scheme	- 0.49(1)	-0.585(5)	-0.590(5)	- 0.45(5)	-	-		
	scaling method	- 0.59(1)	-0.620(5)	-0.615(5)	-	-	-	-0.55(5)	3×10^{-2}
	10/3 effect	-	-	-	-	-	0.52(8)		
$Cu(N_2H_5)_2(SO_4)_2$	Heisenberg model	- 1.65(5)	-2.10 (5)	-2.00 (5)	- 1.87	-	-	-1.9 (1)	$<1.5\times10^{-1}$
$Fe(N_2H_5)_2(SO_4)_2$	interpolation scheme	- 2.22(4)	-	≈-2.2	- 2.90	-			
	scaling method	- 2.59(5)	-	-	-	-	-	≈-2.5	3×10^{-2}
	Ising model	- 2.04(4)	-	-	-	-3.28	-		
$Co(N_2H_5)_2(SO_4)_2$	XY model	- 8.9 (3)	-	-	- 6.7				
	Heisenberg model	- 4.5 (1)	-5.40 (5)	-	- 4.47	-	-	≈-7	1×10^{-2}
	Ising model	-11.5 (3)	-	-	-10.3	-			

We will first try to describe the magnetic properties of $Fe(N_2H_5)_2(SO_4)_2$ within the Heisenberg model applied to antiferromagnetic chains with S=2 (in this model D is neglected). By means of the interpolation scheme of Weng (7), described in Section IV-2.2, theoretical suceptibility and specific heat curves for such chains are calculated. For χ_{max} and $T_{max}(\chi)$ the relations

$$kT_{max}(\chi)/|J| = 6.9 \quad (14) \text{ and}$$

$$|J|\chi_{max}/Ng^2\beta^2 = 0.0937 \quad (15)$$

are derived.

Theoretical susceptibility curves are also obtained by applying eq. (14) of the scaling method, also described in Section IV-2.2, to the case S=2. This method yields

$$kT_{max}(\chi)/|J| = 5.9 \quad (16) \text{ and}$$

$$|J|\chi_{max}/Ng^2\beta^2 = 0.1004 \quad (17).$$

Because the latter approximation method becomes poorer for smaller spin values, eq. (14) and (15) are probably more reliable than eq. (16) and (17).

With eq. (14) and (16) and the experimental value of $T_{max}(\chi)$ (Table IV-1) the values $J/k = -(2.22 \pm 0.04)K$ and $J/k = -(2.59 \pm 0.05)K$ are calculated respectively (Table IV-2). The spectroscopic splitting factor g of $Fe(N_2H_5)_2(SO_4)_2$ is not known, but is usually anisotropic for Fe^{2+} compounds. Hence eq. (15) and (17) cannot be used. For these relations also another problem arises because the Van Vleck paramagnetism probably cannot be neglected for the Fe compound. With our data it is not possible to determine the contribution of this effect to the total susceptibility. It is clear, however, that, corrected for the Van Vleck term, the value of χ_{max} will become smaller. Neglecting the Van Vleck contribution and trying to fit the high-temperature part of the experimental susceptibility curve by means of the interpolation scheme, only very poor fits are found for J/k in the range -(2.2-2.3)K and g in the range 3.1-3.2.

The magnetic anisotropy of the Fe compound motivates the use of the Ising model. For the interpretation of the experimental data one can consider, therefore, the following Hamiltonian:

$$H = -2J \sum_{<i,j>} S_i^z S_j^z + D \sum_i (S_i^z)^2,$$

where D is the crystal-field splitting parameter. In the case that the magnitude of D is comparable to J, the mathematics of the model become intractable. To obtain an estimate of J, we have neglected, therefore, the crystal-field splitting and apply the Ising model with S=2. Within the Ising model no results were known for the parallel susceptibility $\chi_{//}$ of linear chains with S=2 (magnetic field parallel to the axis of anisotropy). Therefore $\chi_{//}$ is calculated by means of a matrix method described in literature (37) and used before by Wagner and Friedberg (21) for the case S=5/2.

The partition function of an Ising chain with n spins is given by $Z=Tr(P)^n$ where P is the symmetric matrix

$$P_{S_z S_z'} = \exp\left[\frac{2J}{kT} S_z S_z' - \frac{g\beta H}{kT} (S_z + S_z')\right].$$

In approximation the partition function is given by $Z = [\lambda(P)]^n$ with $\lambda(P)$ = largest eigen value of matrix P. For any case with specific S-, J/k-, and g-value, $\chi_{//}$ can be obtained numerically by computer calculations of $\lambda(P)$ and $\partial[\lambda(P)]/\partial H$, using the relation

$$\chi = \lim_{H \to 0} \frac{kT}{H} \frac{\partial(\ln Z)}{\partial H} .$$

From the numerical results obtained for S=2 and a set values of J/k and g the theoretical curve in which the dimensionless quantity $|J|\chi_{//}/Ng^2\beta^2$ is given as a function of the dimensionless quantity $kT/|J|$, is composed (fig. IV-6). In this curve

$$kT_{max}(\chi)/|J| = 7.5 \quad (18) \text{ and}$$

$$|J|\chi_{max}/Ng^2\beta^2 = 0.1009 \quad (19).$$

The validity of this method is supported by the very good agreement between the $\chi_{//}$ curves for S=1 and 3/2, obtained in the way described above, and the curves obtained by Suzuki et al. (38) for Ising chains with the same spin values.

Describing now the linear chains in $Fe(N_2H_5)_2(SO_4)_2$ with the Ising model, the value $J/k = -(2.04 \pm 0.04)K$ is found by means of eq. (18) (Table IV-2). But if J/k is calculated in this way an error is introduced because the powder susceptibility curve is made up of $\chi_{//}$ and $\chi_{\perp}$ (magnetic field perpendicular to the direction of anisotropy). Unfortunately, for $\chi_{\perp}$ of Ising chains a theoretical result (39) is only known for spin S=1/2. For S=2 nothing definite can be said about the influence of $\chi_{\perp}$ on the behaviour of the susceptibility curve.

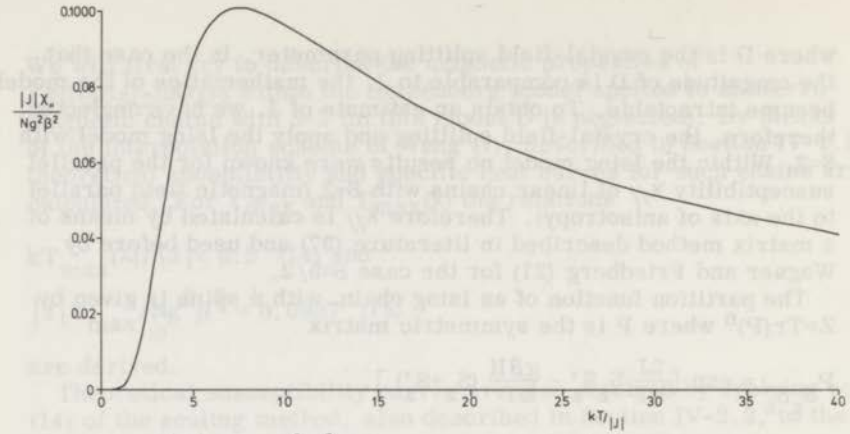

Fig. IV-6 $|J|\chi_{//}/Ng^2\beta^2$ as a function of $kT/|J|$ for an antiferromagnetic Ising linear-chain system with S=2

Again, relation (19) cannot be used because the g-value and the Van Vleck paramagnetism are unknown.

The specific heat measurements (1) give the experimental values $T_{max}(C) = 12.3K$ and $C_{max}/R = 0.96$. From the specific heat data no indications are found that D is much larger than J. Therefore, the possibility that the magnetic system of the compound can be described by the Ising model with effective spin S=1/2 can probably be excluded. For the antiferromagnetic Heisenberg linear-chain system with S=2 the interpolation scheme yields the relations $C_{max}/R = 0.67$ and $kT_{max}(C)/|J| = 4.25$. For antiferromagnetic Ising chains with S=2 it is known (40) that $C_{max}/R = 1.48$ and $kT_{max}(C)/|J| = 3.75$. So the experimental value of C_{max}/R lies between the theoretical values of the Heisenberg and Ising model, which is probably an indication that the character of the chain system in $Fe(N_2H_5)_2(SO_4)_2$ is intermediate between the two models. The experimental value of $T_{max}(C)$ gives $J/k = -2.90K$ and $J/k = -3.28K$ for the Heisenberg and Ising model respectively.

Summarizing all results obtained for J/k in the different theoretical models, it seems reasonable to estimate the value $J/k = -(2.5 \pm 0.5)K$ for the intra-chain coupling. Without more experimental data and more sophisticated theoretical approximation methods it is not possible to calculate a more precise result.

For $Fe(N_2H_5)_2(SO_4)_2$ a reasonably trustworthy value of the transition temperature T_N at which 3D ordering sets in, can be obtained from the susceptibility data, because for linear-chain compounds

there are reasons to believe (41) that in the powder susceptibility curve T_N occurs at the maximum value of $\partial\chi/\partial T$ (arguments for this assumption were discussed in Chapter III-2.3). In fig. IV-5 this maximum is located at $T_N=(5.5\pm0.5)K$. This value is confirmed by the specific heat measurements, that revealed a transition temperature $T_N=5.9K$.

IV-2.5 $Co(N_2H_5)_2(SO_4)_2$

The experimental susceptibility curve of $Co(N_2H_5)_2(SO_4)_2$ is depicted in fig. IV-7. The susceptibility appeared to be field independent up to about 10 kOe. The results quoted refer to measurements at about 3 kOe. The broad maximum is noticed again and the high-temperature part of the reciprocal susceptibility curve obeys the Curie-Weiss law with $\theta=-(22\pm1)K$.

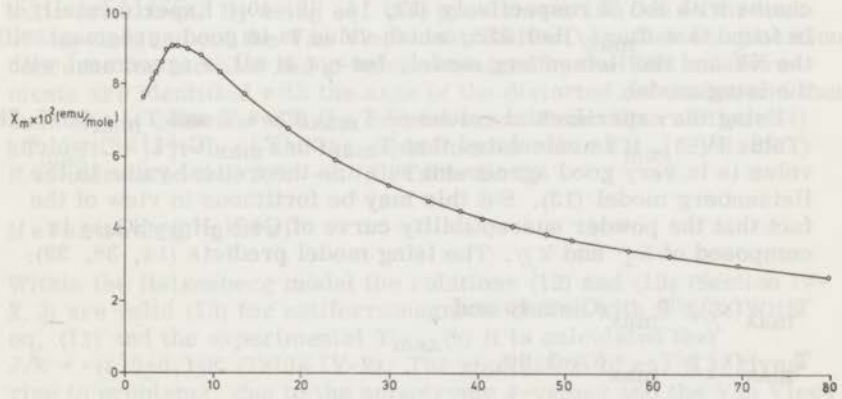

Fig. IV-7 Molar susceptibility χ_m of $Co(N_2H_5)_2(SO_4)_2$ as a function of temperature; o = experimental points. A smooth curve is drawn through the experimental points

In a cubic octahedral field the ^4F orbital state of the free Co^{2+} ion splits into three levels of which the lowest level ^4T, is triply degenerate. Under the action of an axial or rhombic distortion of the crystal field in combination with spin-orbit coupling the ^4T level splits into six Kramers doublets (42), causing the ground state of the Co^{2+} ion to be a doublet. Usually the splitting between the lowest lying doublets is so large that at low temperatures an effective spin $S=1/2$ can be used for the description of the spin system of Co^{2+}

compounds with the Co ions in a distorted octahedral coordination, as is also the case for $Co(N_2H_5)_2(SO_4)_2$. From the entropy at low temperatures, determined by the specific heat measurements, an effective spin S=1/2 is indeed found. Furthermore, one derives from the specific heat measurements that the splitting between the two lowest lying doublets is about 180K, so that the contribution of the Van Vleck term to the susceptibility cannot be neglected.

Due to the pronounced anisotropic character of many Co^{2+} compounds the Ising model is often used to describe the magnetic properties (23). However, the results of the specific heat measurements of $Co(N_2H_5)_2(SO_4)_2$ indicate that for this compound the Heisenberg and XY model (see Chapter I-1) cannot be excluded in the first instance in the theoretical description (vide infra).

From theoretical calculations it has been found that $C_{max}/R=0.326$, 0.350 and 0.445 for the XY, Heisenberg and Ising model of linear chains with S=1/2 respectively (13, 14, 38, 40). Experimentally it is found that $C_{max}/R=0.325$, which value is in good agreement with the XY and the Heisenberg model, but not at all in agreement with the Ising model.

Using the experimental values of $T_{max}(C)=4.3$ and $T_{max}(\chi)=5.7K$ (Table IV-1), it is calculated that $T_{max}(\chi)/T_{max}(C)=1.33$, which value is in very good agreement with the theoretical value in the Heisenberg model (13). But this may be fortituous in view of the fact that the powder susceptibility curve of $Co(N_2H_5)_2(SO_4)_2$ is composed of $\chi_\perp$ and $\chi_{//}$. The Ising model predicts (14, 38, 39):

$T_{max}(\chi_{//})/T_{max}(C)=2.40$ and

$T_{max}(\chi_\perp)/T_{max}(C)=1.00$.

It is possible, therefore, that a mixture of both ratios gives a value for $T_{max}(\chi_{powder})/T_{max}(C)$ that is in accordance with the value obtained from the Heisenberg model.

ESR measurements carried out at liquid hydrogen temperature on a sample of the compound $Zn(N_2H_5)_2(SO_4)_2$ doped with about 1% Co^{2+}, revealed the following values of the g-components:

$g_1=2.20\pm0.01$ $g_2=4.40\pm0.02$ $g_3=5.45\pm0.02$,

which values will probably not differ very much from the g-values of the undiluted compound $Co(N_2H_5)_2(SO_4)_2$. From the difference in magnitudes of the g-values it is obvious that a considerable anisotropy is present. It may be noted that one g-value is relatively small and the other two g-values are much larger. This fact in combination with the experimental value of C_{max}/R (see above) indicates

that the XY model could be the appropriate model to describe the magnetic properties of $Co(N_2H_5)_2(SO_4)_2$. Besides this model also the Heisenberg and Ising model will be used for the interpretation.

XY model

Calculations on basis of this model (14, 23) give

$kT_{max}(\chi_\perp)/|J| = 0.64$ (20) and

$|J|\chi_{max}(\perp)/Ng^2\beta^2 = 0.174$ (21).

Combining the experimental value of $T_{max}(\chi)$ with eq. (20) yields $J/k = -(8.9\pm0.3)K$ (Table IV-2), but in this way the contribution of $\chi_{//}$ to χ_{powder} is neglected. However, for $\chi_{//}$ no theoretical results are known. By using eq. (21) problems arise due to the lack of knowledge about the Van Vleck contribution. Another complication concerns the fact that the g-values obtained by the ESR measurements are identified with the axes of the distorted octahedra and these axes do not coincide with the crystal axes. From the relation (14) $kT_{max}(C)/|J| \approx 0.64$ and the experimental value $T_{max}(C)=4.3K$ it is calculated that $J/k=-6.7K$ (Table IV-2).

Heisenberg model

Within the Heisenberg model the relations (12) and (13) (Section IV-2.3) are valid (13) for antiferromagnetic chains with S=1/2. With eq. (11) and the experimental $T_{max}(\chi)$ it is calculated that $J/k = -(4.5\pm0.1)K$ (Table IV-2). The application of eq. (13) gives rise to problems, due to the anisotropic g-values and the Van Vleck term. Neglecting the Van Vleck term and using the experimental value of χ_{max} (Table IV-1) and the g-value $g_{av} = [\frac{1}{3}(g_1^2+g_2^2+g_3^2)]^{\frac{1}{2}} = 4.23$, the intra-chain interaction is calculated to be $J/k=-5.40K$. If the χ-curve were corrected for the Van Vleck contribution, $\chi_{max}(exp.)$ would be lower and $|J/k|$, therefore, higher.

A theoretical fit with the experimental curve was not found within the Heisenberg model.

From the experimental $T_{max}(C)$ and the relation (13) $kT_{max}(C)/J = 0.962$ the value $J/k = -4.47K$ is obtained (Table IV-2).

Ising model

If we want to describe the powder susceptibility curve with the Ising model $\chi_{//}$ as well as $\chi_{\perp}$ have to be taken into account. For $\chi_{//}$ it is calculated theoretically (13) that

$kT_{max}(\chi_{//})/|J| = 1$ (22) and

$|J|\chi_{max}(\perp)/Ng^2\beta^2 = 0.09197$ (23).

For $\chi_{\perp}$ one knows (39) that

$kT_{max}(\chi_{\perp})/|J| = 0.4186$ (24 and

$|J|\chi_{max}(\perp)/Ng^2\beta^2 = 0.2999$ (25).

From relations (22) and (24) the values $J/k = -5.7K$ and $J/k = -13.6K$ are obtained. In a powder susceptibility curve $T_{max}(exp)$ will lie between $T_{max}(exp.)$ of $\chi_{\perp}$ and $T_{max}(exp.)$ of $\chi_{//}$, so that the real value of J/k would lie between -5.7K and -13.6K. The averaged value $J/k = -9.7K$ of these two results provides a rough estimate of the exchange interaction. Due to reasons mentioned above the use of eq. (23) and (25) gives rise to problems again.

By means of the results (13, 39) for $\chi_{//}$ and $\chi_{\perp}$, as calculated in the Ising model with S=1/2:

$\chi_{//} = (Ng^2\beta^2/4kT) \exp(-|J|/kT)$ (26)

$\chi_{\perp} = (Ng^2\beta^2/4|J|)(\tanh(|J|/2kT) + (|J|/2kT) \operatorname{sech}(|J|/2kT)$ (27)

and the formula $\chi_{powder} = \frac{1}{3}\chi_{//} + \frac{2}{3}\chi_{\perp}$ (28), we have tried to find a best fit with the experimental susceptibility curve. However, this was not feasible. Of course the Van Vleck contribution plays a role here. Also the discrepancy between the real magnetic system and the Ising model may be too large to justify the use of the pure Ising system. But it was possible with eq. (26), (27) and (28) to obtain agreement between the theoretical value of $T_{max}(\chi)$ and the experimental value (Table IV-1) for $J/k \approx -11.5K$ (Table IV-2) and $g \approx 3.5$.

By means of the experimental value of $T_{max}(C)$ and the relation $kT_{max}(C)/|J| = 0.416$, as found for the Ising model (14, 39, 40) we derive $J/k = -10.3K$ (Table IV-2).

Summarizing, we believe, particularly from the specific heat and ESR measurements, that the XY model gives the best approximation

for the magnetic system in $Co(N_2H_5)_2(SO_4)_2$ and that, therefore, $J/k \approx -7$ to -8K (Table IV-2). But our measurements do not give sufficient information to put this assumption on sound footing.

Finally it may be mentioned that the specific heat measurements on $Co(N_2H_5)_2(SO_4)_2$ showed a magnetic transition point at 1.57K, indicating that the inter-chain coupling is much weaker than the intra-chain coupling.

IV-3 Intra- and inter-chain interaction

Summarizing all results obtained on the various $M(N_2H_5)_2(SO_4)_2$ compounds, it is concluded that for the Mn and Cu compound reliable values for the intra-chain interaction are obtained. For the Ni compound the results of susceptibility and specific heat measurements show large differences that possibly can be explained by the presence of a single-ion anisotropy of the same order of magnitude as J. The J/k-value calculated from the susceptibility data seems to give a reasonable estimate. For the Fe and Co compounds no precise values of J/k can be derived because both compounds are probably examples of magnetic systems intermediate between the Heisenberg and Ising model and between the Heisenberg and XY model respectively. Estimates about the order of magnitude of J/k are given in Table IV-2, together with the J/k-values of the other compounds.

The question arises, what is the origin of the relatively strong intra-chain coupling, in spite of the presence of three intervening non-magnetic ligands in the most probable superexchange path in the chains: M-O-S-O-M. Usually such a number of intervening ligands allows only a very weak interaction.

This long range superexchange mechanism is probably of the same nature as is found in $LiMnPO_4$ (43) (superexchange path Mn-O-P-O-Mn), $LiCuVO_4$ (44) (superexchange path Cu-O-V-O-Cu) and in a number of other compounds which have been reviewed by Blasse (45). It can be explained by assuming strongly covalent S-O bonds, due to the high electron affinity of the S^{6+} ion in the $(SO_4)^{2-}$ group.

The specific heat and susceptibility data indicate that the inter-chain coupling is much weaker than the intra-chain coupling. This is probably due to the weak hydrogen bonds that form the links between the N_2H_5 groups and SO_4 groups of neighbouring chains. About the ratio between the inter-chain coupling J' and the intra-chain coupling J the following can be remarked.

Oguchi has calculated (46) by means of Green function techniques an approximate, numerical relation between the transition point T_N of an antiferromagnetic Heisenberg linear-chain system (with general

spin S and inter-chain coupling J') and the ratio $|J'/J|$ for a tetragonal lattice structure (see also Chapter III-2.3 and fig. III-6). By means of these results information about the magnitude of the ratio $|J'/J|$ is obtained, using the experimentally determined T_N-values. This method can only give an order of magnitude estimate in our case since the crystal structure of the $M(N_2H_5)_2(SO_4)_2$ compounds is triclinic and several of the compounds cannot be described by the Heisenberg model. Another complication is that the inter-chain interactions along the a- and c-axes are probably not equal, due to the difference between the lengths of these axes (ratio between the lengths ≈ 0.8).

Using (a) the experimentally determined T_N-values for the Mn, Fe and Co compound (b) the fact that for the Ni and Cu compound no transition point is detected down to 1.5K, and (c) the J/k-values, which are estimated for the different compounds (Table IV-2), the rations $|J'/J|$, given in Table IV-2, are obtained. It is seen clearly that $|J'| \ll |J|$.

The main conclusion to be drawn from these numbers is that J' is very much smaller than J, so that the analysis in terms of linear-chain models is very appropriate for these compounds.

References

1. F.W. Klaaijsen and F. Dokoupil, to be published
2. C.K. Prout and H.M. Powell, J. Chem. Soc. 1961, 4177 (1961)
3. D.W. Hand and C.K. Prout, J. Chem. Soc. A1966, 168 (1966)
4. A. Nieuwpoort and J. Reedijk, J. Inorg. Chim. Acta, in press
5. P.W. Selwood, Magnetochemistry, Interscience Publishers, Inc. New York (1956).
6. I. Dzualoshinsky, J. Phys. Chem. Solids 4, 241 (1958)
7. T. Moriya, Phys. Rev. 120, 91 (1960)
8. A.P. Ginsberg, R.L. Martin and R.C. Sherwood, Inorg. Chem. 11, 2884 (1972)
9. F.W. Klaaijsen, J. Reedijk and H.T. Witteveen, Z. Naturf. 27a, 1532 (1972)
10. N. Achiwa, J. Phys. Soc. Jap. 27, 561 (1969)
11. J. Smith, B.C. Gerstein, S.H. Liu and G. Stucky, J. Chem. Phys. 53, 418 (1970)
12. M. Mekata, K. Adachi, H. Takaki and N. Achiwa, Proc. 12th Int. Conf. Low. Temp. Kyoto, p. 801 (1970)
13. J.C. Bonner and M.E. Fisher, Phys. Rev. 135, A640 (1964)
14. S. Katsura, Phys. Rev. 127, 1508 (1962)
15. S. Inawashiro and S. Katsura, Phys. Rev. 140, 892 (1965)
16. R.B. Griffiths, Phys. Rev. 133, A768 (1964)

17. T. Haseda and H. Kobayashi, J. Phys. Soc. Jap. 19, 1260 (1964)
18. M. Matsuura, Phys. Letters, 34A, 274 (1971)
19. M.E. Fisher, Am. J. Phys., 32, 343 (1964)
20. G.S. Rushbrooke and P.J. Wood, Mol. Phys. 1, 257 (1958)
21. G.R. Wagner and S.A. Friedberg, Phys. Letters 9, 11 (1964)
22. F. Smith and S.A. Friedberg, Phys. Rev. 176, 660 (1968)
23. L.J. de Jongh and A.R. Miedema, Advances in Physics, in press
24. L.C. Jackson, Proc. Roy. Soc. (London), A140, 695 (1933)
25. L.C. Jackson and H. Kamerlingh Onnes, Proc. Roy. Soc. (London), A104, 671 (1923)
26. M. Date, J. Phys. Soc. Jap. 12, 1314 (1957)
27. M. Leconte, J. de Gunzbourg, M. Feyral, A. Meedan-Gros and G. Allain, Solid State Commun. 10, 235 (1972)
28. J. Skalyo jr. and G. Shirane, Phys. Rev. B2, 4632 (1970)
29. V.J. Minckiewicz, D.E. Cox and G. Shirane, Solid State Commun. 8, 1001 (1970)
30. R. Kubo and K. Tomita, J. Phys. Soc. Jap. 9, 888 (1954)
31. E.J. Pleau and G.F. Kokoszka, Inorg. Nucl. Chem. Letters 8, 779 (1972)
32. T. Moriya, Progr. Theor. Phys. 16, 23 (1956)
33. R.D. Dowsing, B. Nieuwenhuijse and J. Reedijk, Inorg. Chim. Acta 5, 301 (1971)
34. S. Hillaert, to be published
35. K. Inomata and T. Oguchi, J. Phys. Soc. Jap. 23, 765 (1967)
36. J.S. Griffith, The theory of transition-metal ions, p. 357, Cambridge University Press (1961)
37. G.F. Newell and E.W. Montroll, Revs. Mod. Phys. 25, 353 (1953)
38. M. Suzuki, B. Tsujiyama and S. Katsura, J. Math. Phys. 8, 124 (1967)
39. M.E. Fisher, J. Math. Phys. 4, 124 (1963)
40. T. Obakata and T. Oguchi, J. Phys. Soc. Jap. 25, 322 (1968)
41. L.J. de Jongh, private communication
42. A. Abragham and M.H.L. Pryce, Proc. Royal Soc. (London), A206, 173 (1951)
43. J.M. Mays, Phys. Rev. 131, 38 (1963)
44. H. Saji, J. Phys. Soc. Jap. 33, 671 (1972)
45. G. Blasse, Philips Res. Repts. 20, 327 (1965)
46. T. Oguchi, Phys. Rev. 133, A1098 (1964)

CHAPTER V - LINEAR-CHAIN ANTIFERROMAGNETISM IN THE COMPOUNDS MnX_2L_2 WITH X=Cl, Br AND L=PYRAZOLE, PYRIDINE

V-1 Introduction

As part of an experimental study on magnetic interactions in coordination compounds, which may be expected to show properties of magnetic linear-chain systems, we have investigated a group of compounds having the general formula MX_2 (ligand)$_2$ with M=Mn^{2+}, Fe^{2+}, Ni^{2+}, Cu^{2+} and X=Cl, Br and as ligands pyrazole ($N_2C_3H_4$) and pyridine (NC_5H_5).

Ligand field spectra and infrared spectra of several of these compounds indicate octahedral geometry for the metal ions with unidentate, non-bridging ligands. The halide ions form the bridges between the metal ions (1-3). On basis of this geometry one expects the octahedra to share edges of halogen ions, so that chains of M ions are formed, separated by the ligands. Hence, it may be conjectured that the inter-chain interaction is much weaker than the intra-chain interaction.

In this chapter results for the compounds MnX_2L_2 are reported. The preparation method of these compounds was already discussed in Chapter II-2.10, where also the results of the chemical analysis of the samples used for the susceptibility measurements are listed (Table II-8).

For the compound $MnCl_2(pz)_2$ (pz=pyrazole) a single crystal X-ray investigation has been carried out, of which the details will be published elsewhere (4). In this chapter only some preliminary results are mentioned, that confirm the expectations about the crystal structure (fig. V-1a). The cell parameters of the chemical unit cell are a=18.26Å, b=3.76Å, c=13.84Å, α=90°, β=94.8° and γ=90° (monoclinic structure). The Mn ions are located at the positions (0,0,1/4), (0,0,3/4), (1/2, 1/2, 1/4) and (1/2, 1/2, 3/4). Along the c-axis a two-fold axis is found. The space-group is C2/c. It is noticed that along the b-axis chains of di-chloride bridged Mn^{2+} ions are formed (fig. V-1b; in fig. V-1a the Cl^- ions are omitted) and that the distance between nearest Mn neighbours in adjacent chains is much larger than the distance between nearest Mn neighbours within the chains.

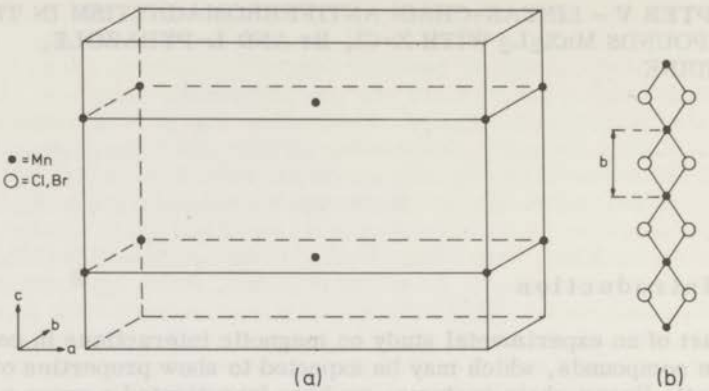

Fig. V-1a Illustration of the structure of $MnCl_2(pz)_2$
Fig. V-1b Di-chloride bridged Mn^{2+} chains formed along the b-axis in the structure of $MnCl_2(pz)_2$

X-ray powder diffraction patterns reveal that the compounds $MnBr_2(pz)_2$, $MnCl_2(py)_2$ and $MnBr_2(py)_2$ (py=pyridine) are isomorphous with $MnCl_2(pz)_2$.

To investigate the character of the magnetic interactions in these compounds susceptibility, heat capacity and paramagnetic resonance experiments have been carried out. The heat capacity results are mentioned only briefly and will be published elsewhere (5).

V-2 Results and discussion

V-2.1 Susceptibility and specific heat

The observed susceptibility versus temperature curves of the compounds, corrected for diamagnetism according to the tables of Selwood (6), are shown in fig. V-2-5. In the high-temperature region the suceptibility curves obey Curie-Weiss relations having a negative asymptotic Curie temperature θ (Table V-1). The result of the crystal structure investigations and the appearance of a broad maximum in the χ-curves provide evidence that the compounds are antiferromagnetic linear-chain systems.

Because of the isotropic character of the Mn^{2+} ions (S-state ions) the Heisenberg model is appropriate for the theoretical description of the magnetic behaviour. Within the Heisenberg model two theoretical approximations are known to describe antiferromagnetic linear

Table V-1. Experimental quantities of the compounds MnX_2L_2 obtained from susceptibility and heat capacity measurements

Compounds	$\chi_{max} \times 10^2$ (emu/mole)	$T_{max}(\chi)$ (K)	C_{max}/R	$T_{max}(C)$ (K)	θ (K)	T_N (K)	$T_{max}(\chi)/T_N$
$MnCl_2(pz)_2$	16.8(2)*	6.5(2)	$\approx$0.99	3.25	-12(1)	<1.3	>5
$MnBr_2(pz)_2$	16.3(2)	6.3(2)	$\approx$0.88	$\approx$3.1	-13(1)	1.9	3.3
$MnCl_2(py)_2$	26.3(3)	4.0(2)	$\approx$0.87	$\approx$2.2	- 9(1)	1.4	2.8
$MnBr_2(py)_2$	20.3(2)	4.7(2)	-	-	-11(1)	2.05	2.3

* The values between parentheses indicate the experimental uncertainty

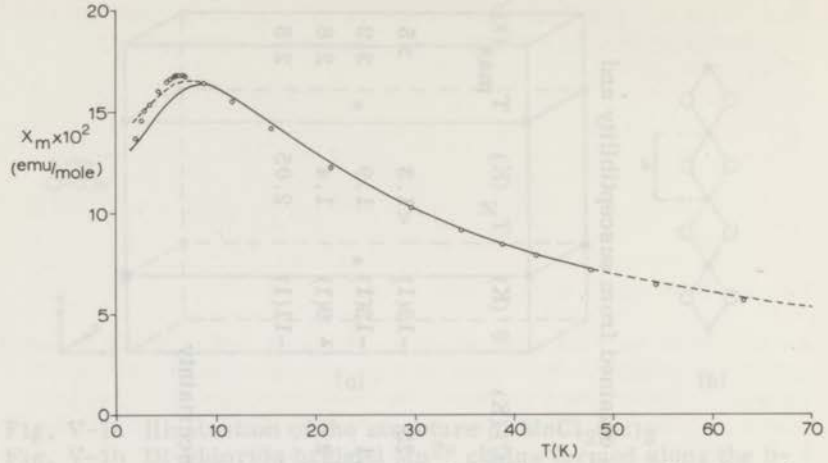

Fig. V-2 Molar susceptibility χ_m of $MnCl_2(pz)_2$ as a function of temperature. o = experimental data. ___ : best fit according to Weng's interpolation scheme. --- best fit according to the scaling method

chains with S=5/2, viz. the scaling method of Wagner and Friedberg (7) and the interpolation scheme developed by Weng (8). These methods were already discussed in Chapter IV-2.2 in order to apply them to the antiferromagnetic linear-chain compound $Mn(N_2H_5)_2(SO_4)_2$. For convenience the results of these approximation methods are reported briefly. In the scaling method the molar susceptibility χ_m is described by the expression

$$\chi_m = \frac{Ng^2\beta^2 S(S+1)}{3kT} \cdot \frac{1+U(K)}{1-U(K)} \quad (1), \text{ where}$$

$U(K) = \coth(K) - 1/K$ and $K = 2JS(S+1)/kT$

The maximum in the susceptibility χ_{max}, and the temperature $T_{max}(\chi)$, where the maximum occurs, are related to the intrachain coupling for the case S=5/2 by the equations:

$|J|\chi_{max}/Ng^2\beta^2 = 0.1004$ (2) and

$kT_{max}(\chi)/|J| = 8.2$ (3).

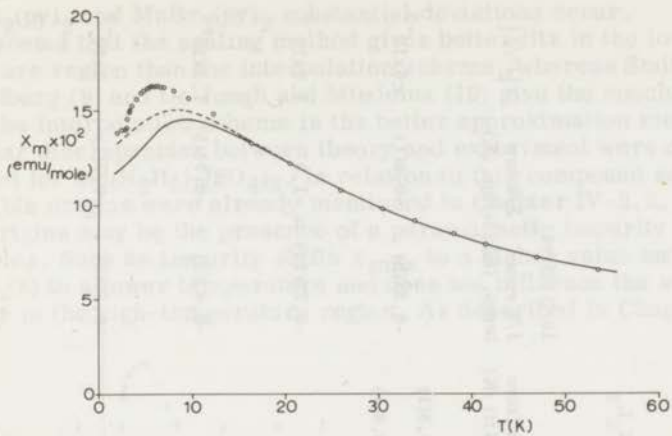

Fig. V-3 Molar susceptibility χ_m of $MnBr_2(pz)_2$ as a function of temperature. o = experimental data.——: best fit according to the interpolation scheme. ---: best fit according to the scaling method

By means of the interpolation scheme of Weng the following relations are found:

$|J|\chi_{max}/Ng^2\beta^2 = 0.0949$ (4) and

$kT_{max}(\chi)/|J| = 9.8$ (5)

Within these two approximations the best fits of the theoretical curve to the high-temperature part of the experimental curve of the compounds are obtained for the J/k-values listed in Table V-2. For these fits is was assumed that, as usual for Mn^{2+} compounds, g=2.00. The J/k-values that are calculated by means of eq. (2), (3) and eq. (4), (5) and the experimental values of χ_{max} and $T_{max}(\chi)$ (Table V-1) are also given in Table V-2.

Just as for the compound $Mn(N_2H_5)_2(SO_4)_2$ (Chapter IV-2.2), discrepancies are noticed between the J/k-values obtained from the best fits and the J/k-values derived from χ_{max} and $T_{max}(\chi)$. Therefore, deviations also exist between the extension of the best fits in the high-temperature region to lower temperatures and the experimental susceptibility around $T_{max}(\chi)$. For $MnCl_2(pz)_2$ the differences between experimental and theoretical results in the region around $T_{max}(\chi)$ are not so large, but especially for

Table V-2. Intra- and inter-chain exchange interaction in the compounds MnX_2L_2

Compound		Susceptibility			specific heat		10/3 effect		
		J/k from $T_{max}^{(\chi)}$ (K)	J/k from χ_{max}(K)	J/k from best fit (K)	J/k from T_{max}(C) (K)	J/k from best fit (K)	J/k room temp. (K)	J/k low temp. (K)	$\lvert J'/J \rvert$
$MnCl_2(pz)_2$	scaling method	-0.79(2)	-0.90(1)	-0.91(2)	-	-0.8(1)	-0.52(8)	-0.6(1)	$<6\times10^{-3}$
	interpol. scheme	-0.66(2)	-0.85(1)	-0.87(2)	-0.58(2)	-0.8(1)			
$MnBr_2(pz)_2$	scaling method	-0.77(2)	-0.92(1)	-1.00(2)	-	-	-0.75(10)	≈ -1.0	1.2×10^{-2}
	interpol. scheme	-0.64(2)	-0.88(1)	-0.98(2)	-0.55	-			
$MnCl_2(py)_2$	scaling method	-0.49(2)	-0.58(1)	-0.70(2)	-	-	-0.43(5)	-0.75(5)	1.3×10^{-2}
	interpol. scheme	-0.41(2)	-0.54(1)	-0.69(2)	-0.40	-			
$MnBr_2(py)_2$	scaling method	-0.57(2)	-0.74(1)	-0.86(2)	-	-	-0.50(5)	-0.7(1)	2×10^{-2}
	interpol. scheme	-0.48(2)	-0.70(1)	-0.85(2)	-	-			

$MnCl_2(py)_2$ and $MnBr_2(py)_2$ substantial deviations occur.

It seems that the scaling method gives better fits in the low-temperature region than the interpolation scheme, whereas Smith and Friedberg (9) and De Jongh and Miedema (10) give the conclusion that the interpolation scheme is the better approximation method. Similar discrepancies between theory and experiment were observed for $Mn(N_2H_5)_2(SO_4)_2$. In relation to this compound several possible origins were already mentioned in Chapter IV-2.2. One of the origins may be the presence of a paramagnetic impurity in the samples. Such an impurity shifts χ_{max} to a higher value and $T_{max}(\chi)$ to a lower temperature and does not influence the susceptibility in the high-temperature region. As described in Chapter

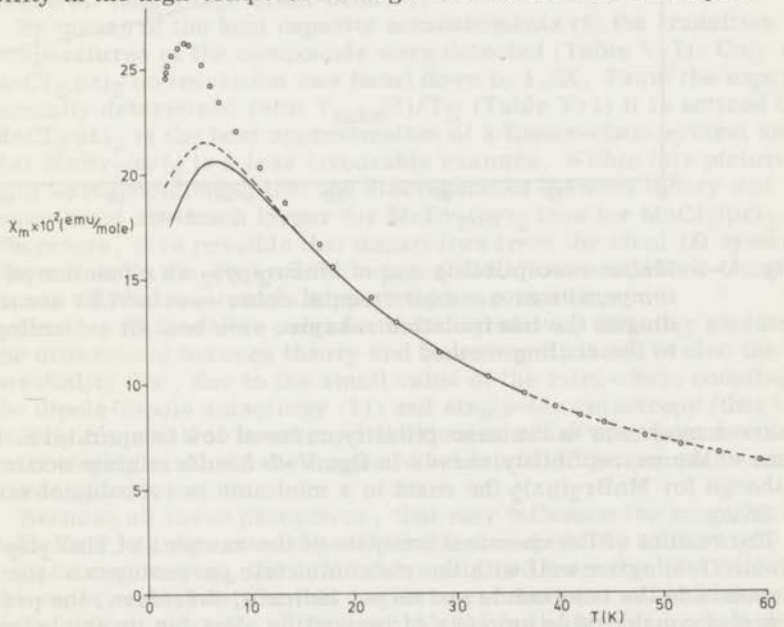

Fig. V-4 Molar susceptibility χ_m of $MnCl_2(py)_2$ as a function of temperature. o = experimental data. ——: best fit according to the interpolation scheme. ---: best fit according to the scaling method

III-2.2, where the influence of paramagnetic impurities on the susceptibility behaviour of the antiferromagnetic linear-chain compounds $ANiX_3$ (X = Cl, Br) is discussed, such an impurity may also

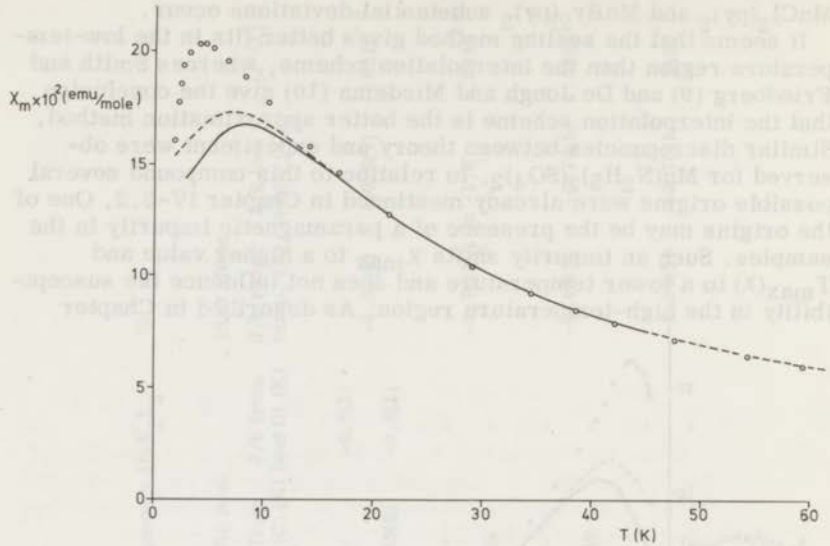

Fig. V-5 Molar susceptibility χ_m of $MnBr_2(py)_2$ as a function of temperature. o = experimental data. ——: best fit according to the interpolation scheme. ---: best fit according to the scaling method

cause a minimum in the susceptibility curve at low temperature. In none of the susceptibility curves in fig. V-2-5 such minima occur, although for $MnBr_2(pz)_2$ the onset to a minimum is probably observed at 3K.

The results of the chemical analysis of the samples of MnX_2L_2 (Table II-8) agree well with the stoichiometric percentages of the elements in the compounds and do not indicate, therefore, the presence of considerable amounts of impurities. But due to the large spin value S=5/2 of the Mn^{2+} ion it is possible that already small amounts of paramagnetic impurities with a low θ-value ($\theta \approx 0$) have a relatively strong influence on the susceptibility curve at low temperatures. One may try to correct the susceptibility data for the influence of a paramagnetic impurity having $\theta = 0$ by including the Curie-law $\chi = C/T$ in the right-hand side of eq. (1). But it appeared to be impossible in this way to find a theoretical fit (with J/k and C as variable parameters) with the experimental χ-curve in the low-temperature region. Thus, it is by no means sure that the dis-

crepancies are explained by the presence of paramagnetic impurities in the samples only.

As remarked in Chapter IV-2.2 another origin of the discrepancies may be the deviation of the ideal 1D magnetic system due to the possible presence of inter-chain interaction in the compounds, that causes a transition to 3D long-range order. For increasing ratio $|J'/J|$ (J' = inter-chain coupling parameter) the deviation from the 1D system increases and it may be expected that this causes the experimental χ-curve to depart from the theoretical χ-curve of 1D systems. A first indication for the magnitude of the deviation from the ideal 1D system is given by the ratio $T_{max}(\chi)/T_N$ (T_N = temperature, where 3D long-range order occurs).

By means of the heat capacity measurements (5) the transition temperatures of the compounds were detected (Table V-1). Only in $MnCl_2(pz)_2$ no transition was found down to 1.3K. From the experimentally determined ratio $T_{max}(\chi)/T_N$ (Table V-1) it is noticed that $MnCl_2(pz)_2$ is the best approximation of a linear-chain system and that $MnBr_2(py)_2$ is a less favourable example. Within this picture it is worth mentioning that the discrepancies between theory and experiment are much larger for $MnBr_2(py)_2$ than for $MnCl_2(pz)_2$. Therefore, it is possible that departures from the ideal 1D system play a role in the observed discrepancies. However, other experiments will be required to support this assumption.

Besides the possible origins mentioned above, that may explain the differences between theory and experiment, there is also the possibility that, due to the small value of the intra-chain coupling, the dipole-dipole anisotropy (11) and single-ion anisotropy (that is usually too small to be of any importance in Mn^{2+} compounds) start to play a role in the magnetic behaviour of the compounds at low temperatures.

Because all these phenomena, that may influence the magnetic behaviour, do not noticeably affect the susceptibility in the high-temperature region, the J/k-values obtained from the best fits to the experimental data in this region seem the most reliable ones.

To give an estimate of the ratio $|J'/J|$ in the Mn compounds discussed we use again the theory that has been developed by Oguchi on basis of Green function theory (12) and that was already discussed in Chapter III-2.3 (fig. III-6) and IV-3, although Oguchi's results apply strictly to a tetragonal lattice structure of coupled antiferromagnetic linear chains. Combining Oguchi's relation, the experimental T_N-values (Table V-1) and the J/k-values obtained from the best fits, we calculated the $|J'/J|$-values listed in Table V-2. These values show that, as was already remarked above, the inter-chain coupling increases with respect to the intra-chain coupling if going

from $MnCl_2(pz)_2$ to $MnBr_2(py)_2$.

The values of the maximum in the specific heat curves, C_{max}, and the temperature $T_{max}(C)$, where the maximum occurs (as obtained after correction for the lattice contribution to the specific heat) are given in Table V-1. These values could not be determined very accurately because the strong peaks that occur in the curves due to the transition to long-range order, partly overlap the broad maxima in the curves. For $MnBr_2(py)_2$ it was not even possible to obtain values of C_{max} and $T_{max}(C)$.

By means of the interpolation scheme of Weng (8) the theoretical relations

$$kT_{max}(C)/|J| = 5.6 \quad (6) \text{ and}$$

$$C_{max}/R = 0.71,$$

where R is the gas constant (R=8.31 J/mole K), are derived.

It is noticed that the experimental values of C_{max}/R (Table V-1) are higher than the theoretical value. Using eq. (6) and the experimental $T_{max}(C)$-values, the J/k-values listed in Table V-2 are calculated. Also the result for the best theoretical fit to the high-temperature part of the experimental specific heat curve of $MnCl_2(pz)_2$ is given (J/k=-(0.8±0.1)K). This value agrees with the J/k-value obtained from the best fit to the susceptibility curve. Furthermore, the J/k-values calculated from $T_{max}(\chi)$ and $T_{max}(C)$ show reasonable agreement.

When we compare for the various Mn compounds the J/k-values found from the best fits of the susceptibility, we find that the replacement of Cl^- ions by Br^- ions causes the exchange parameter J to increase. The same effect was noticed for the linear-chain compounds $ANiX_3$ with X = Cl, Br (Chapter III). This is another indication that superexchange via Br^- ions may be stronger than via Cl^- ions. The same effect is found when the ratios $|J'/J|$ within each pair of compounds $MnX_2(pz)_2$ and $MnX_2(py)_2$ (X = Cl, Br) are compared. Probably the halogen ions are also involved in the superexchange mechanism between neighbouring chains.

It is remarked that the intra-chain coupling parameters J/k of the various compounds do not differ much: $J/k \approx -0.7$ to -1.0K. Possibly these values are typical of di-halogen bridged Mn^{2+} ions. A confirmation for this idea is found in $MnCl_2.2H_2O$, which compound shows chains of di-chloride bridged Mn^{2+} ions having an intra-chain interaction J/k=-0.45K (13).

V-2.2 Electron paramagnetic resonance study

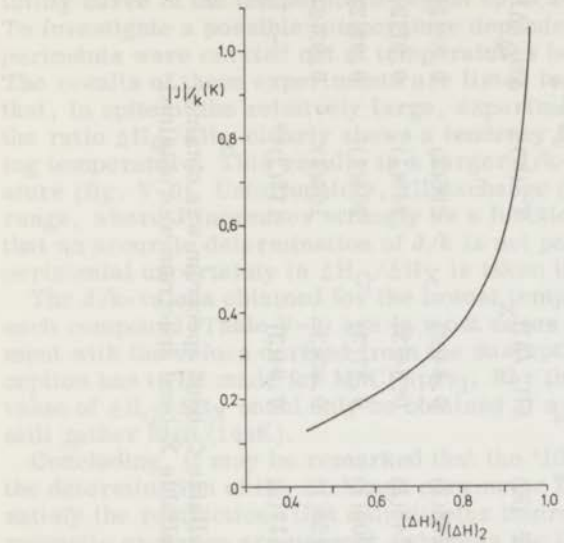

Fig. V-6 Relation between intra-chain interaction J/k and the ratio $\Delta H_1/\Delta H_2$ (ΔH_1 is the line-width of the ESR signal at Q-band frequency (35 GHz), ΔH_2 is the line-width at X-band frequency (9.2 GHz)) for the compounds MnX_2L_2 (S=5/2). The curve is computed according to the '10/3 effect'.

By means of a method, that was employed for the first time by Pleau and Kokoszka (14, 15) it was possible to determine the intra-chain interaction J/k from an electron paramagnetic resonance study (the so-called '10/3 effect'). This method was already described in Chapter IV-2.2. The compounds MnX_2L_2 satisfy the restrictions connected with this method: only dipolar interaction and isotropic magnetic exchange are allowed to be present, whereas the latter must be predominant. By means of eq. (10) and (11) in IV-2.2 (number of nearest magnetic neighbours in the chains is z=2 in eq. (11)) a relation is obtained between the ratio of the line-width of ESR signals recorded at X-band (9.2 GHz) and Q-band (35 GHz) frequency ($\Delta H_Q/\Delta H_X$) and the intra-chain exchange J/k. This relation is depicted in fig. V-6.

From the experiments at room temperature a J/k-value for each Mn compound was obtained, that was lower than the J/k-value de-

Table V-3. Results from ESR measurements at X- and Q-band frequency

$MnCl_2(pz)_2$		$MnBr_2(pz)_2$		$MnCl_2(py)_2$		$MnBr_2(py)_2$	
T (K)	$\Delta H_Q/\Delta H_X$	T (K)	$\Delta H_Q/\Delta H_X$	T (K)	$\Delta H_Q/\Delta H_X$	T (K)	$\Delta H_Q/\Delta H_X$
296(2)	0.88(3)	296(2)	0.94(2)	296(2)	0.84(3)	296(2)	0.88(2)
237(1)	0.86(3)	248(1)	0.93(2)	248(1)	0.84(3)	249(1)	0.91(2)
192(2)	0.86(3)	200(2)	0.95(2)	206(1)	0.87(3)	204(1)	0.92(2)
144(2)	0.91(3)	148(2)	0.97(2)	159(1)	0.93(3)	164(1)	0.93(2)
111(2)*	-	119(2)	1.01(2)	117(2)	0.94(3)	118(2)**	-

* no line-widt ratio could be determined because no reliable Q-band spectrum was obtained
** no line-widt ratio could be determined because no reliable X-band spectrum was obtained

termined from the best theoretical fit of the experimental susceptibility curve in the temperature region up to about 60K (Table V-2). To investigate a possible temperature dependence of J/k, ESR experiments were carried out at temperatures below room temperature. The results of these experiments are listed in Table V-3. It is seen that, in spite of the relatively large, experimental uncertainties, the ratio $\Delta H_Q/\Delta H_X$ clearly shows a tendency to increase at diminishing temperature. This results in a larger J/k-value at low temperature (fig. V-6). Unfortunately, all exchange parameters lie in the range, where J increases strongly as a function of $\Delta H_Q/\Delta H_X$, so that an accurate determination of J/k is not possible when the experimental uncertainty in $\Delta H_Q/\Delta H_X$ is taken into account.

The J/k-values obtained for the lowest temperature reached for each compound (Table V-2) are in most cases in reasonable agreement with the values derived from the susceptibility data. An exception has to be made for $MnCl_2(pz)_2$. For this compound a reliable value of $\Delta H_Q/\Delta H_X$ could only be obtained at a temperature that was still rather high (144K).

Concluding, it may be remarked that the '10/3 effect' is useful for the determination of the exchange parameter in Mn compounds that satisfy the restrictions that only dipolar interaction and isotropic magnetic exchange are present, whereas the latter is predominant.

References

1. J. Reedijk, Rec. Trav. Chim. 89, 605 (1970)
2. K. Takeda, S. Matsukawa and T. Haseda, J. Phys. Soc. Jap. 30, 1330 (1971)
3. J. Reedijk, J.C.A. Windhorst, N.H.M. van Ham and W.L. Groeneveld, Rec. Trav. Chim. 90, 234 (1971)
4. G.C. Verschoor and S. Gorter, to be published
5. F.W. Klaaijsen and F. Dokoupil, to be published
6. P.W. Selwood, Magnetochemistry, Interscience, New York (1956)
7. G.R. Wagner and S.A. Friedberg, Phys. Letters 9, 11 (1964)
8. C. Weng, thesis, Carnegie-Mellon University (1968)
9. F. Smith and S.A. Friedberg, Phys. Rev. 176, 660 (1968)
10. L.J. de Jongh and A.R. Miedema, Adv. Phys., to be published
11. L.R. Walker, R.E. Dietz, K. Andres and S. Darack, Solid State Commun. 11, 593 (1972)
12. T. Oguchi, Phys. Rev. 133, A1098 (1964)
13. J.N. McElearny, S. Merchant and R.L. Carlin, to be published
14. E.J. Pleau and G.F. Kokoszka, Inorg. Nucl. Chem. Letters 8,

779 (1972)
15. E.J. Pleau and G.F. Kokoszka, J. Chem. Soc., Faraday Transactions II, 69, 355 (1973)

CHAPTER VI - MAGNETIC MEASUREMENTS ON POLYCRYSTALLINE SAMPLES OF THE LAYER-COMPOUNDS Rb_2CuCl_4, Rb_2CuCl_3Br AND $Rb_2CuCl_2Br_2$

VI-1 Introduction

In Chapter II-2.5 the preparation and crystal structure investigations of the compounds Rb_2CuCl_4, Rb_2CuCl_3Br and $Rb_2CuCl_2Br_2$ were discussed. Summarizing the results we can say that the compounds have the so-called $(NH_4)_2CuCl_4$ structure (fig. II-2), which structure is a deformed K_2NiF_4 structure (fig. I-2). In the compound $Rb_2CuCl_2Br_2$ the Br^- ions order at the sites 1 and 2 in the K_2NiF_4 structure (fig. I-2), or in other words, the Cl^- ions lie within the equatorial plane of the octahedron (bc plane) surrounding the Cu ions, and the Br^- ions lie above and beneath this plane. In this way only $[CuCl_4Br_2]$ octahedra are formed. In Rb_2CuCl_3Br probably two kinds of octahedra occur, viz. $[CuCl_6]$ and $[CuCl_4Br_2]$ in the ratio 1:1, that are distributed at random in the structure.

On basis of this crystal structure it is expected that the compounds show properties of 2D magnetic systems. From the magnetic measurements described in this chapter it is concluded that this is indeed the case. The measurements indicate a ferromagnetic intra-layer exchange and a much weaker, antiferromagnetic inter-layer exchange, for all three compounds. In the literature only a few other compounds of this type are known, e.g. $CrCl_3$ (1, 2), $MnAu_2$ (3), $FeCl_2$ (4, 5), $CoCl_2$ (6), $NiCl_2$ (6), $(C_2H_5NH_3)_2CuCl_4$ (7, 8) and $(NH_4)_2CuCl_4$ (9).

In these systems much information can be obtained about the interaction parameters and the anisotropy in the magnetic system by means of susceptibility and magnetization measurements. These measurements and their results are discussed in Section VI-2, along with ESR and some heat capacity experiments. In Section VI-3 the anisotropy fields and magnetic exchange fields due to the antiferromagnetic inter-layer coupling, are calculated. In Section VI-4 a discussion of the results is given. In that section also an analysis of the transition temperatures is given by means of Green function techniques.

VI-2 Experimental results

VI-2.1 ESR experiments

By means of ESR powder spectroscopy we obtained the g-values for Rb_2CuCl_4, Rb_2CuCl_3Br and $Rb_2CuCl_2Br_2$. The measurements were carried out on a commercial Varian E3 instrument at frequencies around 9.3 GHz (X-band) both at room temperature and at liquid nitrogen temperature (77K). The spectra were recorded as the first derivative of the absorption line.

The room temperature powder spectrum of Rb_2CuCl_4 is shown in fig. VI-1a. The spectra of Rb_2CuCl_3Br and $Rb_2CuCl_2Br_2$ show the same features and are, therefore, not given here. No anisotropy was noticed in these spectra, and hence the g-values given in Table VI-1 were determined at the point of zero-derivative.

As can be seen in fig. VI-1b-d the spectra recorded at liquid nitrogen temperature reveal anisotropy. Only for Rb_2CuCl_3Br the anisotropy is less pronounced. Two g-values can be derived from the anisotropic spectra, viz. the first g-value at the point midway the points of maximum and minimum slope in the lower field region (point A), and the second g-value at a point with slightly lower field value than the point of minimum slope B in order to account for the asymmetry in the absorption curves (Table VI-1).

One can compare these values with those found for compounds of the $(C_nH_{2n+1}NH_3)_2CuCl_4$ series with n=1 to 6 (7, 10, 11). Also these compounds have a layer-type structure of Cu^{2+} ions. The layers are separated by the alkyl-ammonium groups. According to the g-values of those compounds the higher g-value in our compounds refers probably to the bc-plane, i.e. $g_{b,\,c}$. The lower value would then be the g-value along the a-axis, i.e. g_a. The calculated g-values (Table VI-1) agree very well with those of the $(C_nH_{2n+1}NH_3)_2CuCl_4$ compounds.

For Rb_2CuCl_3Br only the $g_{b,\,c}$-value can be calculated in the same way as for Rb_2CuCl_4 and $Rb_2CuCl_2Br_2$, due to the less pronounced anisotropic character of the spectrum of the former compound. However, by means of the formula

$$g^2_{\text{powder}} = \frac{1}{3}(g_a^2 + 2g_{b,\,c}^2)$$

the value of g_a is obtained by substituting the values of g_{powder} at room temperature and $g_{b,\,c}$ at low temperature. This appears a reasonable procedure since it gives a good agreement between the measured g-values for the other two compounds.

The absence of the anisotropic character in the low-temperature

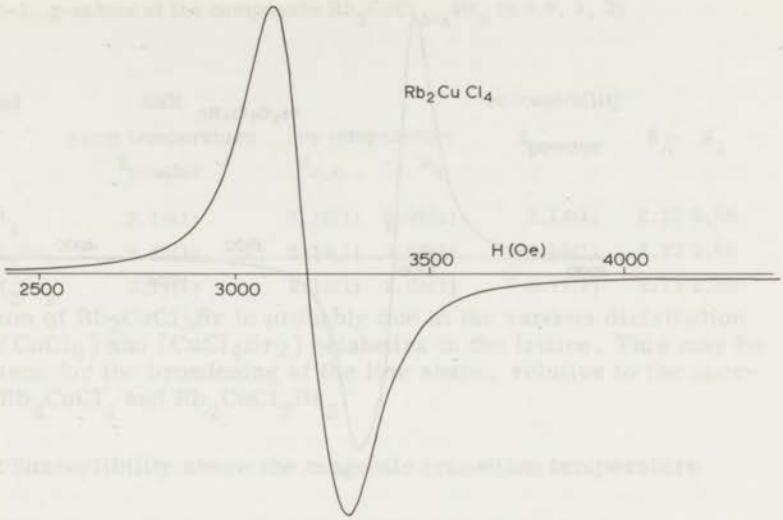

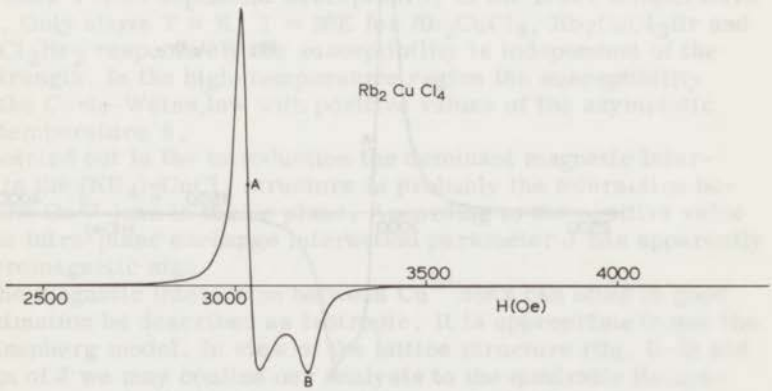

Fig. VI-1a The ESR spectrum of Rb_2CuCl_4 at room temperature
Fig. IV-1b In fig. VI-1b, c, d the ESR spectra at liquid nitrogen temperature of Rb_2CuCl_4, Rb_2CuCl_3Br and $Rb_2CuCl_2Br_2$ are shown respectively. From point A and a slightly lower field value than point B (in order to account for the asymmetry in the absorption curve) the g-values are calculated

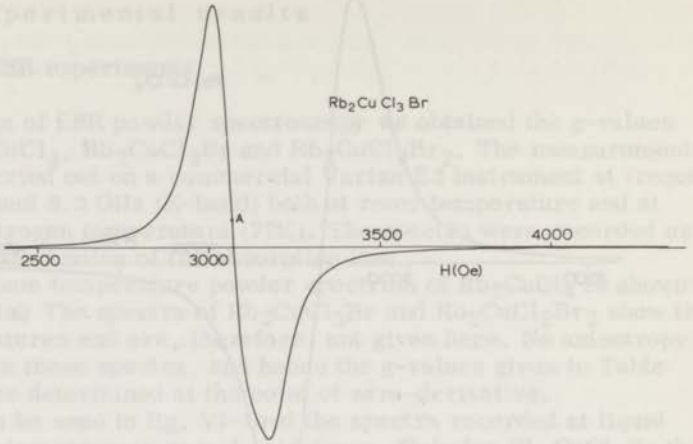
$Rb_2 Cu Cl_3 Br$
A
2500
3000
3500
4000
H(Oe)

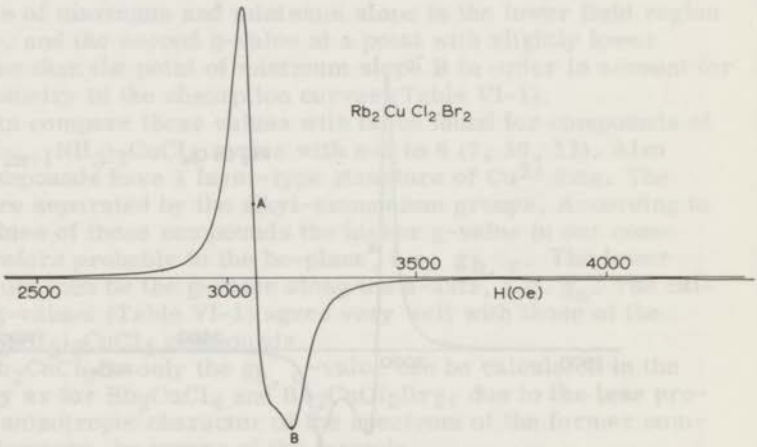
$Rb_2 Cu Cl_2 Br_2$
A
B
2500
3000
3500
4000
H(Oe)

Table VI-1. g-values of the compounds $Rb_2CuCl_{4-x}Br_x$ (x = 0, 1, 2)

Compound	ESR			susceptibility		
	room temperature	low temperature				
	g_{powder}	$g_{b,c}$	g_a	g_{powder}	$g_{//}$	$g_{\perp}$
Rb_2CuCl_4	2.14(1)	2.16(1)	2.06(1)	2.14(1)	2.26	2.06
Rb_2CuCl_3Br	2.11(1)	2.14(1)	2.06(1)	2.10(1)	2.22	2.06
$Rb_2CuCl_2Br_2$	2.11(1)	2.13(1)	2.08(1)	2.11(1)	2.19	2.08

spectrum of Rb_2CuCl_3Br is probably due to the random distribution of the $[CuCl_6]$ and $[CuCl_4Br_2]$ octahedra in the lattice. This may be the reason for the broadening of the line shape, relative to the spectra of Rb_2CuCl_4 and $Rb_2CuCl_2Br_2$.

VI-2.2 Susceptibility above the magnetic transition temperature

The experimental susceptibility data are corrected for diamagnetism according to the tables of Selwood (12). The susceptibility measurements show a field dependent susceptibility in the lower temperature region. Only above T ≈ K, T ≈ 30K for Rb_2CuCl_4, Rb_2CuCl_3Br and $Rb_2CuCl_2Br_2$ respectively the susceptibility is independent of the field strength. In the high-temperature region the susceptibility obeys the Curie-Weiss law with positive values of the asymptotic Curie temperature θ.

As pointed out in the introduction the dominant magnetic interaction in the $(NH_4)_2CuCl_4$ structure is probably the interaction between the Cu^{2+} ions in the bc plane. According to the positive value of θ the intra-plane exchange interaction parameter J has apparently the ferromagnetic sign.

As the magnetic interaction between Cu^{2+} ions can often in good approximation be described as isotropic, it is appropriate to use the 2D Heisenberg model. In view of the lattice structure (fig. II-2) and the sign of J we may confine our analysis to the quadratic Heisenberg ferromagnet. Within this model Baker et al. (13) have calculated 10 terms in the series expansion for the case S=1/2. In powers of J/kT the expansion is written as:

$$\chi T/C = 1+2A+2A^2+1.333A^3+1.083A^4+1.183A^5+0.510^6-0.322^7+$$

$$0.407A^8+1.067A^9-0.657A^{10}\ldots\ ,$$

where $C=Ng^2\beta^2/4k$ and $A=J/kT$.

De Jongh has pointed out (14) that the finite number of known terms in the series expansion provides a good description of the susceptibility in the region $J/kT < 0.6$. We have tried to fit the experimental curves to the theoretical series expansion curve in the region $J/kT < 0.6$ with J/k and g as variable parameters. The best fits, shown in fig. VI-2, were obtained for the J/k- and g-values listed in Table VI-2 and Table VI-1 respectively. The agreement between the g-values obtained from the ESR measurements and the g-values obtained via the susceptibility is very good.

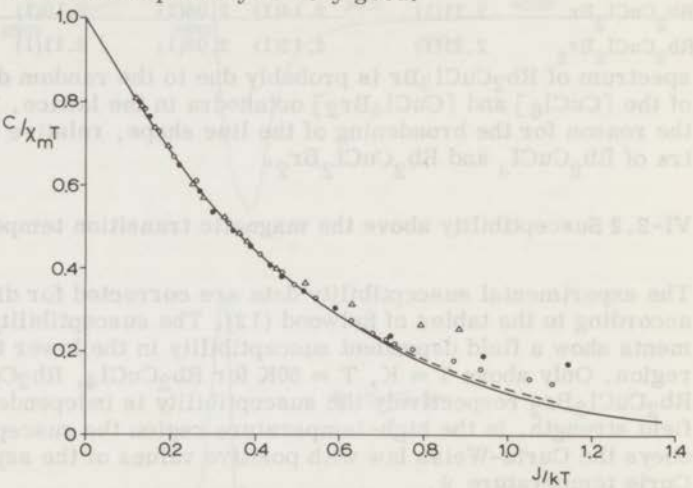

Fig. VI-2 The molar susceptibility of Rb_2CuCl_4, Rb_2CuCl_3Br and $Rb_2CuCl_2Br_2$ plotted as $C/\chi_m T$ versus J/kT in the region $T > T_N$ (C=Curie constant) with J/k and g as variable parameters. o = Rb_2CuCl_4 at H=5.65 kOe, ● = Rb_2CuCl_3Br at H=5.65 kOe, △ = $Rb_2CuCl_2Br_2$ at H=5.63 kOe. For clearness not all measurements are shown. ——: susceptibility series expansion curve for the 2D square Heisenberg ferromagnet. ---: empirical modification of the susceptibility series expansion curve given by De Jongh (14, 15)

In fig. VI-2 is also shown the modification to the series expansion prediction that De Jongh (14, 15) has given on basis of empirical evidence. This curve is deduced from susceptibility data of several compounds of the series $(C_nH_{2n+1}NH_3)_2CuX_4$ (X=Cl, Br), that can

also be characterized as 2D ferromagnetic Heisenberg systems. The curve seems to be generally applicable up to J/kT=1.1.

From fig. VI-2 it is seen that the fits of the experimental data and the series expansion curve coincide for $J/kT < 0.65$, $J/kT < 0.55$ and $J/kT < 0.45$ for Rb_2CuCl_4, Rb_2CuCl_3Br and $Rb_2CuCl_2Br_2$ respectively. The field dependence of the susceptibility in the higher J/kT region can be neglected for those field strengths which are used in our measurements. The results are reproduced in fig. VI-2.

Compared to De Jongh's curve the susceptibility of Rb_2CuCl_4 fits up to J/kT=0.72. So it seems that of the three compounds discussed, Rb_2CuCl_4 is the best approximation of the 2D ferromagnetic Heisenberg model.

VI-2.3 Antiferromagnetic transition

In fig. VI-3a-c the field dependent behaviour of the molar susceptibility χ_m at low temperatures is depicted. It is noticed that for all three compounds a fairly sharp maximum occurs in the susceptibility. This maximum shifts to lower temperature at increasing field strength. Both these phenomena are characteristic for an antiferromagnetic transition. The zero-field values of the transition temperatures T_N, as obtained from extrapolation of the field dependent values to zero field, are listed in Table VI-2.

The magnetic transitions indicate that an antiferromagnetic coupling J' is present between the layers. Due to this coupling the magnetic system below the transition temperature can be described as 3D antiferromagnetic. The same phenomenon has been found in the compounds $(C_2H_5NH_3)_2CuCl_4$ (7) and $(NH_4)_2CuCl_4$ (9).

In the high-temperature region the inter-plane interaction J' can be neglected because it is much weaker than the intra-plane interaction J. But for decreasing temperature J' becomes more important and in the neighbourhood of the transition the magnetic behaviour is influenced very strongly by J'. This can be deduced from the value χ_m at the transition temperature T_N. According to the series expansion (neglecting the inter-plane coupling J') χ_m at T_N should have been 0.87, 0.43 and 0.21 emu/mole for Rb_2CuCl_4, Rb_2CuCl_3Br and $Rb_2CuCl_2Br_2$ respectively. Application of De Jongh's modification of the series expansion curve would lower these values somewhat, but they remain 2-3 times higher than the experimental values of χ_m. Obviously the antiferromagnetic inter-layer exchange lowers χ_m very appreciably at the transition temperature.

The effect discussed above means that for values $J/kT < J/kT_N$ (J/kT_N-values are given in Table VI-3) $C/\chi_m T$ will exceed the series expansion values. Because

Table VI-2. Experimentally determined quantities of the compounds $Rb_2CuCl_{4-x}Br_x$ (X=0, 1, 2)

Compound	T_N(K)	J/k (K)	χ_p (T=0) (emu/mole)x10^2	$H_{s.f.}$ (Oe)	H_2^a (kOe) power law	H_2^a (kOe) magnetization curves
Rb_2CuCl_4	13.7(1)	18.8(3)	24.00(30)	700(25)	17.0(4)	16.5
Rb_2CuCl_3Br	15.2(1)	17.6(3)	11.65(20)	900(50)	35 (1)	34
$Rb_2CuCl_2Br_2$	17.2(1)	16.3(3)	7.60(15)	1175(35)	56 (1)	57

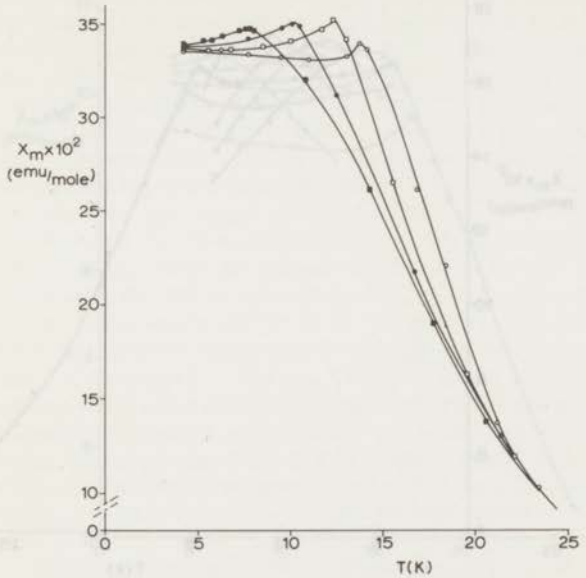

Fig. VI-3a Molar susceptibility χ_m of Rb_2CuCl_4 as a function of temperature and magnetic field. o = H=2.19 kOe, □ = H=8.78 kOe, ● = H=11.26 kOe, ■ = H=13.57kOe

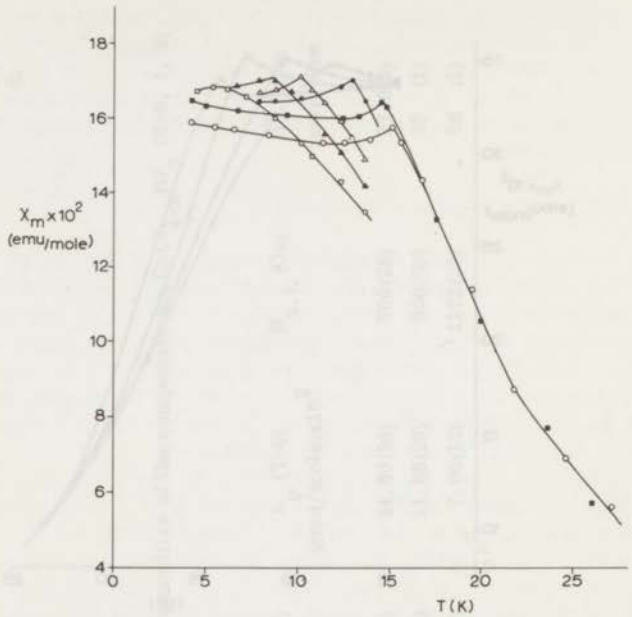

Fig. VI-3b Molar susceptibility χ_m of Rb_2CuCl_3Br as a function of temperature and magnetic field. o = H=1.50 kOe, ■ = H=8.33 kOe, ● = H=19.13 kOe, △ = H=24.52 kOe, ▲ = H=27.22 kOe, □ = H=29.93 kOe

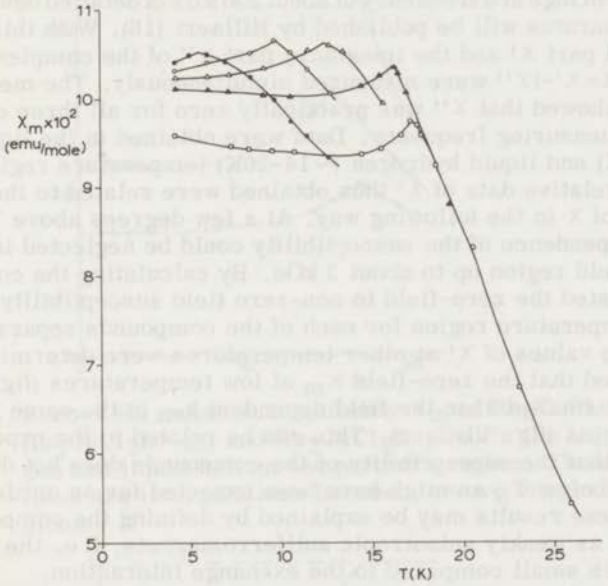

Fig. VI-3c Molar susceptibility χ_m of $Rb_2CuCl_2Br_2$ as a function of temperature and magnetic field. □ = H=1.31 kOe, ▲ = H=21.76 kOe, △ = H=38.15 kOe, ○ = H=43.66 kOe, ● = H=49.23 kOe

J/kT_N ($Rb_2CuCl_2Br_2$) < J/kT_N (Rb_2CuCl_3Br) < J/kT_N (Rb_2CuCl_4) this effect will be strongest for $Rb_2CuCl_2Br_2$ and weakest for Rb_2CuCl_4, which behaviour is indeed noticed in fig. VI-2.

VI-2.4 Zero-field susceptibility and critical fields

Zero-field susceptibility measurements were performed with a twin-T bridge at a frequency of about 250 kHz (a detailed description of this apparatus will be published by Hillaert (16). With this bridge the real part χ' and the imaginary part χ'' of the complex susceptibility $\chi = \chi' - i\chi''$ were measured simultaneously. The measurements showed that χ'' was practically zero for all three compounds at the measuring frequency. Data were obtained in the liquid helium (1-4.2K) and liquid hydrogen (~14-20K) temperature region.

The relative data of χ' thus obtained were related to the absolute values of χ in the following way. At a few degrees above T_N the field dependence of the susceptibility could be neglected in the magnetic field region up to about 3 kOe. By calculating the constant that related the zero-field to non-zero field susceptibility data in this temperature region for each of the compounds separately, the absolute values of χ' at other temperatures were determined. It is noticed that the zero-field χ_m at low temperatures (fig. VI-4) is much smaller than the field dependent χ_m in the same temperature region (fig. VI-3a-c). This can be related to the experimental finding that the susceptibility of the compounds does not decrease steeply below T_N as migh have been expected for an antiferromagnet. These results may be explained by defining the compounds for $T < T_N$ as weakly anisotropic antiferromagnets, i.e. the anisotropy energy is small compared to the exchange interaction.

If to such a system at T=0 a magnetic field is applied along the preferred spin direction in the ordered state (preferential or easy axis), a first order transition occurs at a critical field H_1 (17, 18). At this so-called spin-flop (s.f.) transition the spins flip over to a direction perpendicular to the easy axis because of the gain in magnetic energy. At this field value the magnetization of the system jumps abruptly to a higher value. It keeps rising for increasing magnetic field strength until all spins are oriented parallel to the easy axis at a critical field H_2. At this field, where magnetic saturation is reached, a transition of second order occurs. Such a magnetization behaviour at temperature T=0 is shown in fig. VI-5. Both critical fields H_1 and H_2 are temperature dependent and will vanish at the antiferromagnetic transition temperature.

The fact that the susceptibility of the compounds does not decrease steeply below T_N (fig. VI-3a-c) is understandable if the magnetic

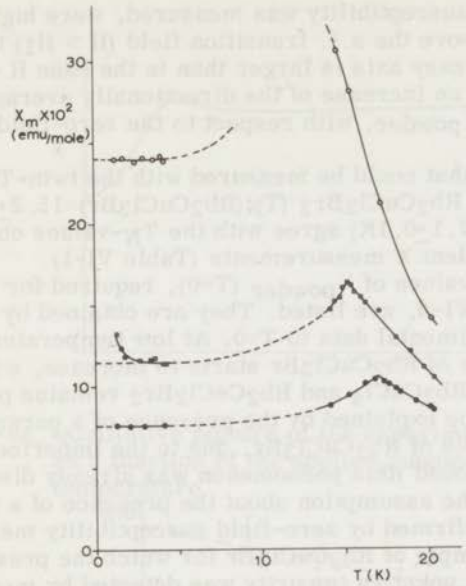

Fig. VI-4 Zero-field molar susceptibility χ_m of Rb_2CuCl_4 (○), Rb_2CuCl_3Br (□) and $Rb_2CuCl_2Br_2$ (●) in the liquid hydrogen and liquid helium temperature region. The dashed lines are interpolations between the two temperature regions

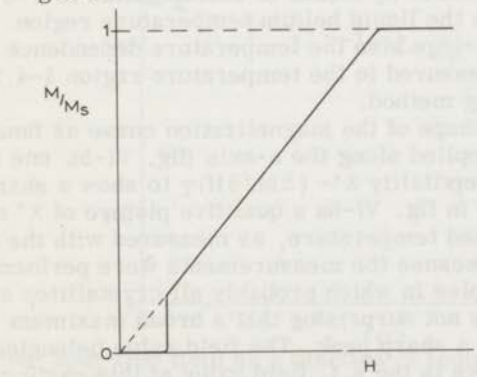

Fig. VI-5 Theoretical behaviour of the magnetization at T=0 as a function of the applied magnetic field H for a weakly anisotropic antiferromagnet with H along the easy direction

fields, at which the susceptibility was measured, were higher than the s.f. field H_1. Above the s.f. transition field ($H > H_1$) the susceptibility along the easy axis is larger than in the case $H < H_1$. This will also cause an increase of the directionally averaged susceptibility, i.e. of χ_{powder}, with respect to the zero-field susceptibility.

The values of T_N that could be measured with the twin-T-bridge for Rb_2CuCl_3Br and $Rb_2CuCl_2Br_2$ ($T_N(Rb_2CuCl_3Br)=15.2\pm0.1K$, $T_N(Rb_2CuCl_2Br_2)=17.1\pm0.1K$) agree with the T_N-values obtained from the field dependent χ measurements (Table VI-1).

In Table VI-2 the values of χ_{powder} (T=0), required for the calculations in Section VI-3, are listed. They are obtained by extrapolation of the experimental data to T=0. At low temperature (about 3K) the susceptibility of Rb_2CuCl_3Br starts to increase, whereas the susceptibility of Rb_2CuCl_4 and $Rb_2CuCl_2Br_2$ remains practically constant. This may be explained by the presence of a paramagnetic impurity in the sample of Rb_2CuCl_3Br, due to the imperfect crystallization of this compound (this phenomenon was already discussed in Chapter II-2.5). The assumption about the presence of a paramagnetic impurity is confirmed by zero-field susceptibility measurements on another sample of Rb_2CuCl_3Br for which the presence of a small amount of an unknown impurity was detected by means of X-ray powder diffraction. The molar susceptibility of this sample was somewhat larger in the liquid helium temperature region than χ_m of the sample used for all our other measurements. The susceptibility started to rise at a higher temperature too. χ_{powder} (T=0) for Rb_2CuCl_3Br was obtained by means of extrapolation to T=0 of the lowest χ_m-values in the liquid helium temperature region.

With the twin-T-bridge also the temperature dependence of the s.f. field H_1 was measured in the temperature region 1-4.2K on basis of the following method.

According to the shape of the magnetization curve as function of the magnetic field applied along the a-axis (fig. VI-5), one expects the differential susceptibility $\chi' = (\partial M/\partial H)_T$ to show a sharp peak at the s.f. field H_1. In fig. VI-6a a qualitive picture of χ' as a function of H at a fixed temperature, as measured with the twin-T-bridge, is shown. Because the measurements were performed on polycrystalline samples in which probably all crystallites are randomly oriented, it is not surprising that a broad maximum in χ' is measured instead of a sharp peak. The field value belonging to the maximum in the curve is the s.f. field value at this particular temperature. In fig. VI-6b the s.f. fields of the compounds are plotted as a function of temperature. Due to the flattening of the maxima an uncertainty appears in the determination of the fields belonging to

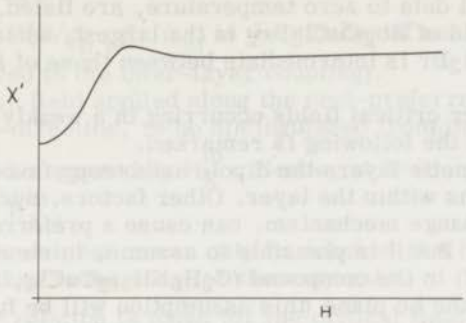

Fig. VI-6a Qualitative picture of the experimentally determined χ' as a function of the applied magnetic field at a fixed temperature

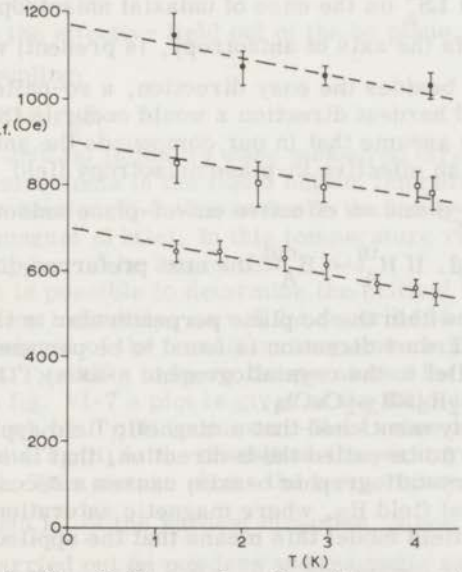

Fig. VI-6b Spin-flop field as a function of temperature in the liquid helium temperature region. o = Rb_2CuCl_4, □=Rb_2CuCl_3Br, ● = $Rb_2CuCl_2Br_2$. The uncertainty in the determined $H_{s.f.}$-values is indicated too

these maxima. These uncertainties are also indicated in fig. VI-6b.

In Table VI-2 the s.f. fields at T=0, obtained by extrapolation of the experimental data to zero temperature, are listed. It is noticed that the s.f. field of $Rb_2CuCl_2Br_2$ is the largest, whereas the s.f. field of Rb_2CuCl_3Br is intermediate between those of Rb_2CuCl_4 and $Rb_2CuCl_2Br_2$.

About the other critical fields occurring in a weakly anisotropic antiferromagnet the following is remarked.

For ferromagnetic layers the dipole anisotropy favours an orientation of the spins within the layer. Other factors, such as anisotropy in the superexchange mechanism, can cause a preferred orientation out of the plane. But it is plausible to assume, in view of the analogous situation (7) in the compound $(C_2H_5NH_3)_2CuCl_4$, that the easy axis lies within the bc plane (this assumption will be further discussed in Section VI-4). Due to the orthorhombic space group of the compounds, it is reasonable to assume an orthorhombic anisotropy (biaxial anisotropy) in our compounds. In the molecular field the biaxial anisotropy is introduced into the Hamiltonian in the form of terms KS_y^2 and LS_z^2 (in the case of uniaxial anisotropy only a term DS_z^2, where z is the axis of anisotropy, is present) with $L > K > 0$. Consequently, besides the easy direction, a so-called next-preferred direction y and hardest direction z would occur in the ordered state. Therefore, we assume that in our compounds the anisotropy manifests itself as an effective in-plane anisotropy field $H_A^{in} = 2KS/g_{b,c}\beta$ and an effective out-of-plane anisotropy field $H_A^{out} = 2LS/g_a\beta$. If $H_A^{in} < H_A^{out}$ the next preferred direction for spin alignment lies within the bc plane perpendicular to the easy axis. In this case the hardest direction is found to be perpendicular to the bc plane (parallel to the crystallographic a-axis). This is actually observed in $(C_2H_5NH_3)_2CuCl_4$.

It was already mentioned that a magnetic field applied along the easy direction (to be called the b-direction, that is to be distinguishing from the crystallographic b-axis) causes a second order transition at a critical field H_2, where magnetic saturation is reached. In the molecular field model this means that the applied magnetic field and the anisotropy field H_A^{in} cancel the effective field of the interplane coupling. Hence, at T=0:

$$H_2^b = 2H_{af}^{in} - H_A^{in},$$

where H_{af}^{in} is the effective field in the bc plane, related to the inter-layer coupling J':

$H_{af}^{in} = 2z_{af} |J'|S/g_{b,c}\beta$, ($z_{af}$ is the number of nearest magnetic neighbours involved in the inter-layer coupling).

A magnetic field applied along the next-preferred direction (to be called the c-direction, to be distinguished from the crystallographic c-axis) will be opposed by H_A^{in}. Hence, at T=0:

$H_2^c = 2H_{af}^{in} + H_A^{in}$,

and magnetic saturation can only be reached at a higher critical field value than is the case for the easy axis.

A similar relation is found for the critical field H_2^a belonging to the hardest direction (that coincides with the crystallographic a-axis):

$H_2^a = 2H_{af}^{out} + H_A^{out}$,

where H_{af}^{out} is the effective field out of the bc plane, related to the inter-layer coupling:

$H_{af}^{out} = 2z_{af} |J'|S/g_a\beta$.

None of the critical fields H_2 were measured directly by means of the χ' measurements in the liquid helium temperature region. As will be seen in Section VI-3 this is due to the limited capability of the available magnet (5 kOe). In this temperature region the critical fields H_2 appear to be larger than 5 kOe.

However, it is possible to determine the critical field along the hardest direction indirectly, as will be described below. Looking at the field dependence of the transition temperature T_N (fig. VI-3a-c) it is clear that T_N shifts to lower temperatures for increasing magnetic field. In fig. VI-7 a plot is given of the field dependence of $T_N(H)/T_N(0)$, where $T_N(0)$ is the zero-field value of the transition temperature and $T_N(H)$ is the transition temperature at a certain magnetic field. This picture shows the temperature dependence of the critical field H_2^a of the hardest direction, since the measurements were carried out on powders and magnetic saturation in the powders can only be reached at magnetic fields higher than the highest critical field value. Extrapolation of the experimental results to T=0 gives the zero-temperature value of H_2^a. It is possible

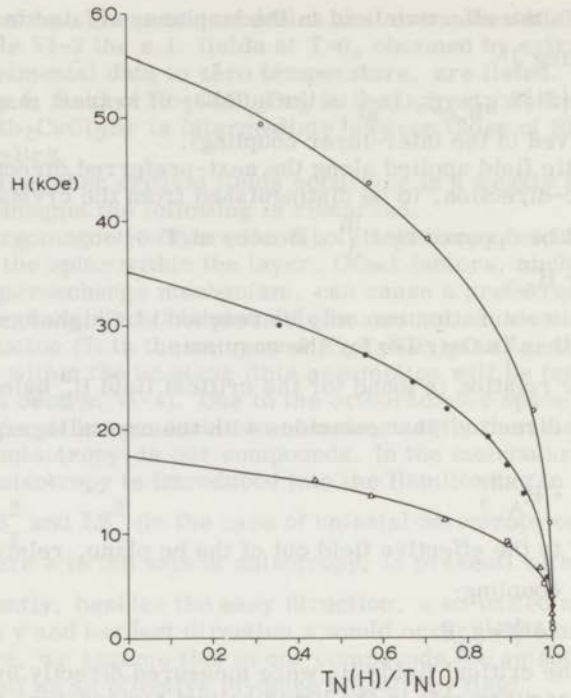

Fig. VI-7 Critical field H_2^a as a function of $T_N(H)/T_N(0)$, where $T_N(0)$=zero-field value of the transition temperature and $T_N(H)$=value of the transition temperature at a certain magnetic field value. △= susceptibility measurements of Rb_2CuCl_4. □= heat capacity measurements of Rb_2CuCl_4. ●= susceptibility measurements of Rb_2CuCl_3Br. ○= susceptibility measurements of $Rb_2CuCl_2Br_2$. The full curves are the best fits, according to the power law $H_2^a \sim [1-T_N(H)/T_N(0)]^{\beta}$

to determine this value fairly accurately, since the experimental curve can be described by a power law (19):

$H_2^a(T) = C[1-T_N(H)/T_N(0)]^{\beta}$ with $C = H_2^a(T=0)$.

The best fits of this power law to the experimental data are obtained for $\beta=0.31\pm0.02$. The $H_2^a(T=0)$-values are listed in Table VI-3.

The value $\beta \approx 1/3$ is usual for 3D Heisenberg systems (19) and thus reflects the 3D character of the magnetic system below the transition temperature, due to the antiferromagnetic inter-layer coupling.

VI-2.5 Magnetization curves

In fig. VI-8a-c the magnetization curves of Rb_2CuCl_4, Rb_2CuCl_3Br and $Rb_2CuCl_2Br_2$ are given for various temperatures. For $T > T_N$ the magnetization behaves like a paramagnetic system (fig. VI-8b,c). Below T_N it is seen that the curves do not show the S-form istic for a spin flop. Probably the S-form is suppressed by the influence of the shape of the magnetization curves belonging to the other crystal directions that occur in the polycrystalline samples and that do not show a s.f. transition.

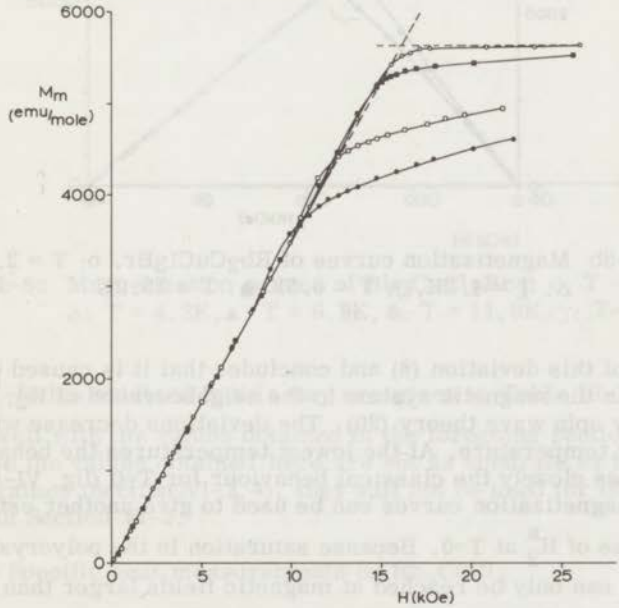

Fig. VI-8a Magnetization curves of Rb_2CuCl_4. o: T = 2.0K, ■: T = 4.2K, □: T = 8.4K, ●: T = 10.6K

At high fields a deviation occurs from the linear behaviour of the magnetization, i.e. the slope of the magnetization curve increases before saturation sets in. De Jongh has given a review of the possible

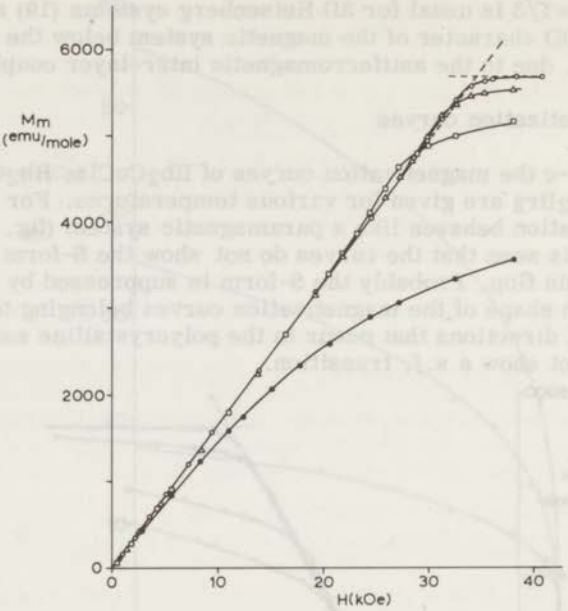

Fig. VI-8b Magnetization curves of Rb_2CuCl_3Br. o: T = 2.0K, △: T = 4.2K, □: T = 6.5K, ●: T = 15.0K

origins of this deviation (8) and concludes that it is caused by instabilities in the magnetic system in the neighbourhood of H_2, as predicted by spin wave theory (20). The deviations decrease with decreasing temperature. At the lowest temperatures the behaviour resembles closely the classical behaviour for T=0 (fig. VI-5).

The magnetization curves can be used to give another estimate of the values of H_2^a at T=0. Because saturation in the polycrystalline samples can only be reached at magnetic fields larger than H_2^a, the point of intersection of the extrapolated linear part of the magnetization curves and the extrapolated horizontal part of the curves (where saturation is reached) gives the value H_2^a (T=0). For $Rb_2CuCl_2Br_2$ the applied fields could not cause total saturation, but assuming that the saturated magnetization value of this compound is just as large as for Rb_2CuCl_4 and Rb_2CuCl_3Br, a good extrapolation can be achieved.

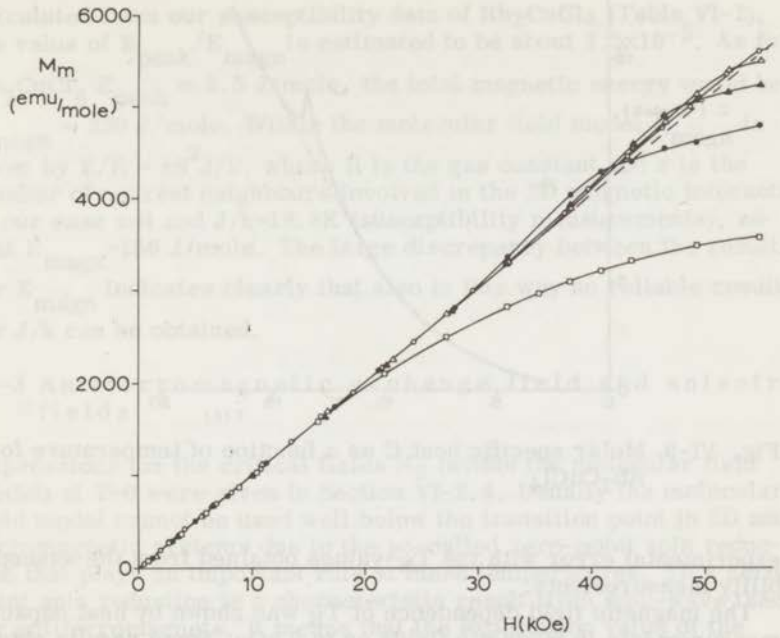

Fig. VI-8c Magnetization curves of $Rb_2CuCl_2Br_2$. o: T = 2.1K, △: T = 4.2K, ▲: T = 6.9K, ●: T = 11.0K, □: T= 15.3K

The H_2^a-fields obtained in this way are given in Table VI-2. They agree well with the values obtained in the foregoing section VI-2.3. Because the values obtained here are not as accurate as the other set of values (Section VI-2.4), they will not be used for the calculation in Section VI-3.

VI-2.6 Specific heat measurements on Rb_2CuCl_4

To obtain information about the magnetic properties of Rb_2CuCl_4 in a way, independent of the susceptibility experiments, heat capacity measurements were carried out in the temperature region 3-80K. (A detailed description of the apparatus used will be published elsewhere (21)). In fig. VI-9 the molar specific heat in the temperature region 3-17K is plotted. The maximum of the peak indicates the the magnetic transition (T_N=13.55±0.05K). This value agrees within

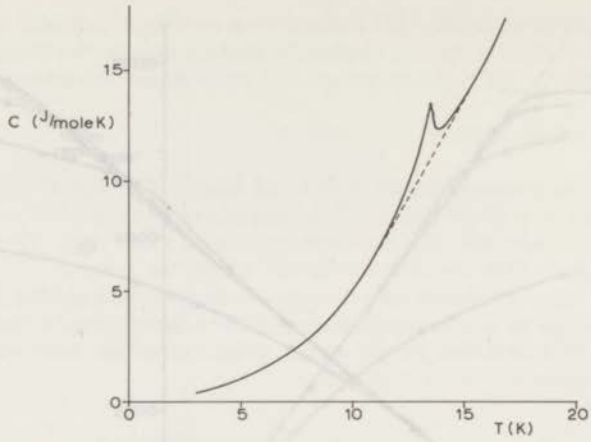

Fig. VI-9 Molar specific heat C as a function of temperature for Rb_2CuCl_4

experimental error with the T_N-values obtained from the susceptibility measurements.

The magnetic field dependence of T_N was shown by heat capacity measurements in magnetic fields up to 9 kOe. Some results obtained in this way are shown in fig. VI-7. It is seen that specific heat and susceptibility data agree well.

Since no reliable estimate of the lattice contribution was obtained the magnetic contribution to the heat capacity could not be precisely determined. Therefore, no value of J/k can be acquired from this experiment. Possibly measurements on a diamagnetic compound, isomorphous to Rb_2CuCl_4 (e.g. Rb_2MgCl_4, see chapter II-2.3), would solve this problem.

Our measurements can be compared to those by Bloembergen et al. (22) on compounds of the series $(C_nH_{2n+1}NH_3)_2CuX_4$ (X=Cl, Br). From their heat capacity data they derived an empirical relation between T_N/θ and E_{peak}/E_{magn} for nearly 2D ferromagnetic systems with $S=\frac{1}{2}$. Here $\theta = 2J/k$ for 2D systems in the molecular field model. Further $E = \int CdT$, where C is the molar magnetic heat capacity, E_{peak} is the energy belonging to the peak of the magnetic transition and E_{magn} is the absolute value of the energy of the magnetic system at absolute zero.

Combining this empirical relation and the value $T_N/\theta = 0.37$ as

calculated from our susceptibility data of Rb_2CuCl_4 (Table VI-2), the value of E_{peak}/E_{magn} is estimated to be about 7.5×10^{-3}. As for Rb_2CuCl_4 $E_{peak} \approx 2.5$ J/mole, the total magnetic energy would be $E_{magn} \approx 330$ J/mole. Within the molecular field model E_{magn} is given by $E/R = zS^2J/k$, where R is the gas constant and z is the number of nearest neighbours involved in the 2D magnetic interaction. In our case z=4 and J/k=18.8K (susceptibility measurements), so that E_{magn}=156 J/mole. The large discrepancy between the results for E_{magn} indicates clearly that also in this way no reliable result for J/k can be obtained.

VI-3 Antiferromagnetic exchange field and anisotropy fields

Expressions for the critical fields H_2 (within the molecular field model) at T=0 were given in Section VI-2.4. Usually the molecular field model cannot be used well below the transition point in 2D antiferromagnetic systems due to the so-called zero-point spin reduction that plays an important role at these temperatures. This zero-point spin reduction is a characteristic result from spin-wave theory for antiferromagnets. It means that the expectation value of the spin per atom of a system of antiferromagnetically interacting atoms is not equal to that of an isolated atom but is lowered by an amount ΔS, where ΔS is the spin reduction. Zero-point corrections for the antiferromagnetic ground-state were first analyzed by Anderson (23). Especially in systems with a low dimension ΔS can be fairly large (17).

However, for our compounds the use of the molecular field model is justified, as far as the spin reduction is concerned, because the antiferromagnetic inter-layer exchange is much smaller than the ferromagnetic intra-layer exchange. A quantitative argument supporting this assumption has been given by De Jongh (8).

For the calculations in this section we use the molecular field relation for the s.f. field H_1^b (spin flop occurs along the easy direction b) (17, 18):

$$(H_1^b)^2 = 2H_{af}^{in}H_A^{in} + (H_A^{in})^2 \qquad (1)$$

and the relation for the critical field H_2^a, that was already derived in Section VI-2.4:

$$H_2^a = 2H_{af}^{out} + H_A^{out} \quad (2) .$$

The expression of the other critical fields H_2^b and H_2^c are of no use because none of these fields could be measured.

The relatively small difference between g_a and $g_{b,c}$ (Table VI-1) warrants a description, in which anisotropy effects are entirely accounted for by the anisotropy fields H_A^{in} and H_A^{out}. Thus, $g_a = g_{b,c} = g$ and $H_{af}^{out} = H_{af}^{in} = H_{af}$. In this case the molecular field expression for $\chi_\perp$ at T=0 reads:

$$\chi_\perp = \chi_\perp^o \left(1 + \frac{H_A}{2H_{af}}\right)^{-1} \quad , \text{ where } \chi_\perp^o = Ng\beta S/2H_{af}$$

denotes the perpendicular susceptibility excluding anisotropy.

The powder susceptibility at T=0 is written as χ_p (T=0) = $\frac{2}{3}\chi_\perp$(T=0), because the parallel susceptibility $\chi_{//}$ vanishes at T=0 for an antiferromagnet. Due to the presence of the orthorhombic anisotropy two contributions to χ_p (T=0) have to be distinguished, viz. $\chi_\perp^c$ for the c-direction (next-preferred direction) and $\chi_\perp^a$ for the a-direction (hardest direction):

$$\chi_p(T=0) = \frac{1}{3}\chi_\perp^{oc}\left(1+\frac{H_A^{in}}{2H_{af}}\right)^{-1} + \frac{1}{3}\chi_\perp^{oa}\left(1+\frac{H_A^{out}}{2H_{af}}\right)^{-1} \quad (3)$$

with $\chi_\perp^{oc} = \chi_\perp^{oa} = Ng\beta S/2H_{af}$.

Eq. (1) can be written as:

$$2H_{af} = \frac{(H_1^b)^2}{H_A^{in}} - H_A^{in} \quad (1a).$$

Substitution of (1a) and (2) in (3) gives:

$$\chi_p\,(T=0) = \frac{1}{3}\,Ng\beta SH_A^{in}/(H_1^b)^2 + \frac{1}{3}\,Ng\beta S/H_2^a \quad (4).$$

Substituting the experimentally determined values of χ_p (T=0), H_1^b, H_2^a and g (Table VI-1, 2), the value of H_A^{in} can be obtained from this last expression.

Using eq. (4), we derive $H_A^{in} \approx 30$ Oe. When this value is substituted in eq. (1a), one finds that a small change in the H_A^{in} -value causes a relatively large change in the H_{af}-value. But it is clear from this calculation that the inequality $H_A^{in} \ll H_{af}$ remains valid. To avoid the large uncertainty in the H_{af}- value, another computation method is followed.

Because $H_A^{in} \ll H_{af}$, eq. (3) can be simplified:

$$\chi_p(T=0) = \frac{1}{3}\chi_\perp^{oc} + \frac{1}{3}\chi_\perp^{oa}\left(1 + \frac{H_A^{out}}{2H_{af}}\right)^{-1} \quad \text{or}$$

$$\chi_p(T=0) = \frac{1}{3} Ng\beta S/2H_{af} + \frac{1}{3} Ng\beta S/H_2^a \qquad (5).$$

By means of eq. (5), and taking into account the experimental errors, we find

$H_{af} = 8.1 \pm 0.3$ kOe. With eq. (1a) and (2) the value

$H_A^{out} = 0.8 \pm 0.3$ kOe and the two solutions

$(H_A^{in})_1 = 30 \pm 10$ Oe and $(H_A^{in})_2 = 16$ kOe are obtained. Comparing the values of

H_A^{in} with the H_A^{in}-value found in $(C_2H_5NH_3)_2CuCl_4$ (7) it is plausible that

$(H_A^{in})_1$ is the physically meaningful solution. This can be confirmed also by substituting $(H_A^{in})_2$ in eq. (1a) in order to calculate H_{af}. This would give a negative value for H_{af}, hence the solution $(H_A^{in})_2$ can be discarded.

The results on Rb_2CuCl_4 are summarized by the following set of values:
$H_{af} = 8.1 \pm 0.3$ kOe, $H_A^{out} = 0.8 \pm 0.3$kOe and $H_A^{in} = 30 \pm 10$ Oe (Table VI-3).

Table VI-3. Antiferromagnetic and anisotropy fields

Compound	H_{af} (kOe)	H_A^{out} (kOe)	H_A^{in} (Oe)	H_{af}/H_f	kT_N/J	T_N/θ
Rb_2CuCl_4	8.1(3)	0.8(3)	30(10)	1.6×10^{-2}	0.73	0.37
Rb_2CuCl_3Br	16.1(7)	2.8(4)	30(10)	3.2×10^{-2}	0.86	0.43
$Rb_2CuCl_2Br_2$	24 (1)	8.5(4)	30(10)	5.2×10^{-2}	1.05	0.53
$(C_2H_5NH_3)_2CuCl_4$*	0.8	1.0	75	1.7×10^{-3}	0.55	0.28
$(NH_4)_2CuCl_4$**	3.1	-	-	6.5×10^{-3}	0.66	0.33

* ref. 7
** ref. 9

Rb_2CuCl_3Br and $Rb_2CuCl_2Br_2$

Repeating the calculation procedure applied to Rb_2CuCl_4, for Rb_2CuCl_3Br, the value $H_{af} = 16.1 \pm 0.7$ kOe is obtained. By means of eq. (1a) and (2) it is found that:

$H_A^{out} = 2.8 \pm 0.4$ kOe and $H_A^{in} = 30 \pm 10$ Oe (Table VI-3).

In the same way, for $Rb_2CuCl_2Br_2$ the following values are obtained:

$H_{af} = 24 \pm 1$ kOe, $H_A^{out} = 8.5 \pm 0.4$kOe, $H_A^{in} = 30 \pm 10$ Oe (Table VI-3).

VI-4 Discussion of the results

VI-4.1 Preferred spin direction

In Section VI-2 it was assumed that for Rb_2CuCl_4, Rb_2CuCl_3Br and $Rb_2CuCl_2Br_2$ below the transition temperature T_N the spins prefer to order in the bc plane. We were led to this assumption by comparing the magnetic properties of the layer-type compounds $CrCl_3$ (1, 2), $MnAu_2$ (3), $FeCl_2$ (4, 5), $CoCl_2$ (6), and $(C_2H_5NH_3)_2CuCl_4$ (7, 8) with those in our compounds. Of all compounds mentioned it is known that the magnetic coupling within the layers is ferromagnetic and that the coupling between the layers is much weaker and antiferromagnetic. Furthermore, of all compounds (except $FeCl_2$) the preferred spin direction lies within the layer. For $FeCl_2$ this preferred direction is perpendicular to the layer.

Particularly the resemblance between the magnetic properties of $(C_2H_5NH_3)_2CuCl_4$ and Rb_2CuCl_4 strongly suggests a preferential orientation of the spins within the bc plane in Rb_2CuCl_4. Comparison with some other compounds gives rise to a different argument for Rb_2CuCl_3Br and $Rb_2CuCl_2Br_2$. In $CrBr_3$ (24-26) and CrI_3 (27), which compounds are isomorphous with $CrCl_3$, the inter-layer exchange has a ferromagnetic character, whereas the spins show a preferred direction perpendicular to the layer. For the compounds $(C_nH_{2n+1}NH_3)_2CuX_4$ (X = Cl, Br) it has been experimentally determined that in the case X=Cl the preferred direction lies within the layer, whereas for X=Br a direction out of the layer is preferred (15, 28). Thus replacement of Cl^- ions by Br^- ions at the sites 1 and 2 (fig. I-2) in Rb_2CuCl_4 could lead to a change of the spin orientation from a direction lying in the bc plane to a direction perpendicular to the bc plane.

Let us assume that this is the case in $Rb_2CuCl_2Br_2$. Then the a-axis in $Rb_2CuCl_2Br_2$ would be the easy axis and the next-preferred and hardest direction would both be found within the bc plane. Eq. (1), (2) and (3) in Section VI-3 now read as follows:

$$(H_1^a)^2 = 2H_{af} H_A^{in} + (H_A^{in})^2$$

$$H_2^b = 2H_{af} + H_A^{out}$$

$$\chi_p (T=0) = \frac{1}{3} \chi^{oc} (1 + \frac{H_A^{in}}{2H_{af}})^{-1} + \frac{1}{3} \chi^{ob} (1 + \frac{H_A^{out}}{2H_{af}})^{-1} ,$$

where b en c are the hardest and next-preferred direction respectively (to be distinguished from the crystallographic b- and c-axis).

Repeating the procedure of Section VI-3, the values of the antiferromagnetic field H_{af} and the anisotropic fields H_A^{in} and H_A^{out} can be obtained. H_{af} will remain the same, but H_a^{in} and H_A^{out} are interchanged. Hence, the out-of-plane anisotropy field would be very small and the in-plane anisotropy field would be very large compared to the original values of H_A^{in} and H_A^{out}, as calculated in Section VI-3. In particular, H_A^{out} (Rb_2CuCl_4) would be much larger than H_A^{out} ($Rb_2CuCl_2Br_2$). However, in $CrCl_3$ and $CrBr_3$ it is found that an important part of the out-of-plane anisotropy in these compounds is associated with the superexchange mechanism via the halogen ions between the layers, causing a larger anisotropy field for $CrBr_3$ than for $CrCl_3$. The same effect has been detected in the compounds $(C_nH_{2n+1}NH_3)_2CuX_4$ (X= Cl, Br), when Cl is replaced by Br (29). Therefore, it seems improbable that in $Rb_2CuCl_2Br_2$ the out-of-plane anisotropy would be smaller than in Rb_2CuCl_4. We conclude that also in $Rb_2CuCl_2Br_2$ the spins prefer an ordering within the layer. For Rb_2CuCl_3Br the same conclusion is reached.

So far nothing has been said about the possibility of a preferred spin direction in the bc plane. The various directions that, at first sight, may be considered as possible preferred spin directions are the in-plane long and short axis of the octahedron and the crystallographic b- and c-axis. Because each long (or short) axis is perpendicular to the long (or short) axis of the neighbouring octahedra, the preferred direction is not uniquely determined in this case. Due to the small value of the in-plane anisotropy it seems improbable that

the spins would all be aligned along the long axis of adjacent octahedra or, alternatively, all along the short axis.

Additional information about a possible alignment along the octahedral axes or the crystallographic b- or c-axis may be obtained by theoretical calculation of the dipole anisotropy fields H^{in}_{Adip} and H^{out}_{Adip} at zero temperature. For these calculations we use a formalism developed by Colpa (28, 30). Combining his expressions pertaining to a tetragonal layer-structure (the orthorhombic distortion in the bc plane of our Cu compounds is so small that b- and c-axis are practically equal; see also Table II-5) and the relations which take into account the anisotropic g-tensor, we obtain:

$H^{in}_{Adip} \approx 55\cos 2\alpha$, $40\cos 2\alpha$ and $30\cos 2\alpha$ Oe for Rb_2CuCl_4, Rb_2CuCl_3Br and $Rb_2CuCl_2Br_2$ respectively (α is the angle between the easy axis and the tetragonal axis of the g-tensor, which is the long axis of the octahedron). The values of the g-tensor, used for the calculations (Table VI-1), are obtained by means of the approximations (28):

$$g_{b,c} = \frac{1}{2}(g_{\perp} + g_{//}) \text{ and}$$

$$g_{\perp} = g_a$$

The calculated values of H^{out}_{Adip} are 840, 830 and 820 Oe for Rb_2CuCl_4, Rb_2CuCl_3Br and $Rb_2CuCl_2Br_2$ respectively.

Comparing the values of H^{in}_{Adip} with the experimentally determined H^{in}_{A} -values (Table VI-3), it is seen that for $\alpha = 0^o$ (that is, if the spins are alternately aligned along the long and short axis of adjacent octahedra) the absolute H^{in}_{Adip}-values are the same as for $\alpha = 90^o$, but that the signs of H^{in}_{Adip} are opposite in the two cases. It is noticed that for these possibilities of spin alignment $H^{in}_{Adip} \approx H^{in}_{A}$ (experimental), so that the dipole anisotropy field would account for the experimentally determined in-plane anisotropy field.

For $\alpha = 45^o$, which means that the easy axis corresponds to the crystallographic b- or c-axis, $H^{in}_{Adip} = 0$. In this case our results agree with the results obtained for $(C_2H_5NH_3)_2CuCl_4$ (7). In this

compound H_{Adip}^{in} is not zero but 5.5 Oe, due to an orthorhombic distortion in the bc plane. The experimental value of H_A^{in} is about 75 Oe. The discrepancy between these two values is assumed to be caused by an anisotropy in the exchange mechanism. Therefore, if the preferred spin direction is parallel to the b- or c-axis, the possibility remains that also in our compounds the value of H_A^{in} is due to such an anisotropy in the exchange mechanism.

VI-4.2 Anisotropy fields and antiferromagnetic fields

Comparison of the H_A^{out}- and H_A^{in}-values listed in Table VI-3, shows that H_A^{out} increases by one order of magnitude when the Cl^- ions at sites 1 and 2 (fig. I-2) are replaced successively by Br^- ions, whereas the anisotropy in the layer is not affected. On basis of the remarks about the anisotropy in Section VI-4.1 it is reasonable to assume that this effect is caused by the anisotropy associated with the superexchange mechanism via the halogen ions between the layers. This assumption is confirmed by the theoretically calculated values of H_{Adip}^{out} (see Section VI-4.1: $H_{Adip}^{out} \approx 840$, 830 and 820 Oe for Rb_2CuCl_4, Rb_2CuCl_3Br and $Rb_2CuCl_2Br_2$ respectively). Comparing the H_{Adip}^{out}-values and the experimentally determined H_A^{out}-values (Table VI-3), it is noticed that H_A^{out} increases strongly, whereas H_{Adip}^{out} remains practically equal, when going from Rb_2CuCl_4 to $Rb_2CuCl_2Br_2$.

Because of the large uncertainty in the experimental value of H_A^{out} for Rb_2CuCl_4 it is not possible to separate the contributions due to the dipole anisotropy and the anisotropy in the superexchange mechanism via the Cl^- ions at sites 1 and 2 in this compound (fig. I-2).

Comparison of the H_{af}-values for the various compounds (Table VI-3) shows that, in spite of the increasing distance between nearest layers, the strength of the antiferromagnetic inter-layer coupling increases too. This is probably due to a larger superexchange interaction via the Br^- ions. The same effect has been found in other compounds (31) (see also Chapter III and V).

VI-4.3 Long-range ordering

De Jongh suggested by comparing the properties of the compounds $(C_2H_5NH_3)_2CuCl_4$ with those of other compounds in the $(C_nH_{2n+1}NH_3)_2CuCl_4$ series that H_{af} is the dominant mechanism that causes the long-range 3D ordering below T_N in $(C_2H_5NH_3)_2CuCl_4$, and that H_A^{out} is ineffective in establishing the long-range order (7). In other words, the quantity $|J'/J|$ is mainly responsible for the value of the transition temperature. This suggestion is supported by comparison of the values kT_N/J, H_{af} and H_A^{out} (Table VI-3) of the compounds Rb_2CuCl_4 and $(C_2H_5NH_3)_2CuCl_4$. In these compounds the H_A^{out}-values are nearly equal, whereas

$H_{af}(Rb_2CuCl_4) > H_{af}((C_2H_5NH_3)_2\ CuCl_4)$ and

$kT_N/J(Rb_2CuCl_4) > kT_N/J\ ((C_2H_5NH_3)_2\ CuCl_4)$.

Because H_A^{out} in Rb_2CuCl_3Br and $Rb_2CuCl_2Br_2$ increases strongly, a comparison with these compounds is not possible.

In Table VI-3, where also the known physical quantities of $(NH_4)_2CuCl_4$ are given, a correlation between kT_N/J and H_{af} is observed. In fig. VI-10 the experimental relationship between H_{af}/H_f and T_N/θ is shown (H_f is the magnetic field due to the ferromagnetic intra-layer exchange, and $\theta = 2J/k$ for a 2D system in the molecular field model). It is seen in fig. VI-10 that a smooth curve can be drawn through the experimental points of the various compounds. Extrapolation for $H_{af} \rightarrow 0$ indicates that the value of T_N/θ is about equal to the value $T_c/\theta=0.22$ that was obtained by Bloembergen et al. (22) from specific heat measurements in the compounds $(C_nH_{2n+1}NH_3)_2CuX_4$ (X=Cl, Br). This T_c/θ-value was interpreted te be characteristic for an ideal, isotropic 2D ferromagnetic system having spin S=1/2, or, in other words, the so-called 'Stanley-Kaplan transition temperature' for such systems (discussed in Chapter I-3) presumably obeys the relation $T_c/\theta=0.22$.

VI-4.4 Analysis of T_N by means of Green function techniques

In this section we compare the experimental T_N-values with theoretical T_N-values calculated by means of double-time temperature dependent Green function techniques. This formalism has been reviewed in detail by Zubarev (32) and has been applied to various magnetic systems (27, 33-37).

It is known that the spin-wave theory and the high-temperature series expansion can be applied with success to temperature regions well below and above the transition temperature respectively, but they do not give reliable results near the transition temperature. Lines (38) has shown that for the calculation of T_N in nearly 2D systems the Green function approximation is to be preferred above other methods, such as the Bethe-Peierls-Weiss and the constant coupling approximation. On the other hand, the Green function formalism underestimates the short-range order in the magnetic system.

In the Green function formalism, as developed by Lines (36, 38, 39) the restrictions hold that there is a single preferred direction of antiferromagnetic spin alignment in the ordered state and that there are only two ferromagnetic sublattices. These restrictions are satisfied by the magnetic model we are dealing with.

Consider a Hamiltonian of the form

$$H = \sum_{<ij>} [2J_{ij}\vec{S}_i.\vec{S}_j + 2D_{ij}S_i^zS_j^z] \quad (7)$$

where $\sum_{<ij>}$ runs over all pairs of spins S_i and S_j and J_{ij} has positive (or negative) sign for antiferromagnetic (or ferromagnetic) interaction. In this Hamiltonian an axially symmetric anisotropy term D_{ij} is included. This simplification of the anisotropy, compared to the orthorhombic anisotropy in our compounds, appears to be justified by the fact that $H_A^{in} \ll H_A^{out}$ (Table VI-3).

Using Ham. (7) we obtain, analogous to the calculations of Lines (39), the following expression for the transition temperature:

$$\frac{S(S+1)}{3kT_N} = \left\langle \frac{\mu}{\mu^2 - \lambda^2} \right\rangle_K \quad (8), \text{ where}$$

$$\mu = \sum_{<ij>}^{s} \{2J_{ij}[\exp(i\vec{K}.(\vec{i}-\vec{j})) - 1] - 2D_{ij}\} + \sum_{<ij>}^{d} [2J_{ij} + 2D_{ij}] \quad (9) \text{ and}$$

$$\lambda = \sum_{<ij>}^{d} 2J_{ij} \exp[i\vec{K}.(\vec{i}-\vec{j})]. \quad (10)$$

$\sum_{<ij>}^{s}$ runs over all values for which i and j are on the same sublattice, $\sum_{<ij>}^{d}$ runs over all values for which i and j are on different sublattices. $\langle \ldots\ldots \rangle_K$ is an average over the wave vector $\vec{K}$ covering $\frac{1}{2}N$ values in the first Brillouin zone of the first reciprocal sublattice, where N is the total number of spins in the lattice.

For our calculations it was necessary to simplify the crystal structure of the compounds to a base-centered tetragonal model. Although this model differs somewhat from that of the Cu compounds discussed (they have a nearly face-centered tetragonal structure), we do not expect the results to be much different. In the simplified model the intra-layer interaction is represented by an isotropic exchange parameter with ferromagnetic sign and an anisotropy parameter D. In the layers each Cu ion has four nearest magnetic neighbours. Similarly, the interaction between nearest neighbours in

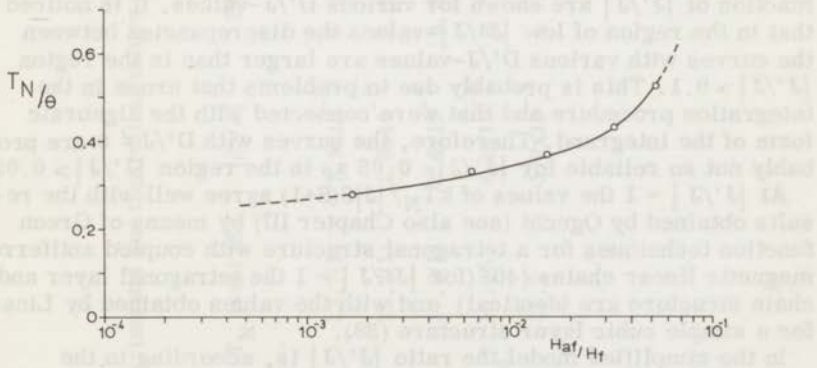

Fig. VI-10 T_N/θ as a function of H_{af}/H_f for the compounds Rb_2CuCl_4, Rb_2CuCl_3Br, $Rb_2CuCl_2Br_2$, $(C_2H_5NH_3)_2CuCl_4$ and $(NH_4)_2CuCl_4$. The dashed portions are extrapolations of the full curve

adjacent layers is represented by an isotropic exchange parameter J' with antiferromagnetic sign and an anisotropy parameter D'. Each Cu ion has two nearest neighbours involved in the inter-layer interaction. We will consider the case D=0. The case J'> 0 and D'<0 (hence D'/J >0) corresponds to a preference for planar alignment.

Taking into account only the nearest neighbour interactions, eq. (9) and (10) in the simplified model give:

$$\mu = 4J\,[\cos(aK_x) + \cos(aK_y)] + 4(J' + D') - 8J \quad (11)$$

$$\lambda = 4J' \cos(\tfrac{1}{2}cK_z) \quad (12),$$

in which a and c are the unit cell parameters of the tetragonal structure. K_x, K_y and K_z are the components of the wave vector $\vec{K}$ along the basic vectors of the reciprocal sublattice, and are subject to the restriction $-\pi \leq aK_x, aK_y, cK_z < \pi$.
The summation $\langle \ldots\ldots \rangle_K$ in eq. (8), in which eq. (11) and (12) are substituted, is evaluated by means of a numerical integration. (The initial computer program used for the integration procedure was handed over to us by J.H.P. Colpa, who has given an extensive discussion of this program in ref. 28. For our purpose the program was modified by W. Vermin at our department.)

In fig. VI-11 the results of the calculation for $kT_N/|J|S(S+1)$ as function of $|J'/J|$ are shown for various D'/J-values. It is noticed that in the region of low $|J'/J|$-values the discrepancies between the curves with various D'/J-values are larger than in the region $|J'/J| > 0.1$. This is probably due to problems that arose in the integration procedure and that were connected with the algebraic form of the integrand. Therefore, the curves with $D'/J \neq 0$ are probably not so reliable for $|J'/J| < 0.05$ as in the region $|J'/J| > 0.05$.

At $|J'/J| = 1$ the values of $kT_N/|J|S(S+1)$ agree well with the results obtained by Oguchi (see also Chapter III) by means of Green function techniques for a tetragonal structure with coupled antiferromagnetic linear chains (40) (for $|J'/J| = 1$ the tetragonal layer and chain structure are identical) and with the values obtained by Lines for a simple cubic layer structure (38).

In the simplified model the ratio $|J'/J|$ is, according to the molecular field expression:

$$H_{exchange} = 2z\,|J_{exchange}|\,S/g\beta\,,$$

written as $|J'/J| = zH_{af}/z'H_f$, where z=4 and z' = 2. The values of H_{af}/H_f for our compounds are listed in Table VI-3. Analogously,

Table VI-4. Experimental and theoretical values of T_N

Compound	T_N (exp) (K)	$\|J'/J\|$	D'/J	T_N(theor) (K)	T_N(theor)/T_N(exp)	T_N (K) mol. field
Rb_2CuCl_4	13.7(1)	7.9×10^{-3}	8×10^{-4}	18.1	1.32	37.6
Rb_2CuCl_3Br	15.2(1)	1.6×10^{-2}	2.8×10^{-3}	19.2	1.26	35.3
$Rb_2CuCl_2Br_2$	17.2(1)	2.6×10^{-2}	9.2×10^{-3}	20.2	1.18	32.9
$(C_2H_5NH_3)_2CuCl_4$*	10.25	8.5×10^{-4}	8×10^{-4}	14.8	1.44	37.2
$(NH_4)_2CuCl_4$**	11.2	3.2×10^{-3}	$\approx 1\times10^{-3}$	15.3	1.37	34.0

* ref. 7
** ref. 9

D' is defined as $H_A^{out} = 2z' |D'|S/g\beta$. In Table VI-4 the values of $|J'/J|$ and D'/J, as calculated for our compounds, are given. To obtain the $|J'/J|$-and D'/J-values in the simplified model, the values in Table VI-4 have to be multiplied by a factor 4, due to the difference in the number of nearest neighbours involved in the inter-layer coupling in the two models. In Table VI-3 and VI-4 are also given the data of $(C_2H_5NH_3)_2CuCl_4$ (7) and $(NH_4)_2CuCl_4$ (9). For $(NH_4)_2CuCl_4$ the D'/J-value is not known, but in view of the values of the other compounds it may be estimated to be about $1x10^{-3}$.

The results of the calculation of T_N by means of the Green function formalism are shown in the fourth column of Table VI-4. By comparison with the experimental T_N-values, it is seen that the theoretical values are always higher and that the ratio $T_N(theor)/T_N(exp)$ decreases for increasing $|J'/J|$ and D'/J. This may be caused by the forementioned problems in the integration procedure in the lower $|J'/J|$-region. It is also possible that the breakdown of the Green function theory in the case of an ideal 2D Heisenberg model (J'=D'=0) plays a role (41). For increasing $|J'/J|$ the deviations from the 2D model become larger and the 3D model will be more closely approached. Since furthermore presumably the Green function approximation is poorer in two dimensions than in three (41) we may expect that for higher $|J'/J|$-values the agreement between theoretical and experimental T_N becomes better, as is indeed the case.

In Table VI-4 also the T_N-values are tabulated, which are obtained from the molecular field relation:

$$kT_N = S(S + 1)(2zJ + 2z'J')/3.$$

As expected for this theoretical model, these values are much too high.

VI-4.5 Conclusions

The magnetic system of the compounds Rb_2CuCl_4, Rb_2CuCl_3Br and $Rb_2CuCl_2Br_2$ can be described by a ferromagnetic intra-layer interaction and a much weaker, antiferromagnetic inter-layer interaction. Below the antiferromagnetic transition temperature T_N the spins probably prefer to order within the layers (bc plane). As a result of the occupation of the sites 1 and 2 in the K_2NiF_4 structure (fig. I-2) by Br^- ions, the inter-plane interaction increases if going from Rb_2CuCl_4 to $Rb_2CuCl_2Br_2$. This is probably caused by a larger superexchange over the Br^- ions compared to the Cl^- ions.

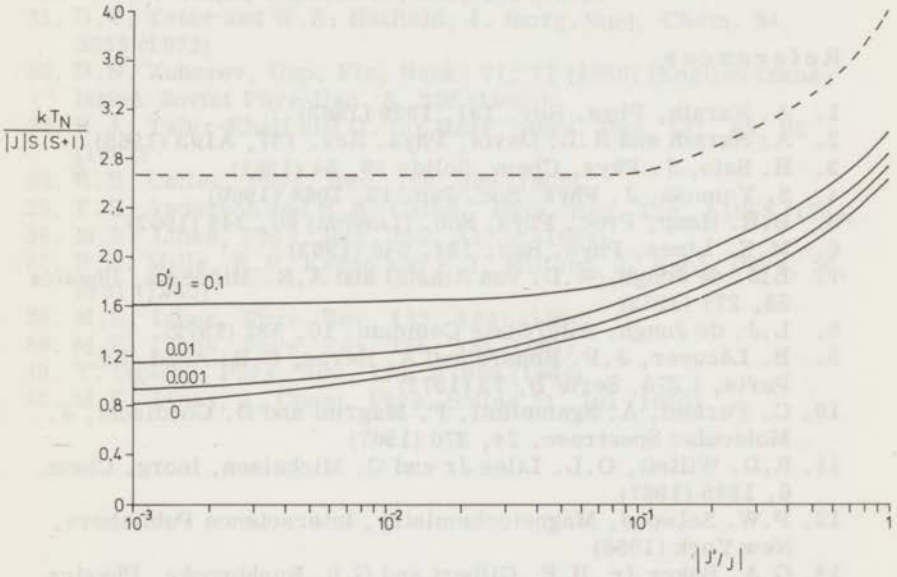

Fig. VI-11 $kT_N/|J|S(S+1)$ as a function of $|J'/J|$ and D'/J. The full curves are the result of calculations by means of Green function techniques. The dashed curve is the molecular field curve

Furthermore, the out-of-plane anisotropy field H_A^{out} increases when Cl^- is partly replaced by Br^-, whereas the in-plane anisotropy field H_A^{in} is not influenced. This phenomenon may be connected with anisotropy in the superexchange mechanism via the halogen ions.

Another result obtained, is that a reasonable explanation of the value of T_N can be given by means of Green function techniques.

References

1. A. Narath, Phys. Rev. 131, 1929 (1963)
2. A. Narath and H.L. Davis, Phys. Rev. 137, A163 (1965)
3. H. Sato, J. Phys. Chem. Solids 19, 54 (1961)
4. S. Yomosa, J. Phys. Soc. Jap. 15, 1068 (1960)
5. B.R. Heap, Proc. Phys. Soc. (London) 80, 248 (1962)
6. M.E. Lines, Phys. Rev. 131, 546 (1963)
7. L.J. de Jongh, W.D. van Amstel and A.R. Miedema, Physica 58, 277 (1972)
8. L.J. de Jongh, Solid State Commun. 10, 537 (1972)
9. B. Lécuyer, J.P. Renard and A. Herpe, C.R. Acad. Sc. Paris, t 275, Serie B, 73 (1972)
10. C. Furlani, A. Sgamelloti, F. Magrini and D. Cordischi, J. Molecular Spectrosc. 24, 270 (1967)
11. R.D. Willett, O.L. Liles Jr and C. Michelson, Inorg. Chem. 6, 1885 (1967)
12. P.W. Selwood, Magnetochemistry, Interscience Publishers, New York (1956)
13. G.A. Baker Jr, H.E. Gilbert and G.S. Rushbrooke, Physics Letters 25A, 207 (1967)
14. L.J. de Jongh and W.D. van Amstel, J. Phys. suppl. no 2-3, Tome 32, 880 (1971)
15. L.J. de Jongh and A.R. Miedema, Adv. Phys. (to be published)
16. S. Hillaert, to be published
17. T. Nagamiya, K Yosida and R. Kubo, Adv. Phys. 4, 1 (1955)
18. F. Keffer, Spinwaves, Handbuch der Physik, Band XVIII, Teil 2, Springer Verlag (1966)
19. M.E. Fisher, Rep. Progr. Phys. Vol. 30, 2, 800 (1967)
20. J. Feder and E. Pytte, Phys. Rev. 168, 640 (1968)
21. F.W. Klaaijsen, to be published
22. P. Bloembergen, K.G. Tan, T.H.J. Lefevre and H.H.M. Bleyendaal, J. Phys., suppl. no 2-3, Tome 32, 879 (1971)
23. P.W. Anderson, Phys. Rev. 86, 694 (1952)

24. H.L. Davis and A. Narath, Phys. Rev. 134, A433 (1964)
25. A. Narath and H.L. Davis, Phys. Rev. 137, A163 (1965)
26. E.J. Samuelson, R. Silberglitt, G. Shirane and J.P. Remeika, Phys. Rev. B3, 157 (1971)
27. A. Narath, Phys. Rev. 140, A854 (1965)
28. J.H.P. Colpa, Physica 57, 347 (1972)
29. L.J. de Jongh, private communication
30. J.H.P. Colpa, Physica 56, 185, 205 (1971)
31. D.Y. Yeter and W.E. Hatfield, J. Inorg. Nucl. Chem. 34, 3055 (1972)
32. D.N. Zubarev, Usp. Fiz. Nauk. 71, 71 (1960) (English translation: Soviet Phys-Usp. 3, 320 (1960))
33. R.A. Tahir-Kheli and D. ter Haar, Phys. Rev. 127, 88, 95 (1962)
34. H.B. Callen, Phys. Rev. 130, 890 (1963)
35. F.B. Anderson and H.B. Callen, Phys. Rev. 136, A1068 (1964)
36. M.E. Lines, Phys. Rev. 135, A1336 (1964)
37. R.E. Mills, R.P. Kenan and F.J. Milford, J. Appl. Phys. 36, 1131 (1965)
38. M.E. Lines, Phys. Rev. 133, A841 (1964)
39. M.E. Lines, Phys. Rev. 156, 534 (1967)
40. T. Oguchi, Phys. Rev. 133, A1098 (1964)
41. M.E. Lines, J. Chem. Phys. Solids 31, 101 (1970)

SUMMARY

In this thesis, the results of magnetic measurements on compounds of 3d-transition metals are reported. Compounds were chosen, which on basis of their crystal structure may show characteristic features of one- or two-dimensional magnetic systems. In particular, we paid attention to the chemical system $AX-BX_2$ (A=K, Rb, NH_4, Tl, Cs; B=Mn, Fe, Co, Ni, Cu; X=F, Cl, Br), since in this system many ABX_3 and A_2BX_4 compounds occur, having respectively the $BaNiO_3$ (h) structure and the K_2NiF_4 structure. In the $BaNiO_3$ (h) structure, chains of metal ions are formed in such a way that the intra-chain exchange interaction may be anticipated to be much larger than the inter-chain coupling. In the layer-type K_2NiF_4 structure, the metal layers are separated by several non-magnetic layers, so that the inter-plane interaction will probably be much smaller than the intra-plane interaction. Experimental evidence for the occurrence of one- or two-dimensional behaviour in compounds with the $BaNiO_3$ (h) and K_2NiF_4 structure was already known in the literature.

However, for X=Cl, Br the knowledge of the system $AX-BX_2$ was still limited. Therefore, we have tried to prepare and to investigate the crystal structure of the compounds in this system for X=Cl, Br. A number of the results obtained are described in Chapter II. Much attention has been paid to the phenomenon of ordering between X and X' halogen ions (X=smaller halogen ion, X'=larger, more polarizable halogen ion) in compounds $A_2BX_{4-x}X'_x$ (x=0, 1, 2) with the K_2NiF_4 structure, where the X' ions prefer to order on sites located between the metal layers.

Besides this part of the experimental program, a few series of coordination compounds were investigated, which on the basis of their structural geometry were expected to show one-dimensional behaviour.

In Chapter III, the results of susceptibility measurements on $ANiX_3$ compounds (A=Rb, NH_4, Tl, Cs; X=Cl, Br) with the $BaNiO_3$ (h) structure are interpreted by means of a theory developed recently by Weng for antiferromagnetic Heisenberg linear chain

systems having spin S=1. With this theory, reliable values for the intra-chain interaction parameter J/k in the various compounds are obtained. By means of Oguchi's theory for coupled antiferromagnetic linear chains, an estimate is given of the magnitude of the much weaker inter-chain coupling J'/k. It is concluded from our results that Weng's theory gives a reliable description of experimental examples of isotropic or nearly isotropic linear-chain systems with S=1.

Weng's theory for S=1, his interpolation scheme for S > 1, and other theoretical models, such as the linear-chain Ising and XY model, were applied to susceptibility and specific heat data obtained for the antiferromagnetic linear-chain compounds $M^{2+}(N_2H_5)_2(SO_4)_2$ with M=Mn, Fe, Co, Ni, Cu (Chapter IV). For M=Mn, Cu, the Heisenberg model for antiferromagnetic linear chains, with S=5/2 and S=1/2 respectively, is appropriate to interpret the experimental results. For M=Ni, a complication occurs, probably due to the presence of single-ion anisotropy of a magnitude comparable to the intra-chain interaction. The development of a theory for linear chains having S=1, including single-ion anisotropy, will be necessary for further investigations on this compound. The description of the magnetic systems in $Fe(N_2H_5)_2(SO_4)_2$ and $Co(N_2H_5)_2(SO_4)_2$ gives rise to several problems that are related to phenomena like crystalline field anisotropy, Van Vleck paramagnetism, and anisotropic exchange. For $Co(N_2H_5)_2(SO_4)_2$, the XY model appears to be the most appropriate one.

In Chapter V, the antiferromagnetic linear-chain compounds MnX_2L_2 (X=Cl, Br; L=pyrazole, pyridine) are discussed. By means of susceptibility and specific heat data, values for the intra- and inter-chain interaction parameters J/k and J'/k are derived. The reliability of the J/k-values is supported by the results of an ESR line-width study (the so-called '10/3 effect') in the temperature region 100-300K, from which also J/k is determined.

The magnetic ions in the compounds Rb_2CuCl_4, Rb_2CuCl_3Br and $Rb_2CuCl_2Br_2$ (Chapter VI), that have the $(NH_4)_2CuCl_4$ structure (a deformed K_2NiF_4 structure) order in ferromagnetic layers coupled by a weak antiferromagnetic exchange interaction. By means of ESR, susceptibility, magnetization, and specific heat measurements, values for the antiferromagnetic transition temperature T_N, the intra- and inter-layer exchange parameters J/k and J'/k, and the anisotropy fields are obtained. As a result of the occupation of sites between the layers by Br^- ions, J'/k increases on going from Rb_2CuCl_4 to $Rb_2CuCl_2Br_2$. This is probably caused by a larger superexchange over the Br^- ions in these compounds, compared to the Cl^- ions (this phenomenon was also observed for

the compounds described in Chapter III and V). Furthermore, the replacement of Cl^- by Br^- was found to introduce a larger anisotropy in the superexchange mechanism. Another result obtained in Chapter VI is, that a reasonable explanation of the value of T_N is given by means of the Green function formalism, in which the parameters J and J', and an anisotropy parameter D' are involved.

SAMENVATTING

In dit proefschrift zijn de resultaten beschreven van magnetische metingen bij lage temperaturen (vanaf ≈ 2K) aan polykristallijne verbindingen van 3d-overgangsmetalen. Op grond van de kristalstrukturen van de beschreven verbindingen werd verwacht dat ze de karakteristieke eigenschappen van één of twee dimensionale magnetische systemen zouden vertonen. Speciaal is aandacht besteed aan het chemische systeem $AX\text{-}BX_2$ (A=K, Rb, NH_4, Tl, Cs; B=Mn, Fe, Co, Ni, Cu; X=F, Cl, Br), daar in dit systeem vele ABX_3 en A_2BX_4 verbindingen bekend zijn, die resp. de $BaNiO_3$ (h) en K_2NiF_4 struktuur hebben. De $BaNiO_3$ (h) struktuur is een ketenstruktuur waarin, zoals in de literatuur bekend is, de magnetische wisselwerking tussen naaste metaal-ionen in de ketens in het algemeen veel sterker is dan de wisselwerking tussen naaste metaal-ionen behorend bij verschillende ketens. Als gevolg hiervan kan het magnetische systeem in goede benadering als één dimensionaal worden beschouwd. Van verbindingen met de K_2NiF_4 struktuur, die is opgebouwd uit metaallagen met daartussen enkele niet magnetische lagen, is bekend dat in het algemeen de magnetische interaktie tussen naaste metaalionen in de laag veel sterker is dan de interaktie tussen naaste metaalionen behorende bij verschillende lagen. Hierdoor zijn verbindingen met de K_2NiF_4 struktuur in goede benadering als twee dimensionale systemen te beschouwen.

Voor X=Cl, Br was de kennis van kristallografische en magnetische eigenschappen van verbindingen in het systeem $AX\text{-}BX_2$ nog tamelijk beperkt. Om een uitgebreider overzicht te krijgen van dit systeem voor X=Cl, Br, hebben we getracht na te gaan welke A_2BX_4 verbindingen bestaan en welke kristalstrukturen ze bezitten. Een aantal van de verkregen resultaten is verwerkt in Hoofdstuk II. Bij de onderzoekingen is veel aandacht geschonken aan het verschijnsel van de ordening die plaats vindt tussen X en X' halogeen ionen (X=kleiner halogeen ion, X'=groter, polariseerbaarder halogeen ion) in verbindingen $A_2BX_{4-x}X'_x$ (x=0, 1, 2) met de K_2NiF_4 struktuur. Het blijkt namelijk dat de X' ionen zich bij voorkeur ordenen op anion posities die gelegen zijn tussen twee metaallagen.

Naast bovenbeschreven onderzoek heeft nog een onderzoek plaats gehad naar de magnetische eigenschappen van enkele series koördinatieverbindingen waarvoor, ook op grond van hun kristalstruktuur, één dimensionaal magnetisch gedrag kon worden verwacht.

In Hoofdstuk III zijn de resultaten besproken van susceptibiliteit metingen van verbindingen $ANiX_3$ (A=Rb, NH_4, Tl, Cs; X=Cl, Br) met de $BaNiO_3$ (h) struktuur. De susceptibiliteit als funktie van de temperatuur kon worden geïnterpreteerd m.b.v. een recentelijk door Weng ontwikkelde, theoretische beschrijving van antiferromagnetische Heisenberg lineaire ketens met spin S=1. De intra-keten magnetische interaktie parameter J/k is berekend. M.b.v. Oguchi's theorie voor een drie dimensionaal systeem van zwak gekoppelde antiferromagnetische lineaire ketens is een schatting gegeven van de grootte van de zwakke inter-keten koppelingsparameter J'/k. De verkregen resultaten tonen aan dat Wengs theorie een redelijk beeld geeft van experimentele voorbeelden van lineaire keten systemen met S=1, die als isotroop of in goede benadering als isotroop kunnen worden beschreven.

Wengs theorie voor S=1, zijn interpolatie schema voor keten systemen met $S > 1$, en andere theoretische modellen, zoals het lineaire Ising en XY keten model, zijn toegepast op de resultaten van susceptibiliteit en soortelijke warmte metingen voor de antiferromagnetische lineaire keten verbindingen $M^{2+}(N_2H_5)_2(SO_4)_2$ met M=Mn, Fe, Co, Ni, Cu (Hoofdstuk IV). In de gevallen M=Mn, Cu blijken de experimentele gegevens in redelijke benadering te kunnen worden geïnterpreteerd met het Heisenberg model voor antiferromagnetische lineaire ketens met resp. S=5/2 en S=1/2. Voor M=Ni treedt een gekompliceerder situatie op, die mogelijk veroorzaakt wordt door een kristalveld anisotropie voor het Ni^{2+} ion, die in grootte vergelijkbaar is met de intra-keten interaktie. Voor een verdere bestudering van deze Ni verbinding is het wenselijk ook de kristalveld anisotropie te betrekken in de theoretische beschrijving van lineaire ketens met S=1. De interpretatie van de experimentele gegevens voor M=Fe, Co levert nogal wat problemen op t.g.v. verschijnselen als kristalveld anisotropie, Van Vleck paramagnetisme en anisotrope magnetische wisselwerking. Voor $Co(N_2H_5)_2(SO_4)_2$ lijkt het XY model de geschiktste benadering van het magnetisch systeem.

In Hoofdstuk V zijn de antiferromagnetische lineaire keten verbindingen MnX_2L_2 (X=Cl, Br; L=pyrazool, pyridine) besproken. De intra- en inter-keten interaktie parameters J/k en J'/k zijn berekend m.b.v. susceptibiliteit en soortelijke warmte gegevens. Ook uit een ESR lijnbreedte studie (het z.g. 10/3 effekt) in het temperatuurgebied 100-300K kon J/k bepaald worden.

De magnetische ionen in de verbindingen Rb_2CuCl_4, Rb_2CuCl_2Br en $Rb_2CuCl_2Br_2$ (Hoofdstuk VI) met de $(NH_4)_2CuCl_4$ struktuur (een vervormde K_2NiF_4 struktuur) ordenen in ferromagnetische lagen, die gekoppeld zijn door een zwakke, antiferromagnetische wisselwerking. ESR, susceptibiliteit, magnetisatie en soortelijke warmte metingen leveren waarden voor de antiferromagnetische overgangstemperatuur T_N, de interaktie parameters J/k en J'/k voor resp. de wisselwerking in en tussen de lagen, en de anisotropie velden. T.g.v. de ordening van Br^- ionen op anion posities tussen de Cu lagen neemt J'/k toe in de reeks Rb_2CuCl_4, Rb_2CuCl_3Br en $Rb_2CuCl_2Br_2$. Dit wordt waarschijnlijk veroorzaakt door een grotere superexchange over Br^- ionen vergeleken met Cl^- ionen (hetzelfde verschijnsel werd ook gekonstateerd bij verbindingen die beschreven zijn in Hoofdstuk III en V). De vervanging van Cl^- door Br^- blijkt ook een grotere anisotropie in het superexchange mechanisme te introduceren. In Hoofdstuk VI is verder beschreven hoe een redelijke theoretische verklaring van de waarde van T_N kan worden verkregen m.b.v. het Green funktie formalisme, waarin J en J', en een anisotropie parameter D' een rol spelen.

Volgens het gebruik in de Faculteit der Wiskunde en Natuurwetenschappen volgt hier een kort overzicht van mijn studie

1956-1961
HBS-b, Stevin HBS, Den Haag

1961-1965
Studie voor kandidaatsexamen: natuur- en wiskunde, bijvak sterrenkunde, aan de Rijksuniversiteit te Leiden. Examen in februari 1965.

1965-1968
Studie voor doctoraal examen. De opleiding op het Kamerlingh Onnes Laboratorium vond plaats onder leiding van prof.dr. N.J. Poulis. De uitgevoerde experimenten waren onderdeel van het onderzoekprogramma van de werkgemeenschap Vaste Stof van de Stichting F.O.M., van welke Stichting ik een studietoelage genoot in de periode 1968-1969. Het doctoraalexamen werd afgelegd in mei 1968.

1968-1973
Promotie onderzoek op de afdeling Anorganische Chemie van de Gorlaeus Laboratoria o.l.v. prof.dr. E.W. Gorter. Na het overlijden van prof.dr. E.W. Gorter in oktober 1972 vond de afronding van het in dit proefschrift beschreven onderzoek plaats o.l.v. dr. W.J.A. Maaskant.
Gedurende de periode 1968-1973 was ik in dienst van de Stichting SON (doktoraal assistent 1968-1969, wetenschappelijk medewerker 1969-1973).

Het in dit proefschrift beschreven onderzoek vond plaats onder de auspiciën van de Stichting Scheikundig Onderzoek Nederland (SON) en is mogelijk gemaakt door financiële steun van de Nederlandse Organisatie voor Zuiver Wetenschappelijk Onderzoek (ZWO).

Allen die hebben bijgedragen aan de totstandkoming van dit proefschrift ben ik zeer erkentelijk. In het bijzonder dank ik de medewerkers van de werkgroep Vaste Stof Chemie voor de samenwerking die ik mocht ondervinden. Ook gaat mijn dank uit naar het personeel van de Gorlaeus Laboratoria. Hun hulp was voor mij onmisbaar.

STELLINGEN

behorende bij het proefschrift van H. T. Witteveen

I De magnetische susceptibiliteit als funktie van de temperatuur van antiferromagnetische lineaire keten verbindingen met spin S=1, waarvan de magnetische wisselwerking in de ketens in goede benadering als isotroop is te beschouwen, kan op redelijke wijze beschreven worden m. b. v. Wengs theorie voor een Heisenberg lineair keten systeem met S=1.
Dit proefschrift, Hoofdstuk III.

II Het bestaan van de verbinding K_2CuCl_4 is door Joly niet bewezen.
E. Joly, C. R. Acad, Sc. Paris, 272, C1302 (1971).
Dit proefschrift, Hoofdstuk II.

III ESR lijnbreedtes kunnen m. b. v. het '10/3 effekt' onder bepaalde voorwaarden een nuttige bijdrage leveren tot het bepalen van de magnetische wisselwerking in verbinding met een isotrope magnetische exchange.
Dit proefschrift, Hoofdstuk V.

IV De wijze waarop Drumheller et al. de asymptotische Curie-Weiss temperatuur van enkele verbindingen van de serie $(C_nH_{2n+1}NH_3)_2CuCl_{4-x}Br_x$ (x=0, 2) hebben bepaald, is niet juist.
J.E. Drumheller, D.H. Dicky, R.P. Reklis en C.E. Zaspel, Phys. Rev. B5, 4631 (1972).

V De konklusie die Speca et al. trekken naar aanleiding van het met een KBr plaatje opgenomen infrarood spektrum van $Ni(pyzNO)_3(ClO_4)_2.2H_2O$, en die inhoudt dat onder grote druk het perchloraat anion in deze verbinding koördineert met het Ni kation, is aan twijfel onderhevig.
A.N. Speca, L.L. Pytlewsky en N.M. Karayannis, Inorg. Nucl. Chem. Letters, 9, 365 (1973).

VI Emori's interpretatie van het scherpe maximum dat bij lage temperatuur optreedt in de susceptibiliteit kurve van de ketenverbinding $CuBr_2$ (pyridazine), is waarschijnlijk niet juist.
S. Emori, M. Inoue en M. Kubo, Bull. Chem. Soc. Jap. 45, 2259 (1972).

VII Het is zeer onwaarschijnlijk dat in de verbindingen MM'_2S_4 met de Th_3P_4 struktuur, kation ordening gevonden zal worden, zoals voorgesteld door Carter.
F. L. Carter, J. Solid State Chem. 5, 300 (1972).
H.H. Davis, J. Bransky en N.M. Tollan, J. Less Comm. Met. 22, 193 (1970).

VIII De door Grambow vermeende overeenstemming tussen de eksperimentele en theoretische spin-spin relaksatie tijd in $Ce_2Mg_3(NO_3)_{12}.24H_2O$ is onvoldoende theoretisch gemotiveerd.
I. Grambow, Z. Physik 257, 245 (1972).

IX Het is te betreuren dat de belangstelling van de fysici voor koördinatieverbindingen geen gelijke tred heeft gehouden met de ontwikkelingen in de koördinatiechemie.

X De struktuur, die Clark mogelijk acht voor een verbinding MX_2 met M in oktaedrische omringing, kan op grond van de door hem geciteerde tweede regel van Pauling worden uitgesloten.
G. M. Clark, The Structures of Non-Molecular Solids, p223, 240, 42, Applied Science Publishers Ltd, London (1972).